REPORT NO. LO341

DRA

(NASA-CR-147984) FLUIDIC HYDROGEN DETECTOR PRODUCTION PROTOTYPE DEVELOPMENT Final Report, Nov. 1974 - Apr. 1976 (McDonnell-Douglas Astronautics Co.) 155 p HC $6.75 CSCL 14B G3/35

N76-33475

Unclas 15409

FLUIDIC HYDROGEN DETECTOR PRODUCTION PROTOTYPE DEVELOPMENT

G. W. ROE

R. E. WRIGHT

MCDONNELL DOUGLAS ASTRONAUTICS - TICO

P. O. BOX 600 TITUSVILLE, FLA.

APRIL 16, 1976

FINAL REPORT

CONTRACT NO. NAS10-8764

NOVEMBER 1974, APRIL 1976

NATIONAL AERONAUTICS AND SPACE ADMINISTRATION

JOHN F. KENNEDY SPACE CENTER

CAPE KENNEDY, FLA. 32899

REPORT DOCUMENTATION PAGE		READ INSTRUCTIONS BEFORE COMPLETING FORM
1. REPORT NUMBER L0341	2 GOVT ACCESSION NO	3 RECIPIENT'S CATALOG NUMBER
4. TITLE (and Subtitle) Fluidic Hydrogen Detector Production Prototype Development		5. TYPE OF REPORT & PERIOD COVERED Final Report November 1974 to April 1976 6. PERFORMING ORG. REPORT NUMBER
7. AUTHOR(s) G. W. Roe, R. E. Wright		8. CONTRACT OR GRANT NUMBER(s) NAS10-8764
9. PERFORMING ORGANIZATION NAME AND ADDRESS McDonnell Douglas Astronautics Co. P. O. Box 600, Titusville, Florida 32780		10. PROGRAM ELEMENT, PROJECT, TASK AREA & WORK UNIT NUMBERS
11. CONTROLLING OFFICE NAME AND ADDRESS National Aeronautics & Space Administration John F. Kennedy Space Center Cape Kennedy, Florida 32899		12. REPORT DATE 16 April 1976 13. NUMBER OF PAGES
14. MONITORING AGENCY NAME & ADDRESS (if different from controlling office)		15. SECURITY CLASS. (of this report) Unclassified 15a. DECLASSIFICATION/DOWNGRADING SCHEDULE
16. DISTRIBUTION STATEMENT (of this report) Unlimited		
17. DISTRIBUTION STATEMENT (of the abstract entered in Block 20, if different from report)		
18. SUPPLEMENTARY NOTES		
19. KEY WORDS (Continue on reverse side if necessary and identify by block number) Hydrogen Detector, Fluidic, Prototype		
20. ABSTRACT (Continue on reverse side if necessary and identify by block number) A fluidic sensor concept, based on the principle that the frequency of a fluidic oscillator is proportional to the square root of the molecular weight of its operating fluid, was utilized. To minimize sensitivity to pressure and temperature fluctuations, and to make the sensor specific for hydrogen, two oscillators are used. One oscillator operates on		

DD FORM 1 JAN 73 1473 EDITION OF 1 NOV 65 IS OBSOLETE

SECURITY CLASSIFICATION OF THIS PAGE

Block 20. (Continued)

sample gas containing hydrogen, while the other operates on sample gas with the hydrogen converted to steam. The conversion is cccomplished with a small catalytic converter. The frequency difference is taken, and the hydrogen concentration computed with a simple digital processing circuit. The sensor output is an analog signal proportional to hydrogen concentration.

REPORT NO. LO341

FLUIDIC HYDROGEN DETECTOR PRODUCTION PROTOTYPE DEVELOPMENT

G. W. ROE
R. E. WRIGHT

MCDONNELL DOUGLAS ASTRONAUTICS - TICO
P. O. BOX 600 TITUSVILLE, FLA.

APRIL 16, 1976

FINAL REPORT
CONTRACT NO. NAS10-8764
NOVEMBER 1974, APRIL 1976

NATIONAL AERONAUTICS AND SPACE ADMINISTRATION
JOHN F. KENNEDY SPACE CENTER
CAPE KENNEDY, FLA. 32899

W. R. HELMS
TECHNICAL REPRESENTATIVE

PREFACE

The author wishes to express his gratitude to Mr. W. B. Depperman for his contribution to the development of the fluidic sensor used in these prototype detectors.

TABLE OF CONTENTS

TABLE OF CONTENTS

LIST OF FIGURES

LIST OF FIGURES

LIST OF TABLES

ABSTRACT

This report describes the work performed by McDonnell Douglas Astronautics Company, TICO (MDAC TICO), under Contract No. NAS10-8764 to the National Aeronautics and Space Administration, Kennedy Space Center, Florida, for the development of production prototype fluidic hydrogen gas detectors. The effort was sponsored by NASA to develop a reliable and relatively maintenance free hydrogen gas sensor that can replace catalytic combustion sensors presently used to detect leaks in the liquid hydrogen transfer systems at Kennedy Space Center. This work culminates previous efforts by MDAC TICO under Contract No. NAS10-8373 to NASA "Fluidic Hydrogen Sensor Development Study" and studies conducted by the University of Florida.

A fluidic sensor concept, based on the principle that the frequency of a fluidic oscillator is proportional to the square root of the molecular weight of its operating fluid, was utilized. To minimize sensitivity to pressure and temperature fluctuations, and to make the sensor specific for hydrogen, two oscillators are used. One oscillator operates on sample gas containing hydrogen, while the other operates on sample gas with the hydrogen converted to steam. The conversion is accomplished with a small catalytic converter. The frequency difference is taken, and the hydrogen concentration computed with a simple digital processing circuit. The output from the sensor is an analog signal proportional to hydrogen content.

Functional and environmental tests have shown the detector to be very accurate, and relatively insensitive to severe environmental disturbances. It is also specific for hydrogen, even with large helium concentrations in the sample gas. The performance of the sensor is adequate for the intended application, and the basic concept can be adapted to provide a reliable gas detector for numerous government and commercial requirements.

SECTION 1
INTRODUCTION

For over a decade, it has been recognized that fluidic technology offered promise in the area of gas detection. An application of the phenomena involved exists at Kennedy Space Center (KSC) where the detection of trace amounts of hydrogen gas is required as a safety precaution, since the existence of such gas would indicate a potentially dangerous leak. Realizing this application of fluidics to a hydrogen sensor for the Space Shuttle era, KSC sponsored a study in 1971-72 with the University of Florida to investigate promising but untried theories which might yield such a sensor. Numerous fluidic techniques were considered, and of the three which showed promise the study indicated the concept which utilized the principle that the frequency of a fluidic oscillator is proportional to the square root of the molecular weight of its operating fluid was the most practical. Although this study demonstrated the feasibility of a fluidic sensor, it also identified several problems inherent to this approach.

In 1973, a study was conducted by MDAC TICO for NASA under Contract NAS10-8373 to develop an engineering prototype sensor using the fluidic oscillator principle, but designed to overcome these inherent problems. This study successfully demonstrated a sensor which was capable of measuring hydrogen concentrations over a range from 0 to 10% by volume with an accuracy of ± 500 ppm. The sensor was essentially unaffected by changes in launch site variables, such as inlet gas temperature, humidity and helium concentrations.

In 1974, a development program was started by MDAC TICO, which this report describes, to develop production prototype models of a relatively inexpensive hydrogen sensor which could be used at KSC. Program objectives were to "production engineer" the electronic and fluidic circuits so that a simple, reliable and inexpensive end product could be realized, to obtain extensive environmental test data that will be required to establish a production configuration, and to determine maintenance and calibration requirements. The program was conducted in the four phases described below.

Phase I consisted of production engineering and designing, the electronics, fluidic circuit, catalyst system, and the transducers. In addition, operating environment life tests of the fluidic system, including oscillators, heat exchangers, and the catalytic converter, were conducted to determine, early in the program, if any design refinements must be incorporated to compensate for specific environmental conditions.

Phase II consisted of fabrication and testing a design verification model, which incorporated the results of the production engineering and design recommendations obtained during Phase I, and updating this model as required by results of the environmental life test units. Functional tests were then performed on this unit, and a production prototype design established.

During Phase III, environmental perturbation tests were conducted on the design verification model. The unit was subjected to extreme temperature, pressure, and humidity environments to determine their effects on system operation. Various gas background concentrations, dust and salt spray environments were also investigated.

In Phase IV, seven production prototype fluidic hydrogen detectors were built and functionally tested.

A block diagram of the hydrogen detector developed is given in Figure 1-1. Development and testing of each component is described in Sections 2 through 5. Section 2 discusses development of the fluidic sensor, including an edgetone oscillator, reluctance pick up, heat exchanger, catalytic converter, and manifold assembly. Section 3 describes the electronic processing of fluidic signals, heater control circuit, self test circuit and thermal control assembly. Integration of these two systems into a relatively small self-contained package is covered in Section 4. Testing is discussed in Section 5, including both functional and environmental evaluations. Conclusions and recommendations derived from the program are given in Section 6.

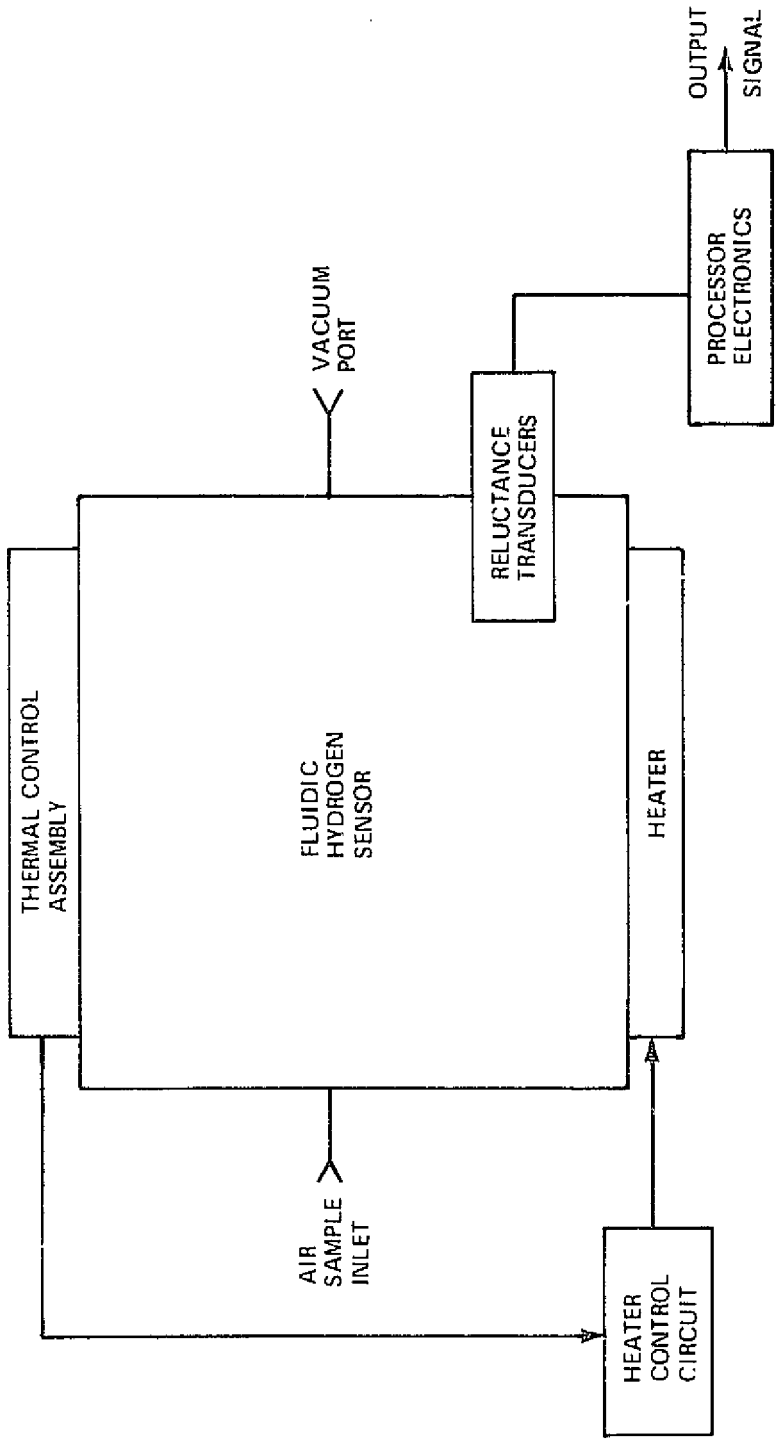

FIGURE 1-1 HYDROGEN DETECTOR BLOCK DIAGRAM

SECTION 2
FLUIDIC SENSOR

The heart of the hydrogen detector is a fluidic sensor that is used to detect variations in sample gas composition. This sensor works on the principle that the operating frequency of a fluidic oscillator is primarily a function of the speed of sound in the gas used as the working fluid. To make a sensor selective to hydrogen only, two oscillators are employed, where one oscillator operates on the sample gas mixture and the other operates on the sample gas mixture with the hydrogen removed from it. This technique also renders the sensor insensitive to pressure and temperature fluctuations, assuming the oscillators track each other as these parameters are varied. Test results indicate that good frequency correlation can be expected if the circuit design has similar flow paths and employs a heat exchanger to match the temperature of the gases entering each oscillator. Successful operation is predicated upon removing hydrogen from the sampled gas supplied to one oscillator. This is accomplished by a catalytic reaction of the hydrogen with oxygen in the background gas using a platinum and palladium compound. This type of catalytic converter can be made practically 100% efficient as long as the background gas contains enough oxygen to oxidize the hydrogen. When hydrogen is present in the sample gas the oscillator receiving the gas mixture of air and hydrogen increases in frequency, while the frequency of the oscillator receiving the gas with hydrogen removed will remain constant. The magnitude of this change in frequency between the two oscillators is directly proportional to the hydrogen concentration in the sample gas.

The fluidic hydrogen sensor utilizes two manifold blocks and a series of etched laminae that comprise the heat exchangers and oscillators. The etched laminae are mounted between the manifold blocks and the components are bolted together to form an assembly. The bottom manifold contains flow passages, the active and inactive catalytic converters, and sintered metal input and output filters that also serve as flame arrestors. The top manifold contains flow passages and two variable reluctance pressure transducers. The assembly measures 2-1/4" x 3" x 1-1/2" and is made from type 302 stainless steel. An exploded view of this

assembly is shown in Figure 2-1 and a schematic of the fluidic circuit is given in Figure 2-2. The theory of operation of the fluidic hydrogen sensor is contained in Appendix A. A discussion of the development of each component follows.

2.1 FLUIDIC OSCILLATORS

Previous development efforts had been directed toward using a bistable element with negative feedback as an oscillator. During this program an edgetone oscillator was evaluated for use in the sensor, because of its high frequency capabilities and construction simplicity. The edgetone oscillator developed has a higher gain and better signal-to-noise ratio than was obtained from the bistable element oscillator. In addition, the edgetone unit did not require a buffer amplifier, which reduced system complexity and power consumption.

An edgetone oscillator was tested in the oscillator evaluation studies conducted during the previous hydrogen sensor contract, but poor performance was obtained from the particular design that was used at that time. The edgetone concept was abandoned at that time in favor of the feedback oscillator concept. However, the advantages offered by the edgetone concept indicated that further development effort was indicated in this area. This work was conducted under IRAD funding, at no cost to the government, and resulted in an edgetone oscillator design that is superior to the feedback oscillator for the hydrogen sensor application.

Four edgetone oscillator configurations were tested to optimize the oscillator cavity shape. A rectangular cavity, a circular cavity, and variations of these basic cavity shapes were investigated, reference Figure 2-3. In all cases, the vacuum port was on the centerline of the oscillator. These investigations were undertaken to determine which cavity shape would produce the best signal quality; that is, a fundamental wave with minimum distortion. Test results indicated that a variation on the rectangular cavity shape (Figure 2-3c) produced the best fundamental signal.

This configuration was selected for additional optimization with respect to location of the vacuum port. As stated, the first design had the vacuum port on the centerline of the device. This porting arrangement had the potential to cause a problem with oscillator response, since the basic sample flow is through the center of the oscillator and the resonant cavities are essentially closed volumes

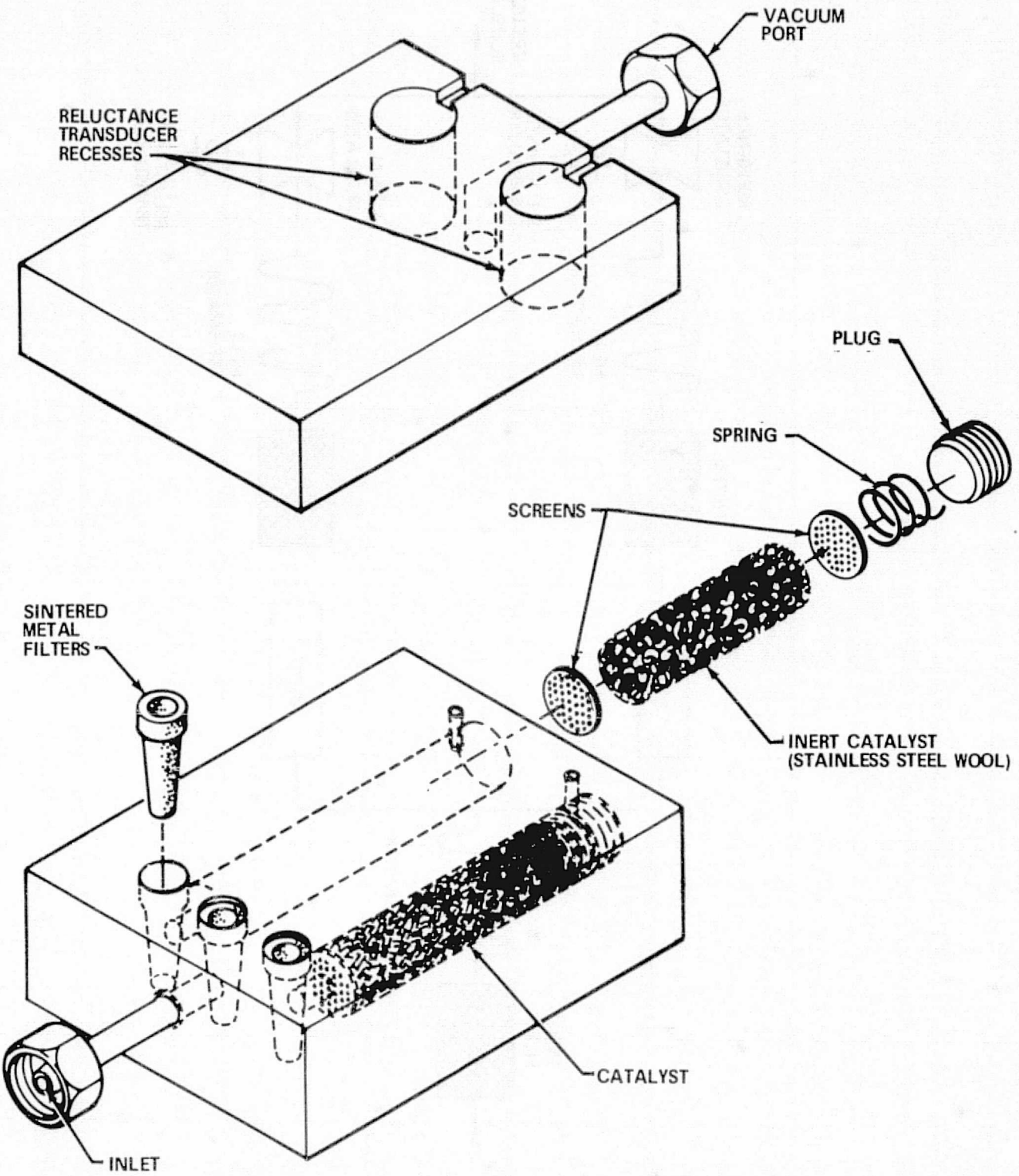

FIGURE 2-1 FLUIDIC HYDROGEN SENSOR

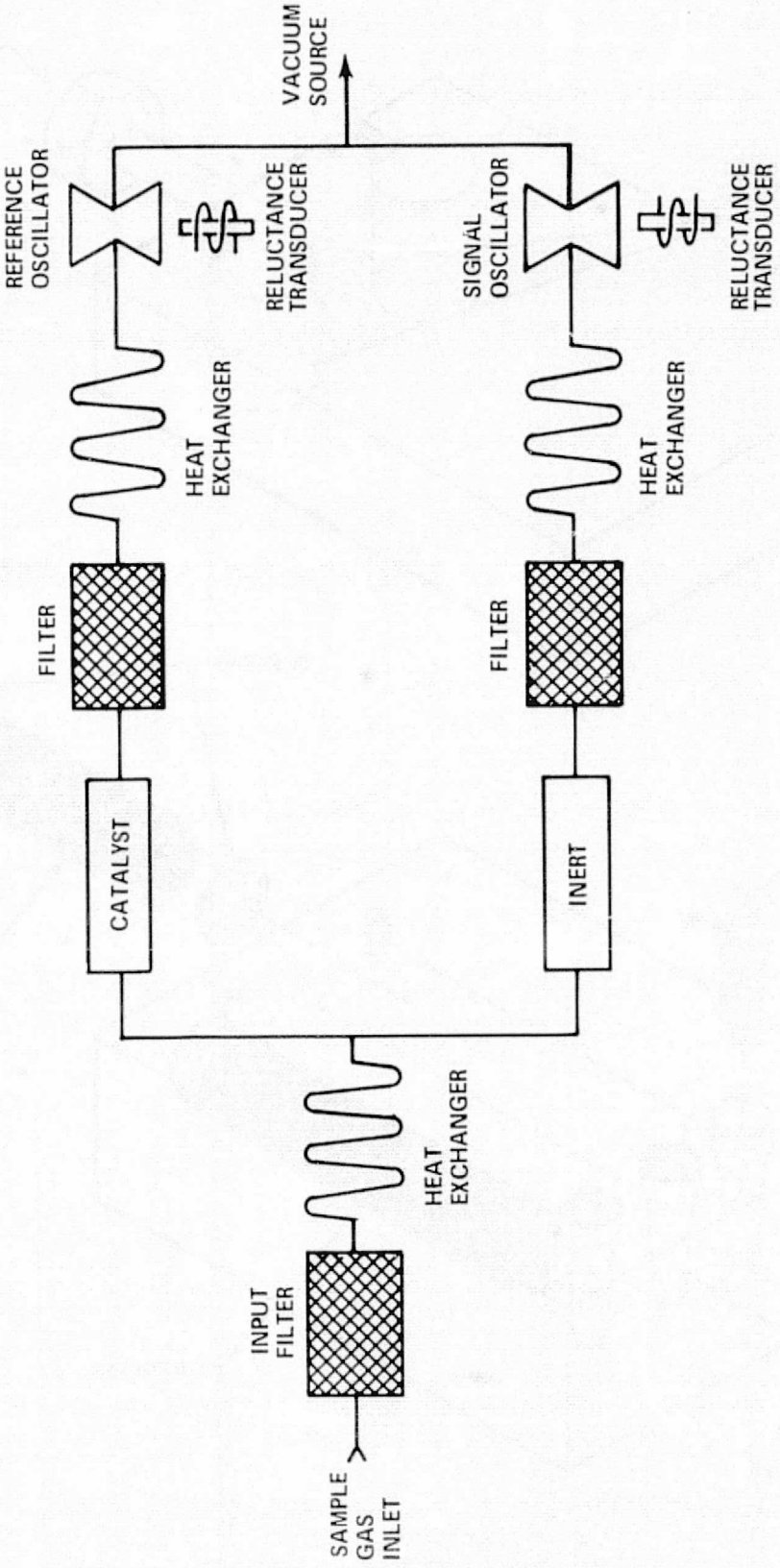

FIGURE 2-2 HYDROGEN SENSOR SCHEMATIC

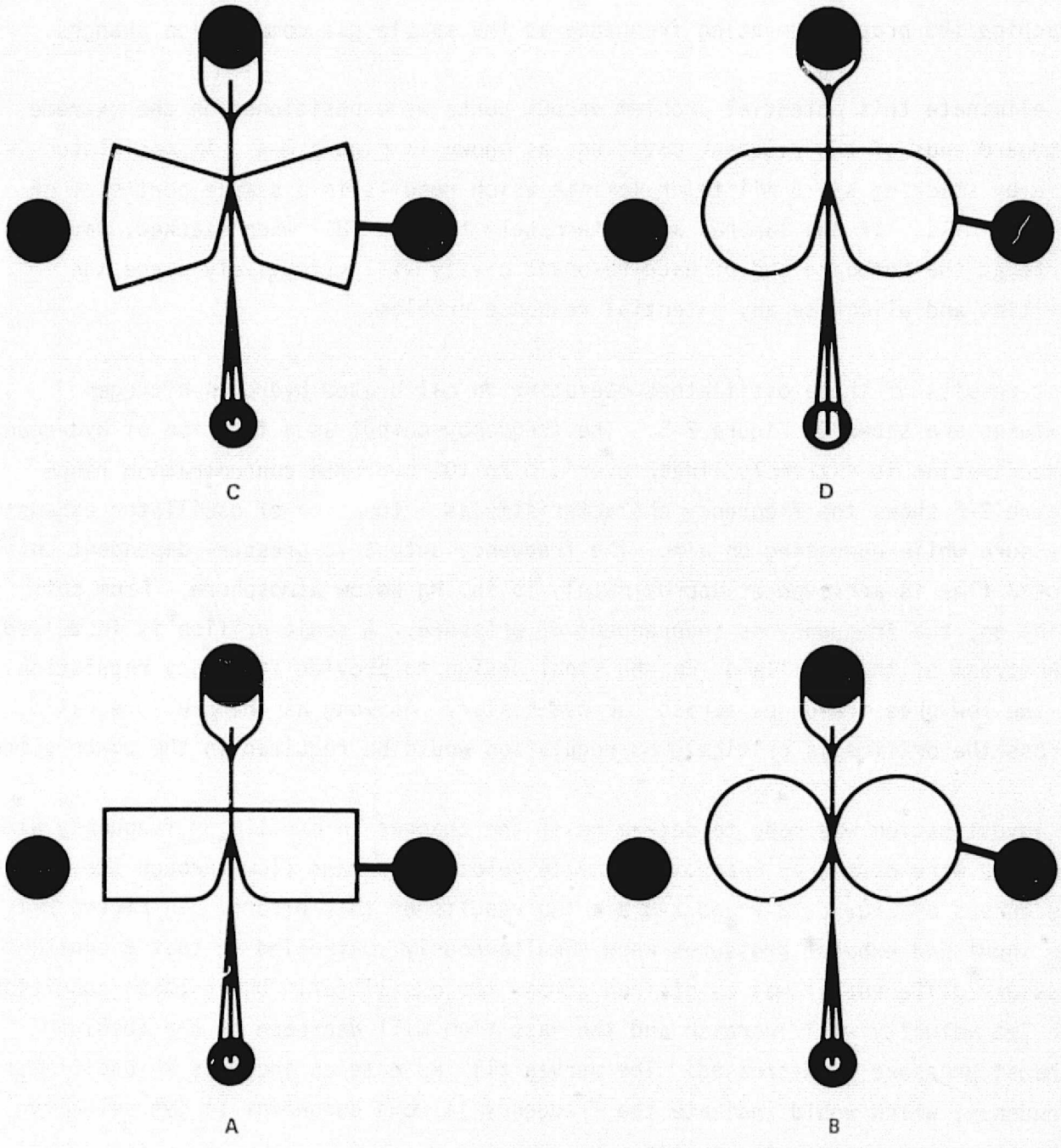

FIGURE 2-3 EDGETONE OSCILLATOR CAVITY CONFIGURATIONS

on each side of the jet. Since the cavities are not actively purged, the gas composition in the cavities could tend to stagnate and would not rapidly track changes in sample gas composition. This stagnation could cause a delay in reaching the proper operating frequency as the sample gas composition changes.

To eliminate this potential problem vacuum ports were positioned on the extreme outboard ends of the resonant cavities, as shown in Figure 2-4. An oscillator is made by stacking six 5 mil thick laminae which results in a sample port size of 10 x 30 mils. If the laminae are alternately flipped 180° when stacked, vacuum ports at the outboard end of each resonant cavity will effectively purge the cavities and eliminate any potential response problem.

Test results of these oscillators operating on calibrated hydrogen-nitrogen mixtures are shown in Figure 2-5. The frequency output as a function of hydrogen concentration is extremely linear over a 0 to 10% hydrogen concentration range. Figure 2-6 shows the frequency characteristic as a function of oscillator exhaust pressure while operating on air. The frequency output is pressure dependent until choked flow is achieved at approximately 15 in. Hg below atmosphere. From this point on, the frequency is independent of pressure. A sonic orifice is installed downstream of the oscillator in the final design to provide frequency regulation at the low pressure drops across the oscillator. As long as the pressure ratio across the orifice is critical, no regulation would be required in the power system.

An investigation was made to determine if the changes in oscillator frequency with pressure were caused by changes in nozzle velocity or mass flow through the system. The curves of Figures 2-7 and 2-8 are the results of this effort. In Figure 2-7, the input and exhaust pressures were simultaneously controlled so that a constant pressure differential was maintained across the oscillator. Under these conditions, the jet velocity will increase and the mass flow will decrease as the absolute exhaust pressure is decreased. The curves all indicate an increase in oscillator frequency, which would indicate the frequency is more dependent on jet velocity than mass flow through the system.

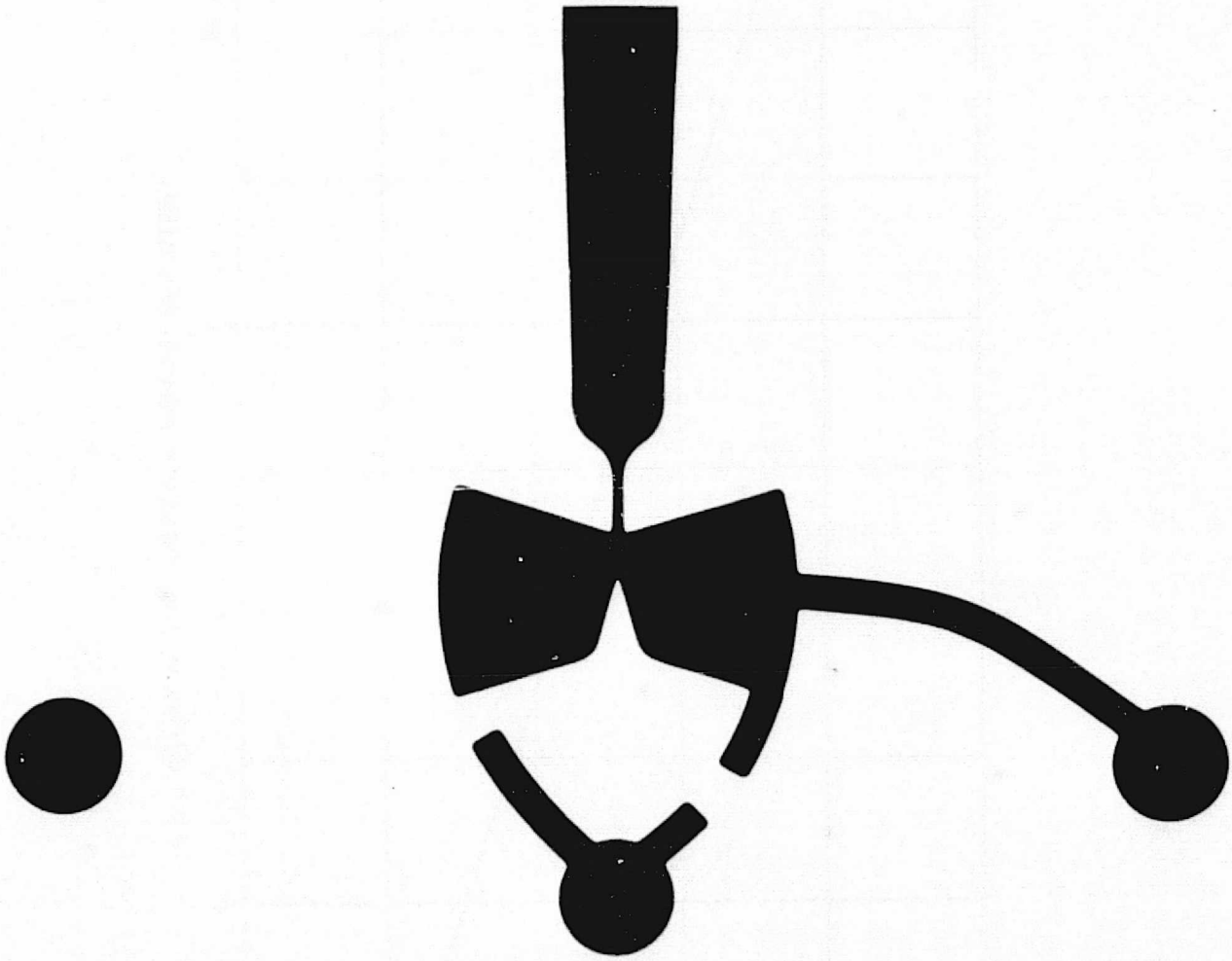

FIGURE 2-4 CAVITY PORTED EDGE TONE OSCILLATOR

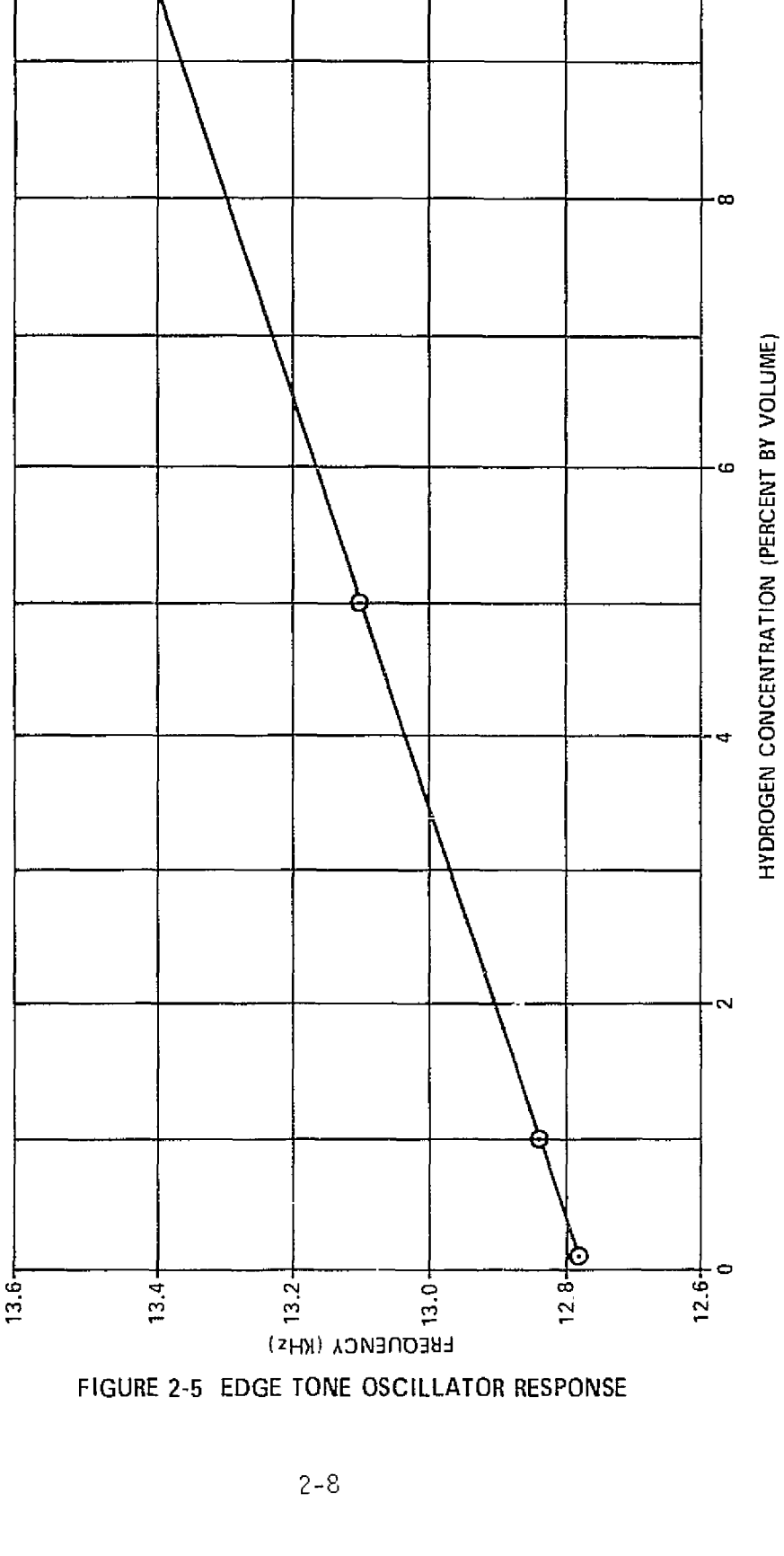

FIGURE 2-5 EDGE TONE OSCILLATOR RESPONSE

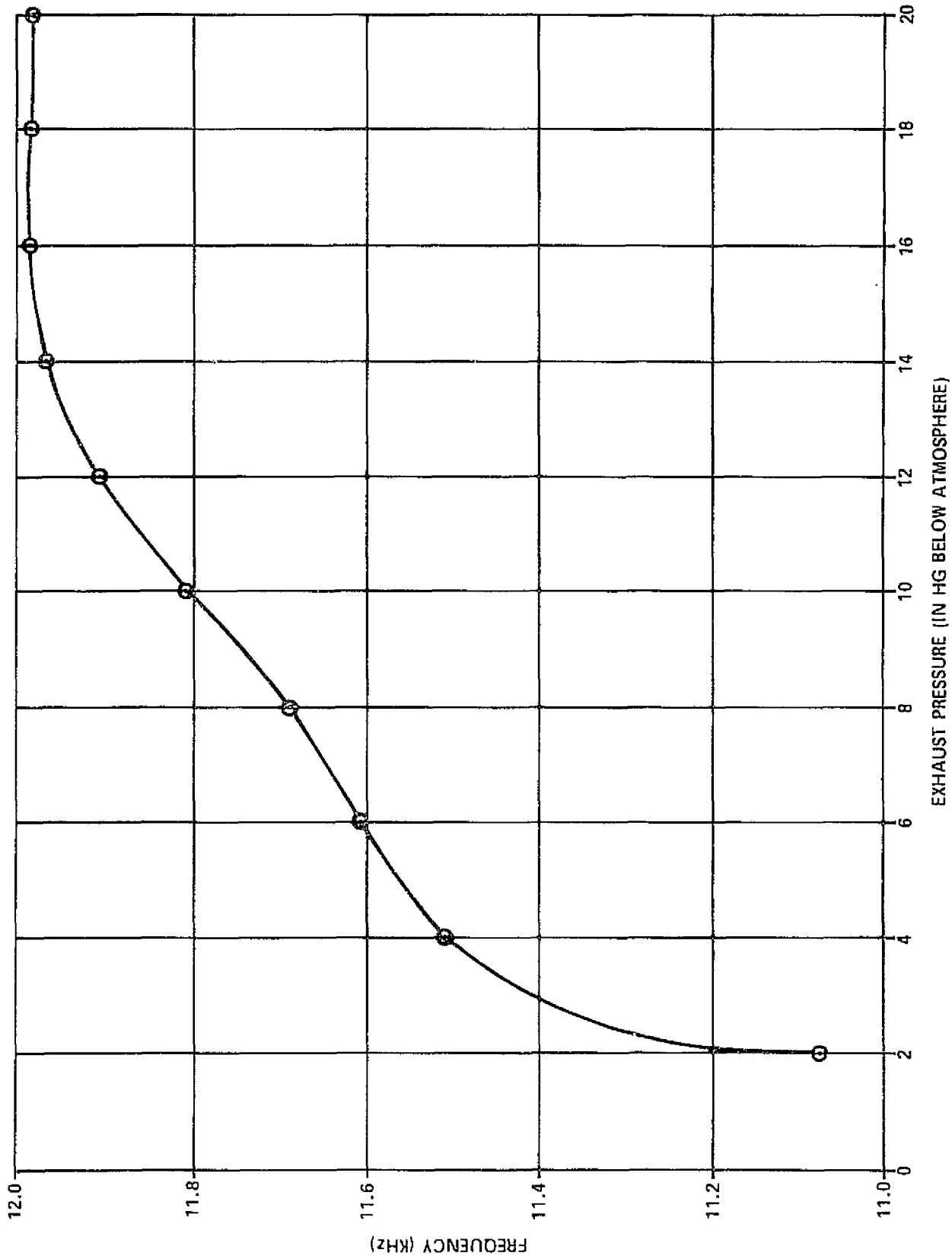

FIGURE 2-6 EDGE TONE OSCILLATOR PRESSURE CHARACTERISTIC

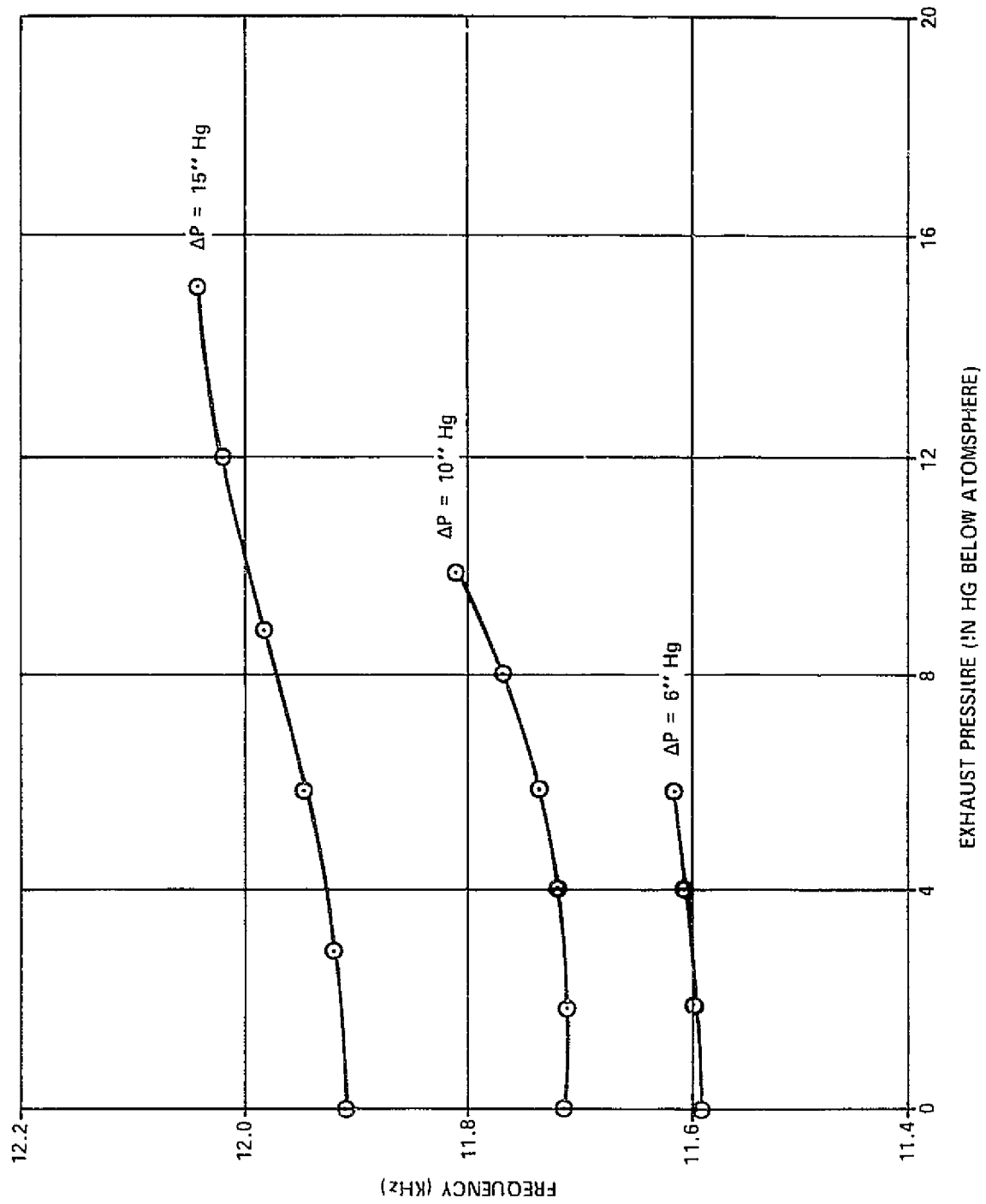

FIGURE 2-7 EDGE TONE OSCILLATOR PERFORMANCE WITH CONSTANT NOZZLE PRESSURE DIFFERENTIAL

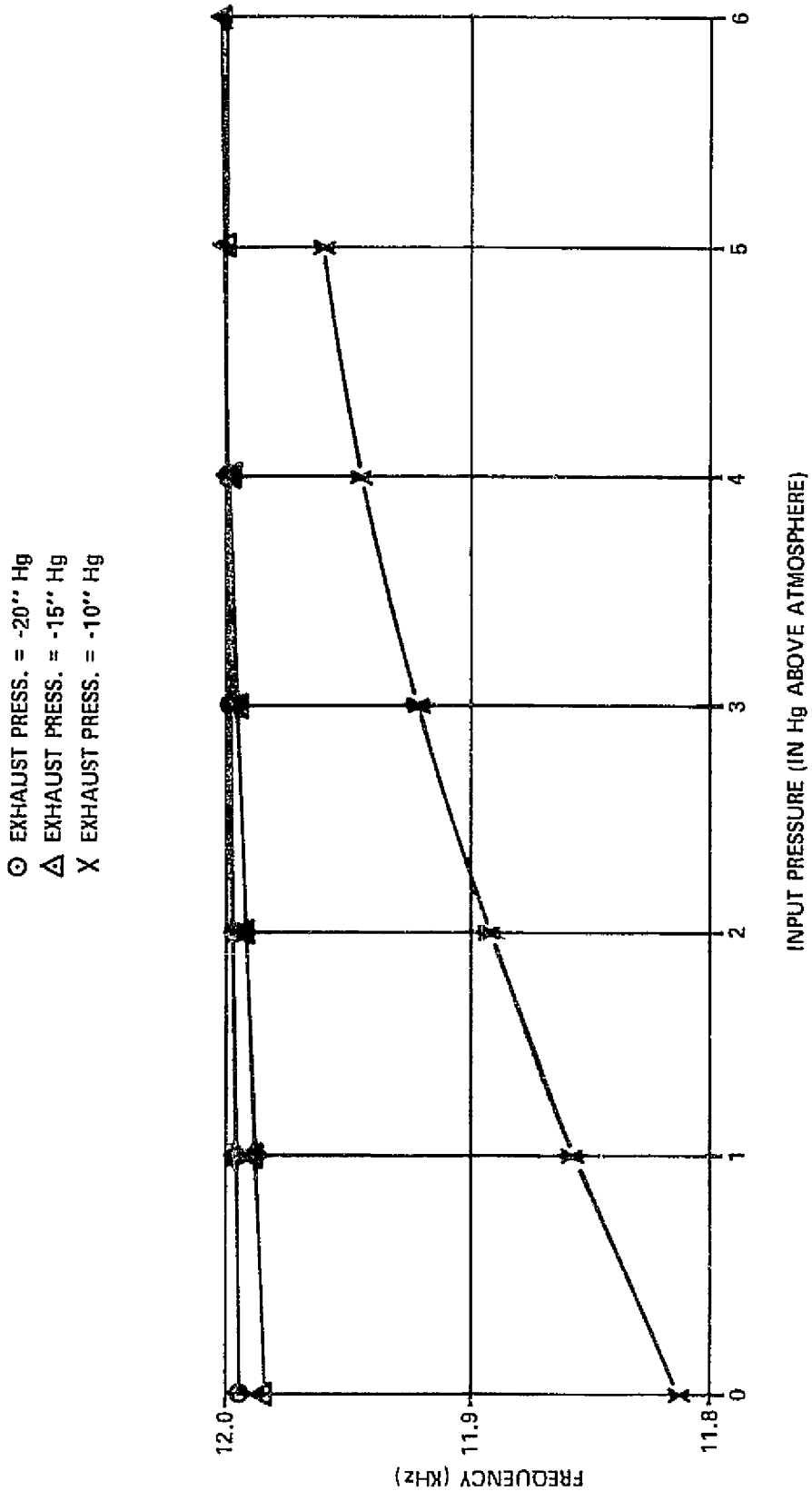

FIGURE 2-8 EDGE TONE OSCILLATOR PERFORMANCE WITH CONSTANT EXHAUST PRESSURE

A constant exhaust pressure was then applied to the oscillator and the input pressure varied. Curves for three different exhaust pressures were developed, and are shown in Figure 2-8. As long as the critical pressure ratio is maintained across the oscillator, output frequency is practically independent of input pressure. This indicates the oscillator can be made insensitive to upstream pressure, and therefore will not respond to day-to-day changes in the barometric pressure level.

An evaluation of the edgetone oscillator output signal was also conducted at varying oscillator exhaust pressures. A plot of transducer output voltage, depicted in Figure 2-9, shows that amplitude is also pressure dependent and becomes constant when the critical pressure ratio is reached. This would indicate the amplitude of oscillation is a function of either the jet velocity or mass flow through the system.

A significant improvement in magnitude and quality of the edgetone oscillator and reluctance transducer (described in Paragraph 2.3) output signals were obtained. Magnitude of the transducer output, under equivalent operating conditions, was approximately four times the value obtained from the bistable element oscillator and piezo-electric crystal transducer combination used in previous work. The photograph of transducer output wave-form in Figure 2-10 shows the unfiltered output to be sinusoidal with practically no distortion. This was an improvement over the previous system and eliminated the need for filter circuits in the transducer amplifiers.

The final oscillator configuration is shown in Figure 2-11. Each oscillator is comprised of three of these elements alternately stacked. It should be noted that the two oscillator laminae shown in Figure 2-11 contain chambers of different sizes. Original development work used oscillators with similar sized chambers, which is normal in fluidic systems. However, when an oscillator is designed for the high frequencies used in the hydrogen sensor, any minute differences in the laminae used to build up an oscillator can cause instabilities. These instabilities were observed when a group of oscillators were being built up. Oscillators using laminae with similar chamber sizes develop a relatively high Q circuit and any

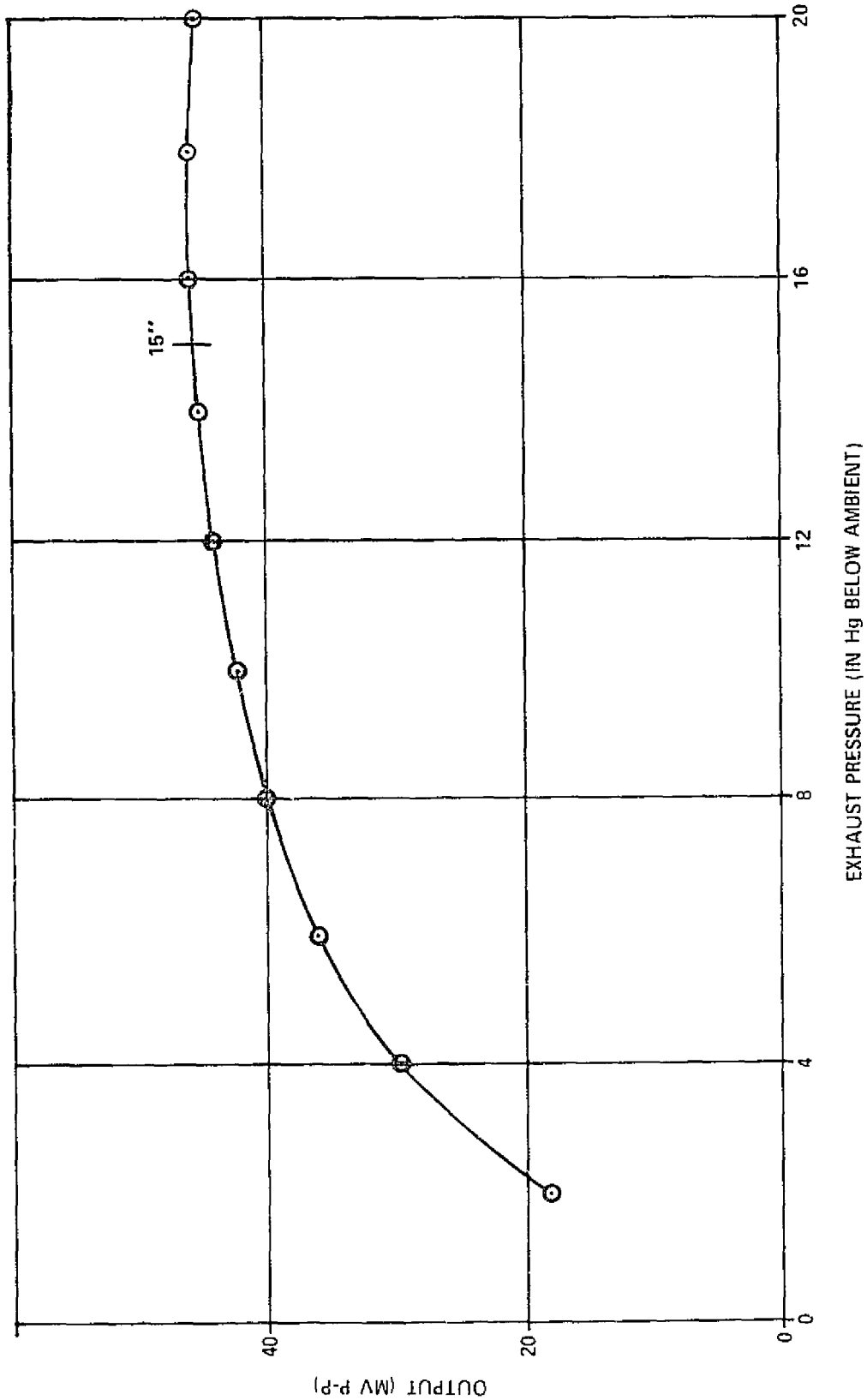

FIGURE 2-9 TRANSDUCER OUTPUT CHARACTERISTIC

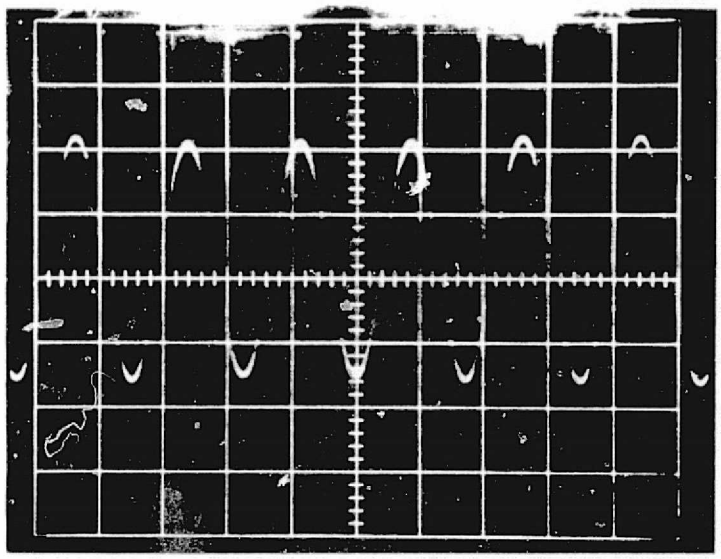

SCALES: VERTICAL 5MV/CM
HORIZONTAL 50μ SEC/CM

FIGURE 2-10 TRANSDUCER OUTPUT WAVEFORM

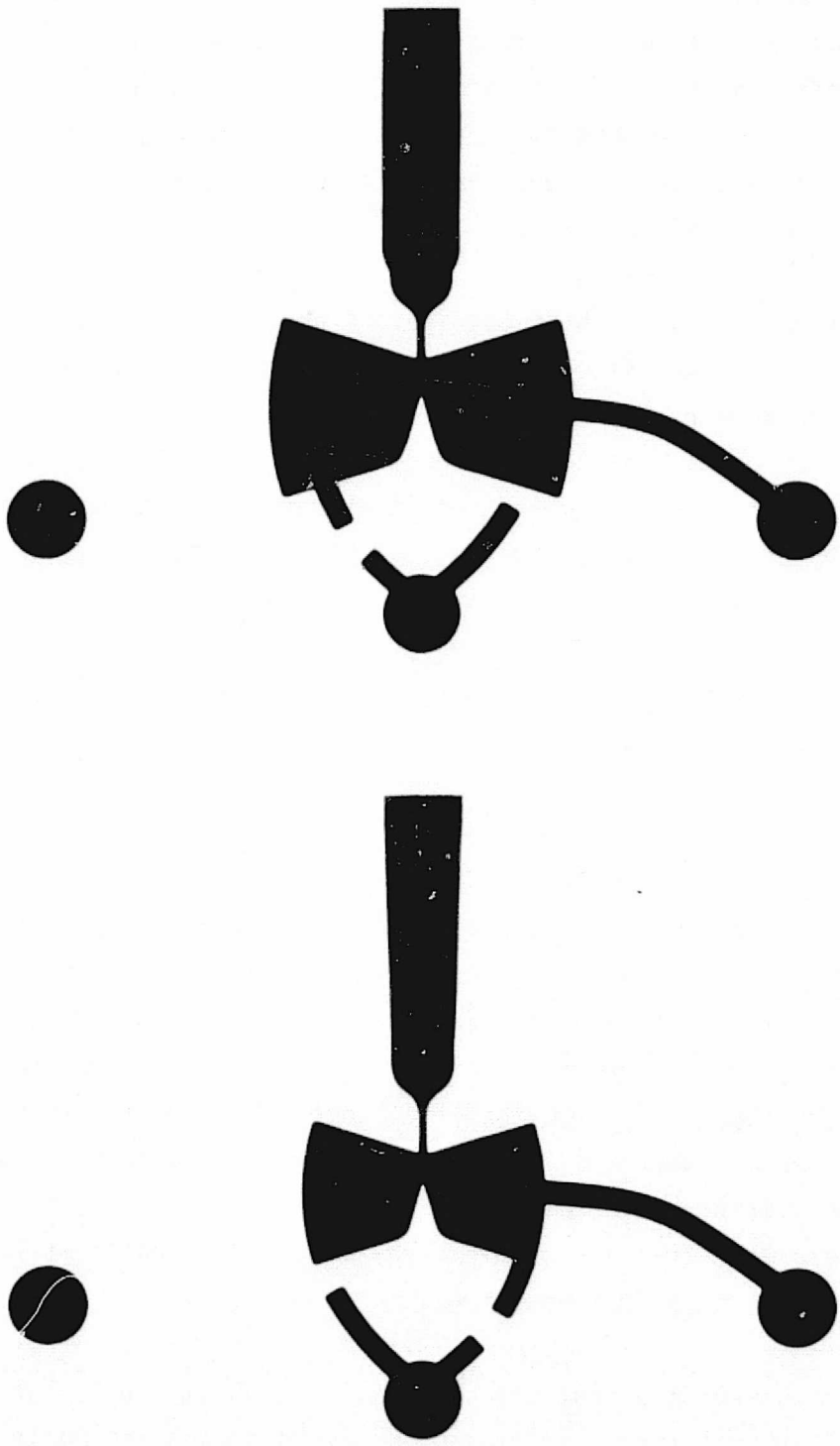

FIGURE 2-11 EDGE TONE OSCILLATOR FINAL CONFIGURATIONS

departure from the oscillator's design frequency causes an abrupt change in output amplitude and/or frequency which is seen as instability. To correct this problem, an oscillator was designed which incorporated two chamber sizes. This, in effect, detuned the chamber, or reduced the circuit Q. This method produces a stable oscillator at the sacrifice of a small amount of gain or output signal amplitude. An analogy of this detuning is common in the high gain I.F. amplifiers used in radio and television receivers.

A problem was discovered with these oscillators when placed in the manifold blocks to make a sensor. When the five environmental test units were built up and tested with various hydrogen-air mixtures, two of the sensors worked properly and three did not. The three units that malfunctioned worked correctly on 2% hydrogen in air, but usually would not function on 0.5% or 1% mixtures. It appeared the catalyst was not operating efficiently on the low hydrogen concentrations, as the frequency of both oscillators was increasing, but they were remaining balanced. In this situation there was no difference frequency and the processor electronics output remained at zero. At the 2% level, however, a difference frequency was produced and the correct output was observed.

These observations led to the conclusion that the catalyst was marginal. In order to further verify this theory, one of the inoperative sensors was packed with a catalyst that was known to be functional, and retested in the oven. This time, the sensor worked properly, which seemed to substantiate the inactive catalyst theory. New catalyst was ordered and installed in one of the sensors. This unit was tested in the oven and proper operation was obtained. The other four sensors were packed and tested in the same manner. Functional problems were again observed with two of the sensors not removing the hydrogen at low concentration levels. These sensors were packed with catalyst that had worked properly in the other sensors. However, this time the problem remained, as the units still did not function at hydrogen concentrations of 0.5%.

At this point, it seemed apparent the catalyst was not at fault, but that there was a basic problem with the oscillators. Analysis showed the units that worked well were not matched in frequency, while the ones that malfunctioned were either initially balanced or passed through the balanced condition at low hydrogen concentrations. The oscillators appeared to "lock on" each other when their natural

frequencies were near each other, which resulted in no system output. Low hydrogen concentrations would not cause a large enough difference frequency to break the oscillators apart, which resulted in erroneous outputs. The oscillators were apparently being acoustically coupled through the thin plate that separates the two circuits. This plate was made thin to promote heat transfer between the two circuits in an effort to minimize thermal effects caused by the hydrogen-oxygen reaction. The circuit was modified so that the thin separator was retained between the secondary heat exchanger passages, while an additional 20 mils separation was added in the area directly between the two oscillators. This change eliminated the acoustic coupling problem while retaining adequate heat transfer capability to minimize thermal drift. The additional 20 mils thickness was the two No. 4 laminae discussed in Paragraph 2.6.

2.2 CATALYTIC CONVERTER

Initial development efforts indicated a catalytic reactor, made from a combination of metal ribbon based and ceramic pellet based materials, should be used. This combination was selected for a number of reasons. First, a reactor made only from the metallic ribbon based catalyst had to operate at about 290°F to be 100% efficient. Since the transducers used in early units were rated at a maximum temperature of 265°F, this reactor could not be used. A reactor made entirely from the ceramic pellet based catalyst was 100% efficient at temperatures as low as 225°F, but caused the output voltage to overshoot and undershoot when step changes were made in the sample gas composition. Therefore, a reactor made from this catalyst was not suitable until a reason for the transient response problems could be identified and corrected. It was assumed the response problem was caused by the hygroscopic nature of the catalyst carrier material and could not be easily resolved. However, a catalystic reactor using a mixture of the two materials could be used, since it was 100% efficient at 240°F; and with a minimum amount of the ceramic pellet based catalyst, the transient response problem was reduced to an acceptable level. This design was used in the engineering prototype model.

In the interest of simplicity, and to eliminate the transient response problem, it was decided to investigate further a reactor made entirely from the metallic ribbon catalyst material for the production prototype sensors. This was possible because the new reluctance transducer design would allow operating temperatures in

excess of 300°F, so the sensor could be operated where the reactor was 100% efficient. However, the manufacturer quoted a price of $118 for the five grams of catalyst material required to pack each reactor tube. This quote of approximately $10,758 per pound was unrealistic, and about two orders of magnitude higher than an equivalent amount of ceramic pellet based catalyst. This dictated that a new catalyst source was required, or a reasonable quotation had to be obtained. Both avenues were investigated.

A platinum plated expanded metal screen used as a catalyst for other processes was investigated. Two screens were obtained for testing, one Tantalum base and the other Columbium base. Since the catalyst carrier was metal similar to the ribbon catalyst, a transient response problem was not anticipated. A reactor tube was fabricated and efficiency tests conducted on these catalysts. Neither platinum plated metal screens would initiate a catalytic reaction at any useful temperature.

Two new types of ceramic pellet catalysts functioned very well as far as removing the hydrogen was concerned. However, these catalysts had essentially the same carrier material as the ceramic pellet catalyst evaluated previously and transient response was again a problem.

Transient response problems with the pellet catalyst had previously been attributed to the fact that the porous ceramic carrier material was hygroscopic, and absorption of steam generated during the reaction was causing the problem. Analysis indicated that improper simulation of the active reactor time delay in the inactive reactor could also cause the same indication in readout voltage. To evaluate this possibility, additional testing was indicated. Untreated pellets, pellets without catalysts, were obtained and a test model of the sensor fabricated. The inactive reactor was filled with untreated pellets, and the active reactor filled with catalyst treated pellets. This sensor was tested with hydrogen-air mixtures and the transient response problem still remained. Two additional types of catalysts, using a ceramic pellet as the carrier material, were also tested. In all cases, the response was the same. Next, the active ceramic based catalyst material was replaced by the metal ribbon based catalyst material, while the untreated ceramic pellets were retained in the inactive reactor. The transient response problem now disappeared when step changes were made in the hydrogen concentration levels.

Since the system was no longer responsive to water generated in the hydrogen-oxygen reaction, this indicated that the ribbon based active reactor was not humidity sensitive. However, when this configuration was alternately supplied with dry and humid air, transient response problems were again observed with the humid air. This indicated that the inactive reactor was affecting the output signal response. Next, the untreated ceramic pellets were removed from the inactive reactor, and the reactor packed with stainless steel wool material to simulate the physical characteristics of the metal based catalyst. In this configuration, transient reponse problems were eliminated under all conditions. From these tests, it was concluded that the hygroscopic nature of the ceramic pellets caused the transient response problem, and that it could not be corrected by physical simulation in the inactive reactor loop.

The need to avoid this response problem, coupled with a somewhat more realistic price quote of $1200 per pound or $13.21 per sensor for the metal ribbon based catalyst, dictated the use of the platinum and palladium coated ribbon catalyst exclusively.

2.3 RELUCTANCE TRANSDUCER

Initial development efforts used a reliable and accurate pair of piezoelectric crystal transducers. This insured that transducer problems would not jeopardize system operation during demonstration tests of the fluidic sensor. These transducers were, however, expensive and limited to a maximum operating temperature of 265°F. A breadboard model of a potentially inexpensive variable reluctance magnetic transducer was fabricated and tested under Internal Research and Development (IRAD) funds. Test results were encouraging, and indicated such a transducer could withstand the temperature requirements, had a relatively high output signal with low distortion, and could easily be employed in a hydrogen sensor.

This low cost variable reluctance pressure transducer was then adapted for use with the hydrogen sensor. The transducer consists of an Alinco ring magnet, a metal core coil, and a diaphragm that is driven by the oscillator. The diaphragm, made from type 910 stainless steel, is part of the etched laminae stack. The magnet and coil assembly are mounted in a hole in the top manifold block (reference Figure 2-1). This design is particularly well suited for this application since

it does not require a power source, has no electronic circuitry other than a simple coil and can be economically produced in quantity. Examples of signal fidelity and amplitude are shown in Figure 2-10.

A cutaway view of the transducer is given in Figure 2-12. Operation of the fluidic oscillators causes variations in their respective chamber pressures which flex the diaphragm laminant. Since this laminant is made of a magnetic material, these flexures change the air gap between the diaphragm and pole piece, which in turn varies the reluctance of this magnetic path. These reluctance changes create a fluctuating magnetic field surrounding the coil and induce a voltage into the coil. The frequency of this voltage is identical to the fluidic oscillator frequency. This analog is then used in the processor electronics described in Paragraph 3.1.

2.4 HEAT EXCHANGERS

Two heat exchangers are employed in the hydrogen sensor; i.e., a primary exchanger to condition incoming sample gas and the secondary exchanger to insure thermal stability between the two fluidic oscillators.

The primary heat exchanger is located directly atop the lower manifold which in turn is atop the heater. This arrangement provides maximum conditioning to the incoming gas flow before it is divided and routed to the active and inactive catalyst, as shown in Figure 2-2. As the sample gas passes through the active catalyst chamber, the gas temperature will rise if hydrogen is present due to the exothermic nature of the reaction. When this happens, the reference oscillator frequency will increase due to this temperature rise. To minimize this effect, a secondary heat exchanger is utilized. This exchanger is comprised of two adjacent channels, one for each oscillator input flow, separated by a 0.010 inch thick laminant. This allows any heat picked up by the one gas during the catalytic reaction to be transmitted to the other. This assures that both oscillators receive gas at an equivalent temperature and no difference frequency is generated due to thermal differences.

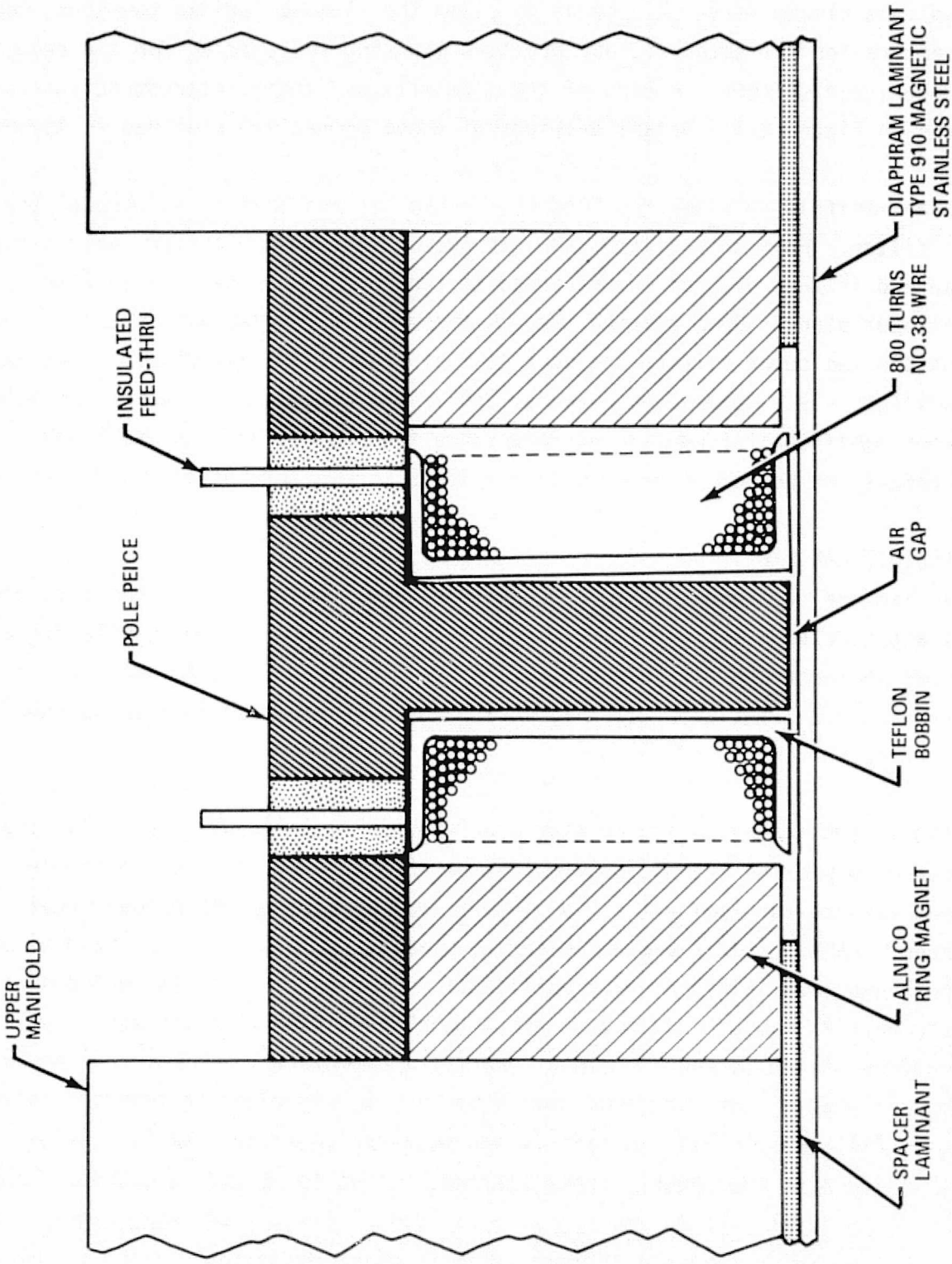

FIGURE 2-12 RELUCTANCE TRANSDUCER

2.5 MANIFOLD BLOCKS

The manifold blocks serve as a means to clamp the fluidic laminae together, contains the chambers for the catalyst, and provides mounting receptacles for the reluctance transducers and filters. A view of these details and their interconnecting passages is given in Figure 2-1. Detail drawings of these blocks are provided in Appendix B.

The lower manifold receives the incoming sample gas and filters it through the center filter. From this filter, the gas passes through the primary heat exchanger laminae and is then divided and returned to the active and inactive catalyst chamber in the lower block. Upon passing through these chambers, the gasses are filtered through the two outer filters and sent to their respective fluidic oscillators. The oscillators are powered by a vacuum applied to a port in the upper manifold. The upper manifold also contains a reluctance transducer for each oscillator. These blocks are bolted together with six 10-32 screws torqued to 7 ± 0.5 ft./lbs.

2.6 FLUIDIC LAMINAE

Fluidic laminae are used in the hydrogen sensor to provide heat exchangers, oscillators and a driving element for the reluctance transducer. The oscillators are described in Paragraph 2.1, the heat exchangers in Paragraph 2.4, and the transducer in Paragraph 2.3. The physical relationship of each of these laminae is shown in Figure 2-13, and described below.

Starting in the center left hand side of Figure 2-13, laminant 1 is a blanking plane used to provide the necessary passages to the lower block and a smooth mounting surface for laminant 2. Six No. 2 laminae make up the primary heat exchanger. Laminant 3 is another blanking plane. Laminant 4 is utilized on both the upper and lower sides of each oscillator to increase the cross sectional area of their heat exchangers and reduce cross coupling between oscillators. Three alternations of the 5_o and 7 laminae comprise a reference oscillator. A No. 4 laminant is used as described and then a No. 6 blanking plane is inserted between the two oscillators. This laminant is the heat exchanger for the two channels of the secondary heat exchanger. Three alternations of the 5 and 7_o laminae flanked by a No. 4 laminant make up the signal oscillator. A No. 8 blanking plane is next. The No. 9 laminant provides a chamber which is continually charged and discharged

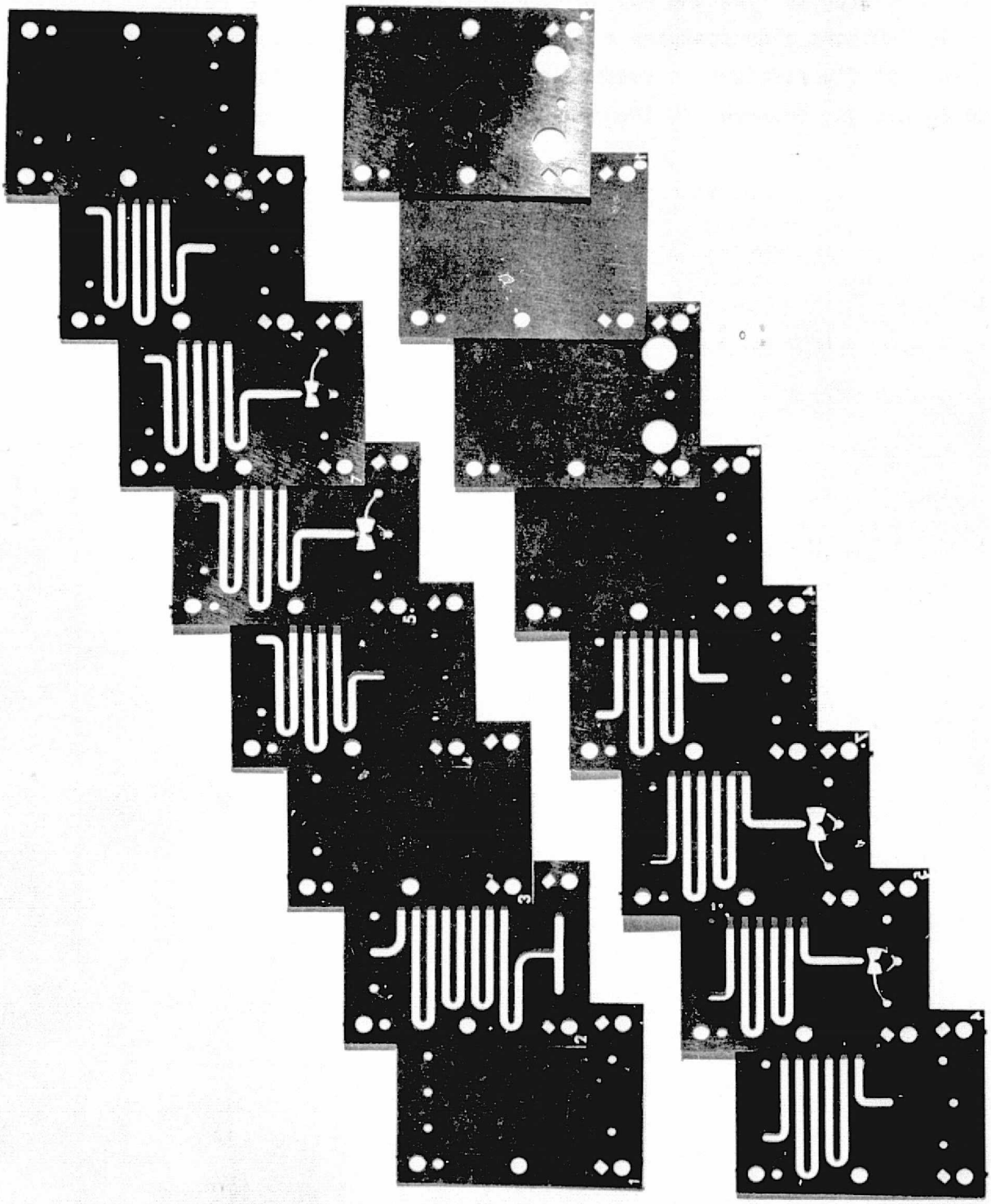

FIGURE 2-13 FLUIDIC LAMINAE STACKING ORDER

by each oscillator to flex the No. 10 laminant which drives the reluctance transducer. The No. 10 laminant also contains a 0.0225 inch diameter orifice provided to minimize the effects of fluctuations in vacuum level. Another No. 9 laminant is used to provide an air gap between the transducer and the No. 10 laminant.

SECTION 3
DETECTOR ELECTRONICS

Hydrogen detector electronics accepts signals from the reluctance transducers, within the fluidic sensor, and processes them to provide an output signal which is proportional to the frequency difference between the two signals. The electronics also provides thermal control of the fluidic sensor and generates a signal reflective of system operating status. In this section, a digital processor is described which gives an output signal proportional to hydrogen concentrations in the sampled air. Temperature control of the fluidics block by a heater circuit which senses block temperature to control heater power is explained. A self test circuit is discussed which monitors critical system parameters and generates a bilevel signal representative of system condition to assure output signal integrity. A thermal control assembly is described which contains three thermally activated system components. Figure 1-1 shows the relationship between these four functions and the fluidic sensor.

The detector design utilizes state-of-the-art circuits described here at a functional block diagram level. Detailed circuit analysis can be obtained from the component manufacturers' data books. Schematics of the three printed circuit boards and the package are given in Appendix C. Electronic requirements are listed in Table 3-1.

3.1 PROCESSOR ELECTRONICS

Initially, the processor electronics design used a phase lock loop to amplify input signals and the initial output signal requirements were for a nine bit digital word whose value indicated the hydrogen level present. The reference and signal frequencies were amplified and filtered in buffer amplifier-filter stages. These outputs were routed to two identical phase locked loop (PLL) circuits

TABLE 3-1

ELECTRONIC REQUIREMENTS

Function	Specification
Input Signal	
Voltage	10 mv p/p minimum
Frequency	Between 15 kHz and 17 kHz
Scale Factor	Difference frequency between 40 and 50 Hz per percent hydrogen
Power	
Voltage	28 ± 2 Vdc
Current	1.7 amps including heater power
Output Signal	
Voltage	0-5 Vdc
Scale Factor	1 Vdc per percent hydrogen
Linearity	±20 mv of nominal
Sampling Time	Less than 2.5 seconds
Self Test Signal	
Operational	$12\ ^{+0.5}_{-1.0}$ Vdc
Failed	0 ± 1.0 Vdc
Heater Control	
Temperature	245 ± 1°F

which incorporated divide-by-four counters in their feedback loops such that their output frequency, F_0, was four times the input frequency. The digital processor of the initial design used the same basic processor as the present design. The output stage, however, incorporated a buffer storage register and line drives to provide a nine bit, parallel output, digital word. Changes in system output requirements and problems encountered with the PLL dictated changes that evolved to the present design.

Fundamental to proper operation of the digital processor is control of a timing gate. Proper control of gate opening permits enough pulses to reach the digital to analog (D/A) convertor to achieve the desired output voltage. The D/A output scale factor is one volt per 50 input pulses; therefore, with a system requirement of one volt per % H_2, 50 pulses/% H_2 must enter the D/A. A simplified block diagram of the processor (Figure 3-1) shows difference frequency (Δf) pulses are gated to the D/A. These Δf pulses are generated in a difference circuit which is fed by two comparators. Low level signals from both transducers are applied to the comparators whose high gain causes their output to switch between full on and off. These square wave signals thus generated are applied to the difference circuit whose output frequency is equal to the difference between the two input frequencies. For an initial explanation it is assumed, with no H_2 present, the two oscillators operate at the same frequency of 16 kHz, and that the signal oscillator frequency increases 50 Hz per % H_2. Under these assumptions, with no hydrogen, the Δf will be zero and operation of the gate is irrelevant, since open or closed, the D/A input and thus output will be zero.

With hydrogen present, assume 1%, the signal frequency now becomes 16,050 Hz and Δf becomes 50 Hz. Now, control of the gate time is very important. The gate is opened when the input from the divide by M (:M) circuit is high. This :M circuit is a switch selectable divide circuit whose input is from the reference comparator. For the assumptions made, M must equal 32,000 and the frequency of the gate control

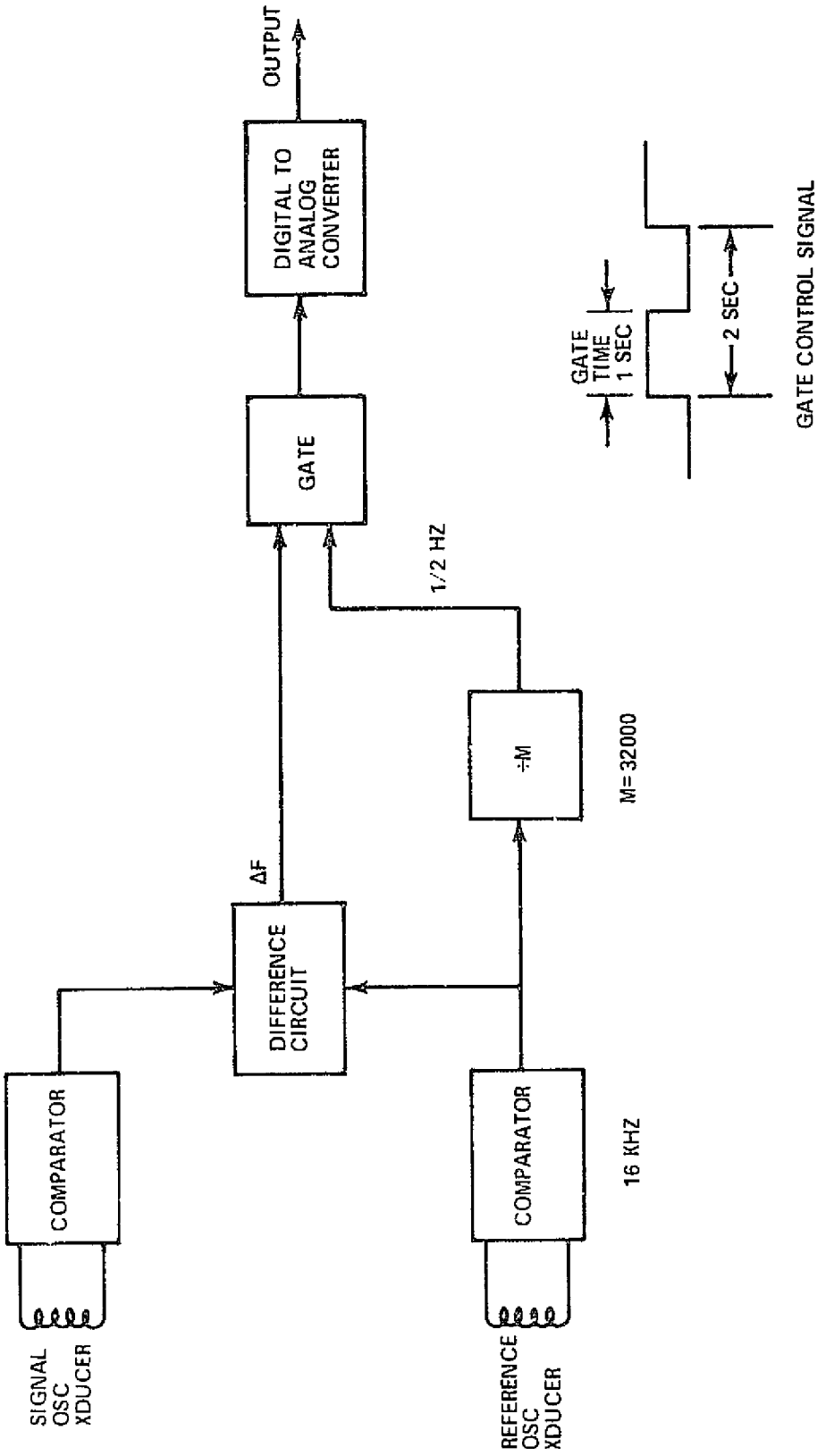

FIGURE 3-1 SIMPLIFIED DIGITAL PROCESSOR

signal will be 0.5 Hz, which gives a period of two seconds. This means the gate is open one second and closed one second. During the one second open period, the gate will allow 50 of the 50 Hz Δf pulses to reach the D/A, causing a one volt output signal to be obtained representing one percent hydrogen.

Above assumptions, made to simplify circuit explanation, are not practical in normal operation. For example, a difference of 50 to 100 Hz is normal between the two oscillators with no hydrogen present; also, the fluidic sensor scale factor is not 50 Hz per % H_2, which conveniently coincided with D/A gain. A detailed block diagram of the processor electronics, given in Figure 3-2, shows the additional functions necessary to make the processor practical. A schmitt trigger is used at the comparator outputs to provide a fast rise time square wave to the difference circuit which is necessary for proper operation. The ÷M circuit is now followed by a divide by 10 (÷10) circuit, which was necessary to achieve a capability of dividing by 100,000 and to provide reset signals. Counter and storage capability is required at the timing gate output to change the data format from serial to parallel since the D/A input requires an eight bit binary word. D type latches are used to provide temporary data storage during that portion of time when the gate is closed. Without this storage, the output signal would drop to zero while the gate is closed. A line driver is added to the D/A output to drive some 1,200 feet of line in actual application. A significant change in this diagram is the addition of up/down counters and zero offset switches. A third input to the timing gate from the up/down counters is used to hold the gate closed for a specified period. During this period, Δf pulses generated at 0% H_2, due to the difference between the signal and reference oscillator frequencies, are blocked from entering the output stages.

As stated earlier, the fluidic sensor scale factor is not equal to the required scale factor at the D/A input. Therefore, gain must be provided by the processor. This is accomplished by control of gate times. From the diagram, it is seen that the Δf pulses into the gate are defined as D, which is the fluidic sensor scale factor; i.e., $D = \Delta f/\%\ H_2$. Also, the D/A input scale factor is shown as N, where N is the binary word required by the D/A to give the necessary output scale factor

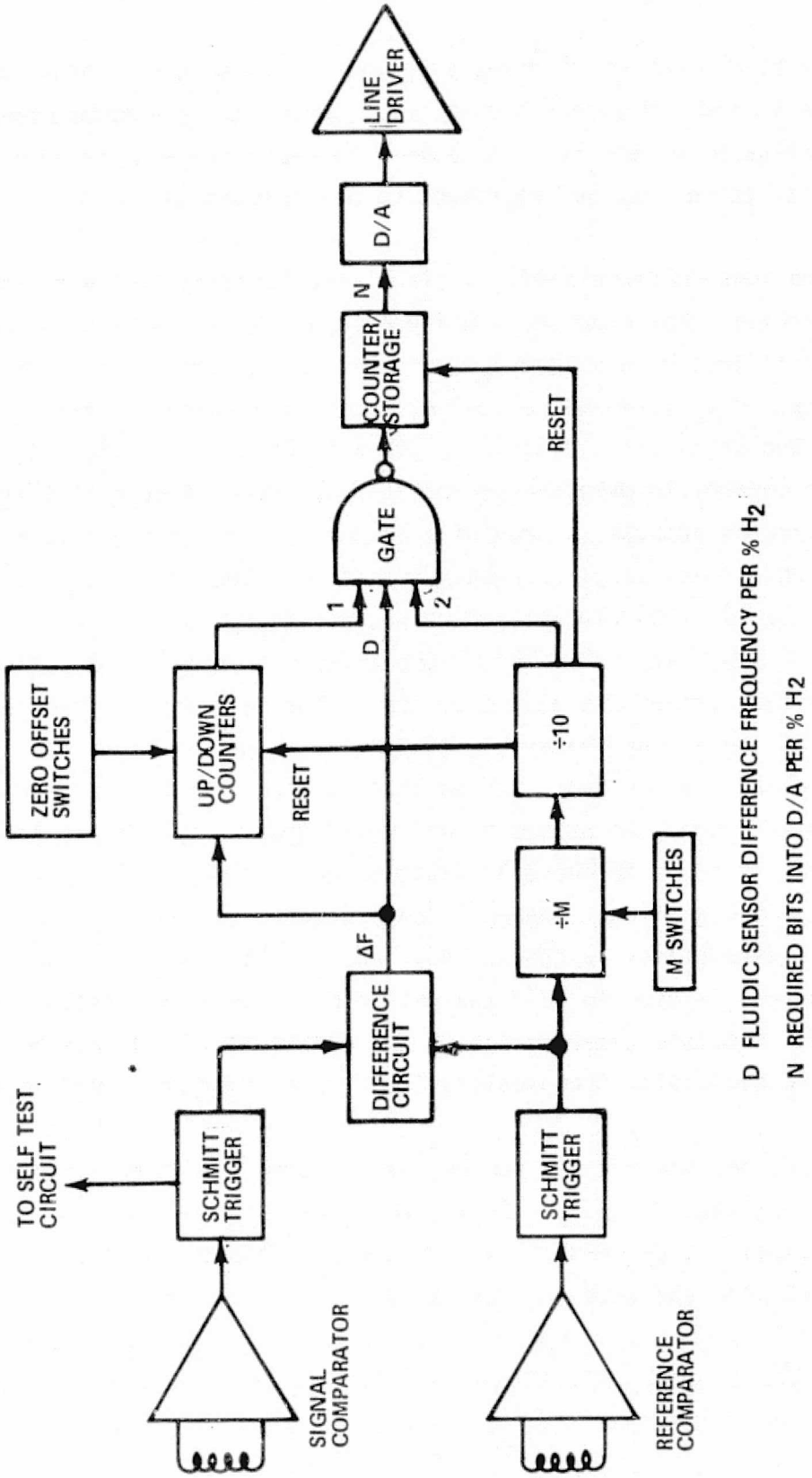

FIGURE 3-2 PROCESSOR ELECTRONICS

of 1 Vdc/% H_2. For the selected D/A, N = 50. Since D is nominally about 45, it can be seen that a gain factor (J) must be incorporated. The derivation of these parameters is discussed in Appendix D.

The zero offset circuit utilizes up/down counters to count Δf pulses which delay the timing gate opening. These counters are connected in the up mode and their output goes high when the counter reaches 255. The counters have jam inputs to allow a preset number to be inserted. Assuming Δf = 60 Hz at 0% H_2, the jam switches would be set to 255 - J60; therefore, the counter output goes high when J60 Δf pulses have been counted. Now, with no H_2 present, the gate will remain closed during the period of the first J times 60 Δf pulses. After these Δf pulses have arrived, the up counters are filled and the output goes high, trying to open the gate. However, as shown in Appendix D, at 0% H_2 this time equals the on time of gate pulse τ_{g2} from the ÷M circuit which now turns off and no Δf pulses are passed to the output stages. When, for example, 1% H_2 is present, the difference between the fluidic oscillators becomes 105 Hz, 60 Hz due to their difference at 0% H_2 and 45 Hz due to the 1% H_2. Since Δf is now 105 Hz, the zero offset circuit will hold the gate closed for a period equal to J times 60 Δf pulses, after which it will open. Since Δf is 105 Hz, where in the 0% H_2 example it was 60 Hz, the elapsed time for these first J 60 pulses is less than before. Now, the gate will open and let a burst of Δf pulses through to the output stages. The gate times are controlled so J times 45 pulses will pass through, or for this example J = 1.1111. Since 1.1111 x 45 = 50, the gate will let 50 Δf pulses into the binary counter, which in turn presents the binary word 50 to the D/A input. With the D/A scale factor (N) of 1 Vdc out for each binary word 50 in, the output becomes 1 Vdc; and the system scale factor of 1 Vdc/1% H_2 is obtained. From this it can be seen that system gain is achieved by applying the factor J to the quantity of Δf pulses which is allowed through the timing gate such that the output circuit receives 50 Δf pulses/1% H_2. This in effect raises the fluidic sensor output scale factor D to equal the D/A input scale factor N, or N = JD.

The value to be inserted into the zero offset switches is:

$$Z = 255 - JX$$

where: Z = the number inserted into the zero offset switches

$J = \frac{N}{D}$ system gain factor

$X = \Delta f$ at 0% H_2

and for this example:

$Z = 255 - JX = 255 - (1.1111)(60)$

$Z = 188$

The value of M can be found from:

$$M = \frac{J f_r}{5}$$

where: M = number inserted into M switches

J = system gain factor

f_r = reference oscillator frequency

and for this example:

$$M = \frac{J f_r}{5} = \frac{(1.1111)(16000)}{5}$$

$M = 3556$

The derivation of these expressions is shown in Appendix D.

During breadboard development of the processor electronics a problem was encountered with the difference circuit. The difference circuit would intermittently generate an erroneous Δf and this error was always an increase in frequency. Logic indicated that noise was present at the inputs, which was causing false triggering of the "D" type latch and generating extra output pulses. This was confirmed by viewing Δf on a scope where the extra, short duration, pulses could be seen. The solution to this problem appeared to be a neat circuit board layout as opposed to the breadboard which had been modified several times and invited noise problems. The design was then committed to a printed circuit (PC) layout to eliminate these problems. After build up of the first set of PC cards, initial testing did not reveal the noise problem and it was thought to be solved. However, further testing with different fluidic sensors caused the problem to return. Since the cause now could be identified with some, but not all, fluidic sensors, the sensors were investigated. After considerable investigation the fluidic oscillator signals were evaluated with a tunable discriminator. The discriminator provided an output voltage which was proportional to input frequency. This output was then recorded

on a strip recorder and is shown in Figure 3-3. These traces show that the instantaneous stability of the fluidic oscillators can vary as much as 30 Hz. In all previous work with these oscillators the output was viewed on a scope for wave shape and the frequency checked with a counter. The counter, however, counted over a one second period and always showed a frequency stability of ± 1 Hz, which was the counter accuracy.

Once this instability was discovered, the difference circuit was modified to incorporate a delay in the latch reset so instantaneous changes of Δf could not retrigger the circuit.

Processor electronics is contained on printed circuit cards 1 and 2 shown in Figures 3-4 and 3-5, respectively. Schematics of these cards are provided in Appendix C.

3.2 HEATER CONTROL CIRCUIT

A thermistor which senses the fluidic hydrogen sensor block temperature is used to control the pulse width of the power applied to the heating element. A block diagram of this control circuit is shown in Figure 3-6. The thermistor is located in one leg of a bridge circuit whose output is sensed by a high gain op amp. Proper operating temperature is selected by adjusting potentiometer R1 until the bridge is balanced when the desired temperature is reached. The op amp is biased such that this balanced condition will provide the Pulse Width Modulator (PWM) with an input voltage that yields an output pulse with a fifty percent duty cycle. The heater is selected, or trimmed with a resistor, to where this fifty percent duty cycle maintains system temperature. Any changes in fluidic block temperature is sensed by the thermistor which upsets the bridge balance. This unbalance is in turn sensed by the op amp, amplified and a new input voltage level is applied to the PWM. This change of input voltage results in a change in output pulse width to correct the block temperature. The oscillator shown in Figure 3-6 provides the base frequency to the PWM circuit for modulation. Power transistor Q1 is used to switch heater current.

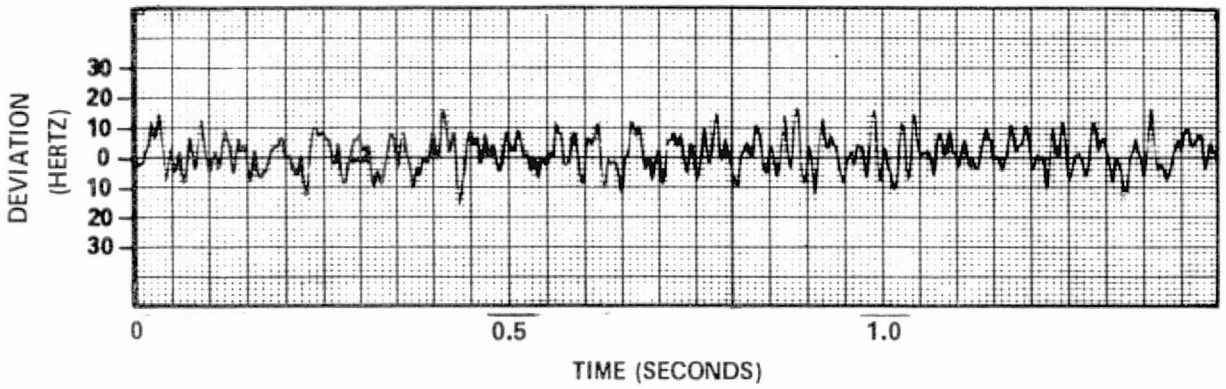

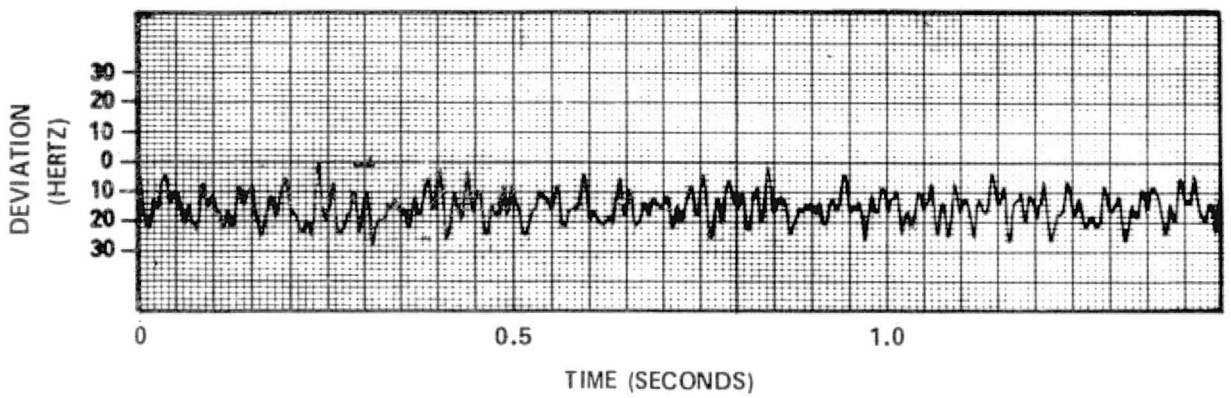

FIGURE 3-3 FLUIDIC OSCILLATOR STABILITY

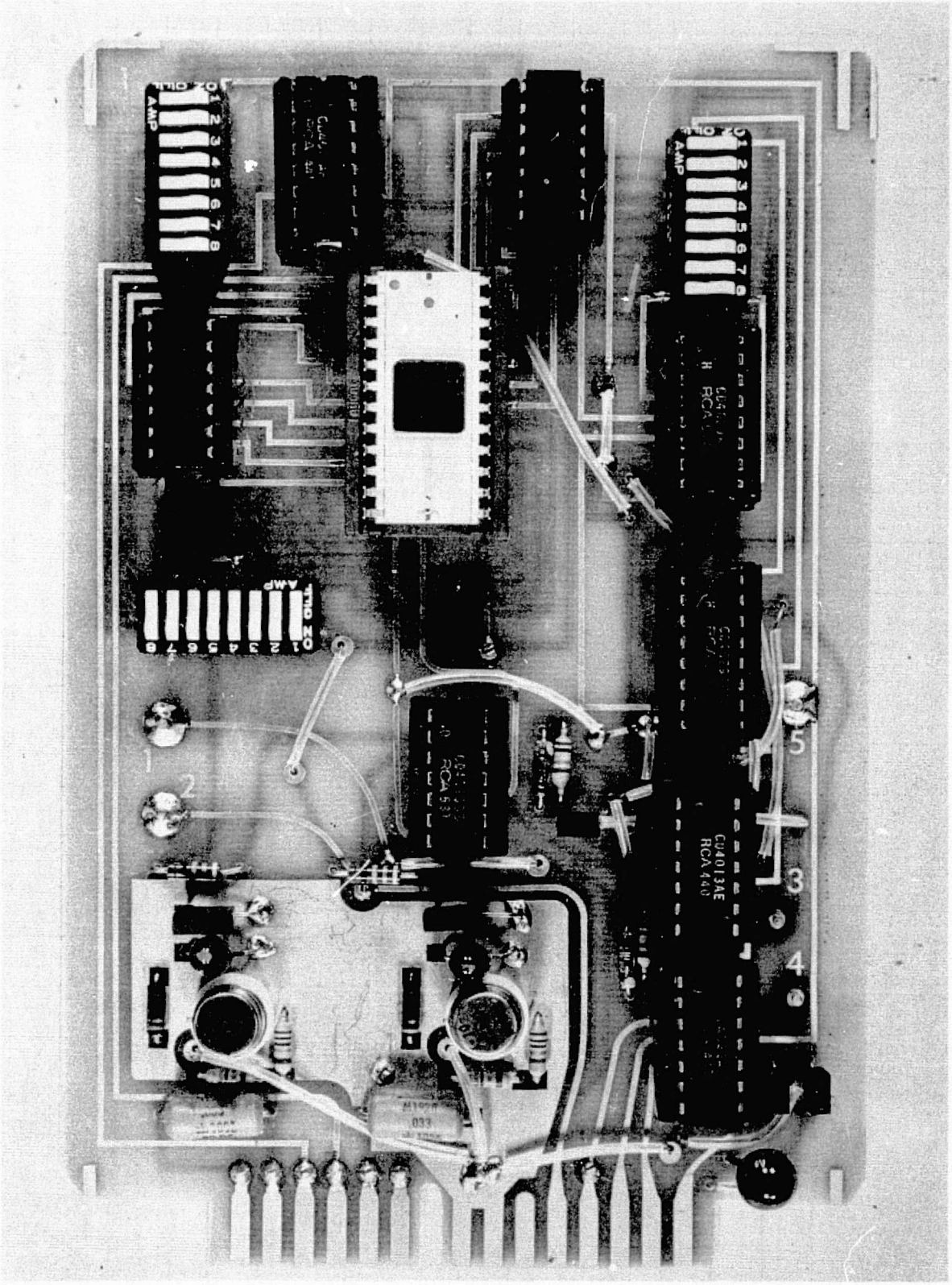

FIGURE 3-4 PRINTED CIRCUIT CARD 1

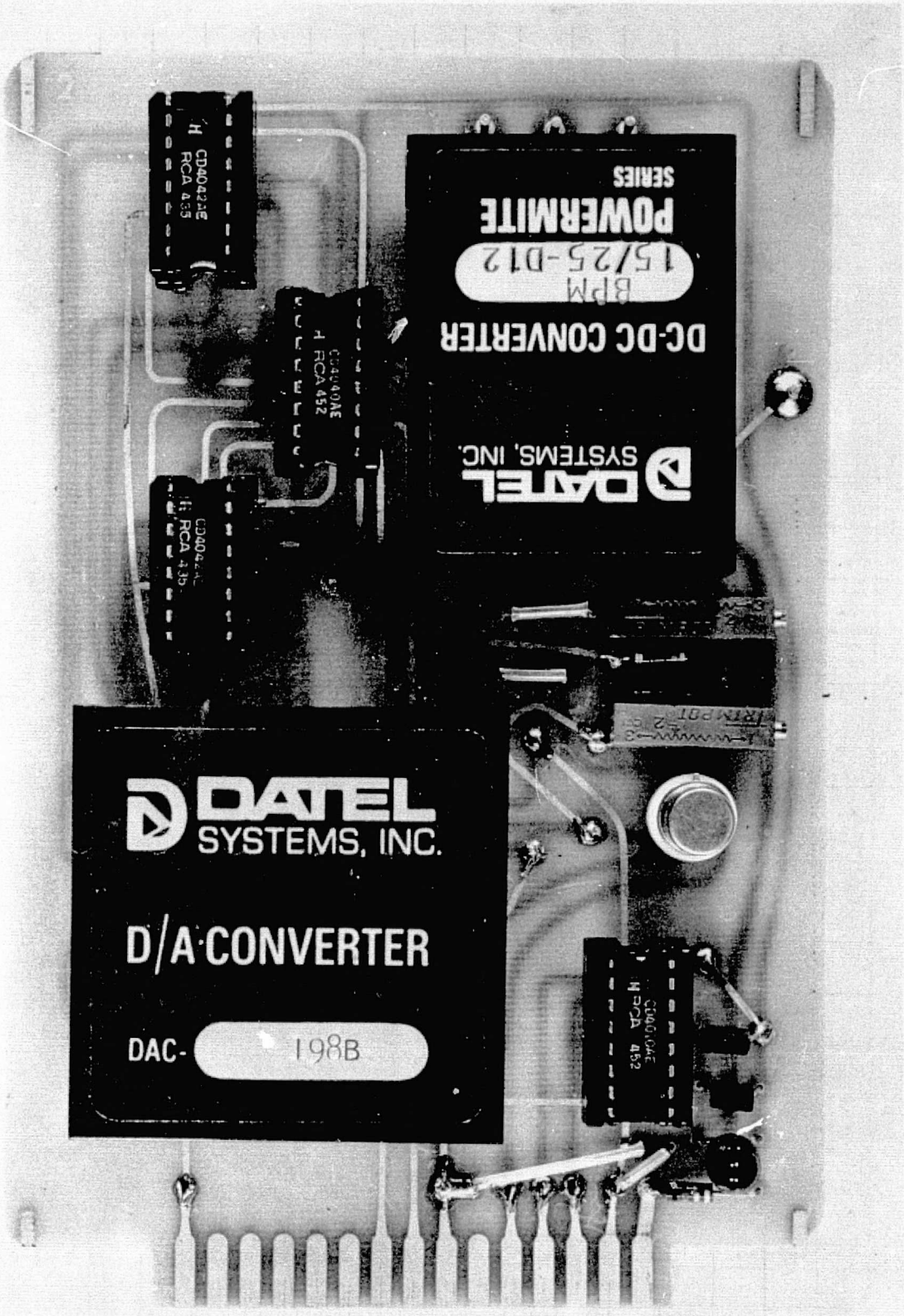

FIGURE 3-5 PRINTED CIRCUIT CARD 2

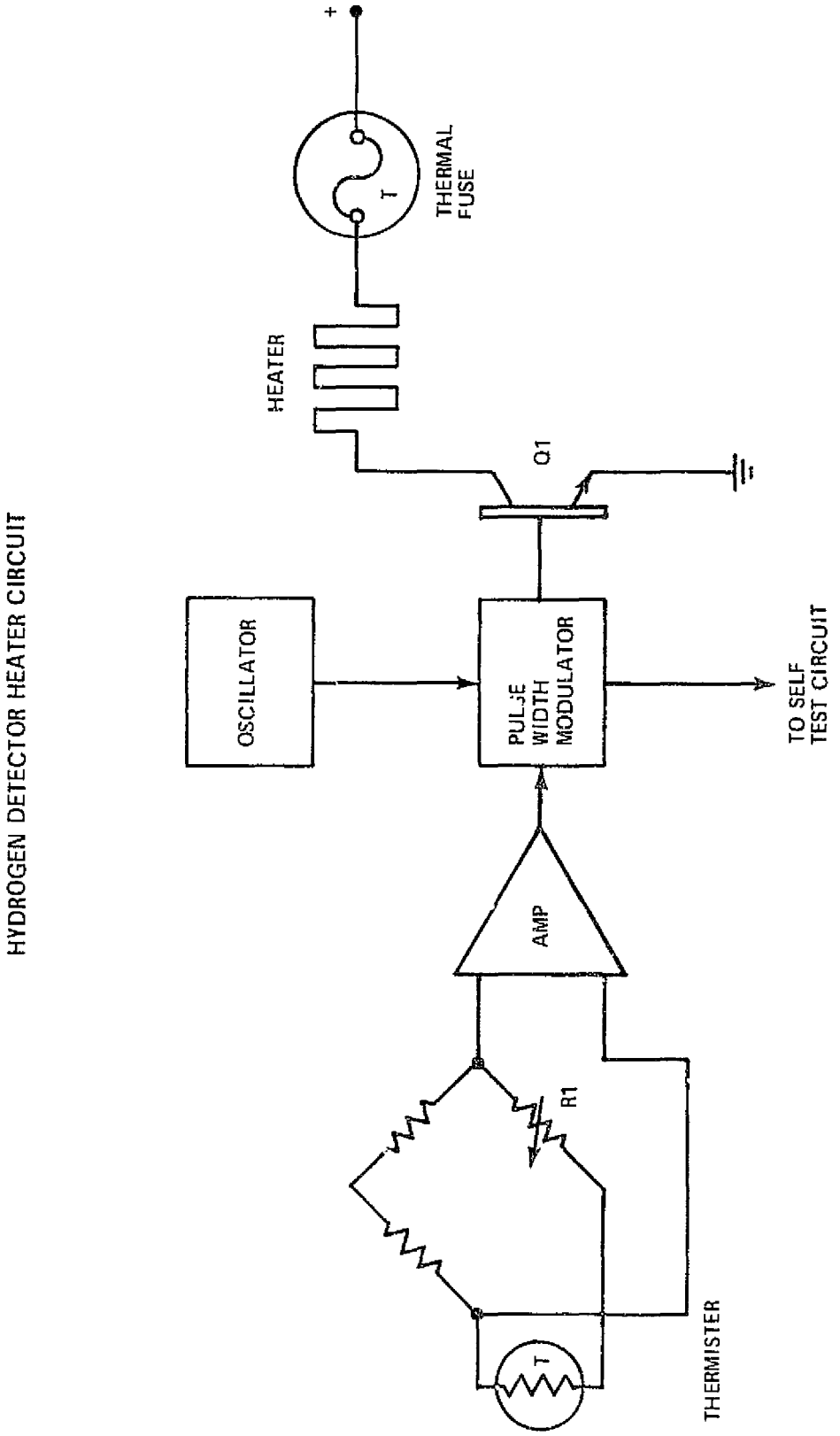

FIGURE 3-6 HEATER CONTROL CIRCUIT

The thermal response of a typical system is shown in Figure 3-7. Although this curve shows that stability is reached in 80 minutes, it is recommended that during normal usage the detectors be allowed a two hour warmup period.

3.3 SELF TEST CIRCUIT

A self test circuit monitors operation of the signal and reference amplifiers and heater oscillator within the detector. Loss of any one of these would cause the resulting output to be questionable. By monitoring the signal and reference amplifier outputs, a failure of reluctance transducers, amplifiers, or the schmitt trigger circuit can be detected. The most critical of these is a loss of reference signal which stops the generation of reset pulses. Should the refer nce signal be lost when the sensor was at null, the most probable condition, and no reset pulses generated, then the sensor output is locked at null. If hydrogen later becomes present, the detector output will not indicate this.

The loss of a heater oscillator will cause the fluidic sensor block temperature to slowly decrease. A decrease in temperature below 212°F places the catalytic converter in an operating range where the generation of steam cannot be assured, making the detector unreliable.

Circuit operation of all three detectors is basically the same. The monostable oscillators shown in Figure 3-8 operate at a slightly lower frequency than the circuit they are monitoring. Output of the monostable oscillator is high until the voltage across the capacitor (C) is sufficient to reset the oscillator. During normal operation the capacitor is continually discharged by transistor (Q) before this reset voltage is reached, since the monitored frequency is higher than the monostable oscillator frequency. Should the monitored signal fail, then the monostable oscillator will reset, causing the output voltage to drop to zero. The output voltage of each self test circuit is applied to the input of a nand gate. When any one of these inputs goes low, the output goes high, indicating a system malfunction.

Both the heater control circuit and the self test circuit are implemented on Card 3, shown in Figure 3-9, with a complete schematic given in Appendix C.

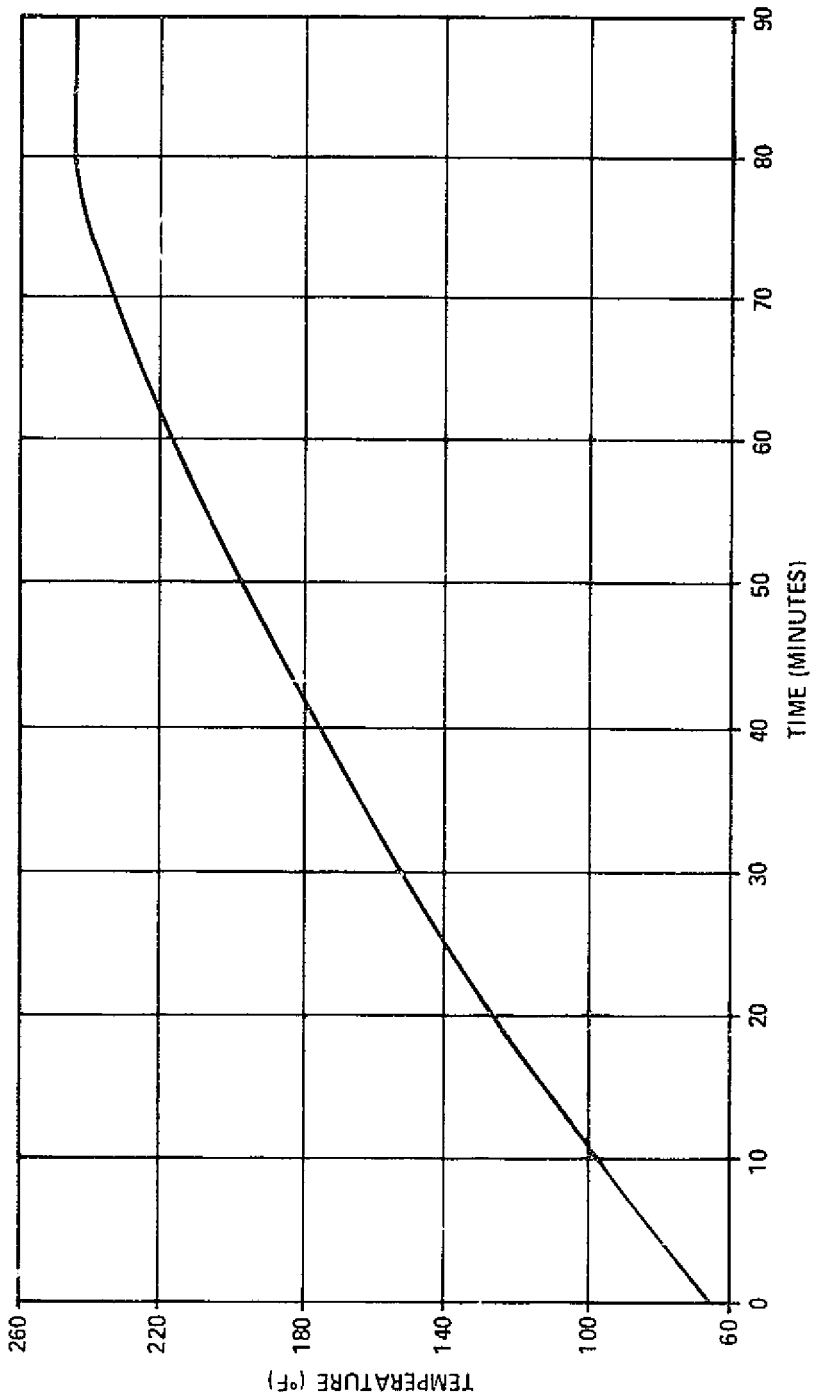

FIGURE 3-7 SENSOR THERMAL RESPONSE

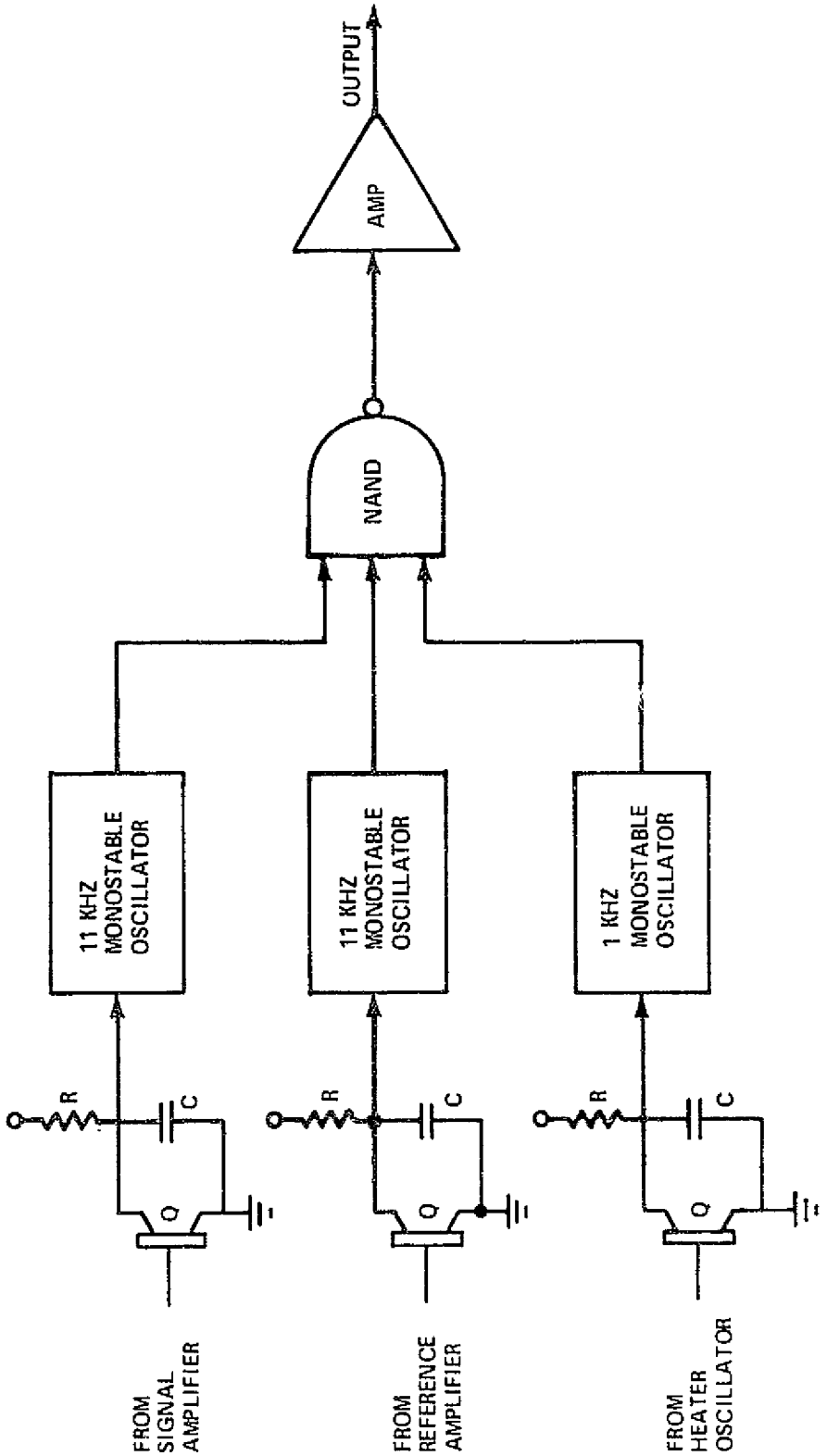

FIGURE 3-8 SELF TEST CIRCUIT

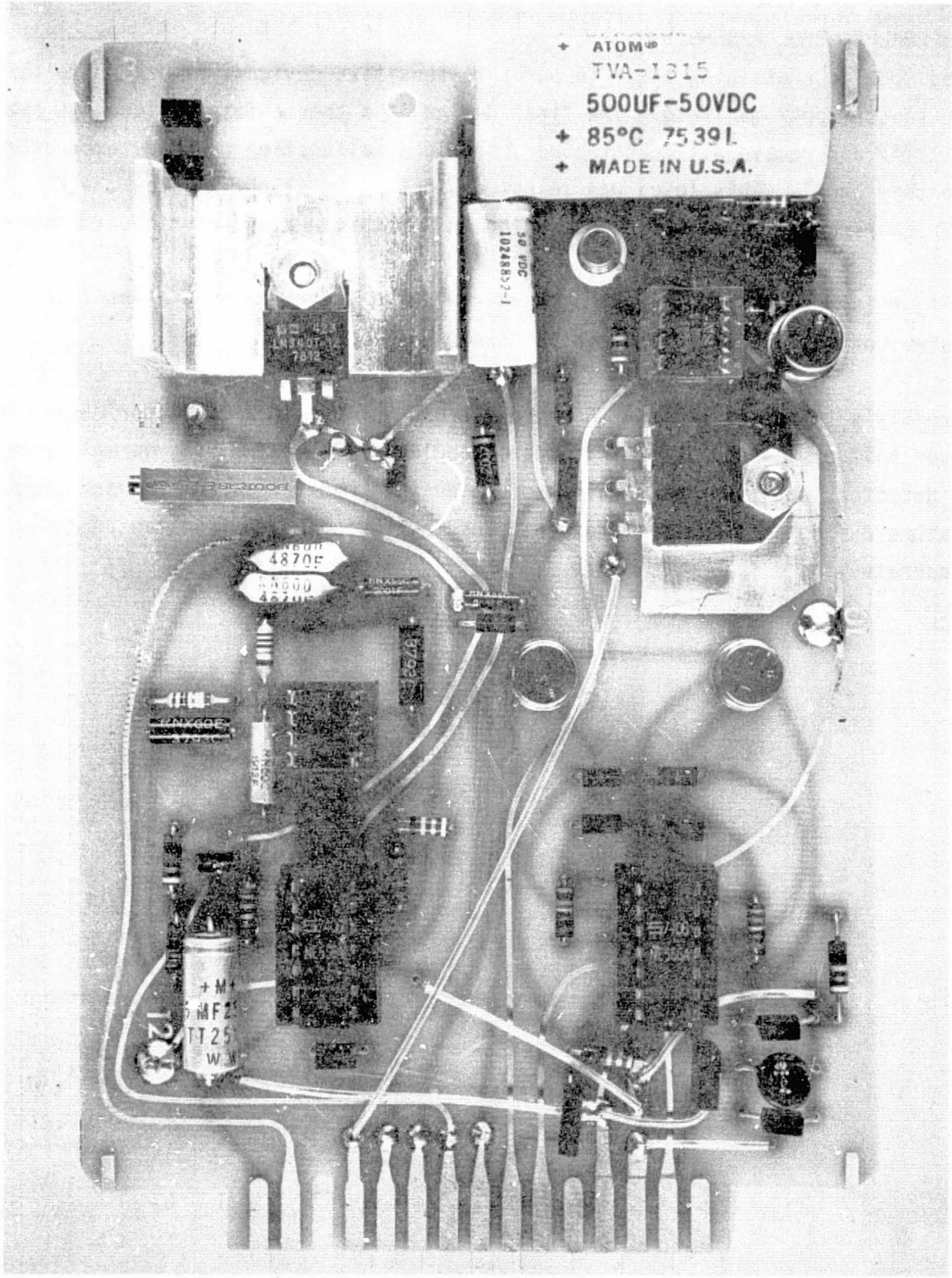

FIGURE 3-7 PRINTED CIRCUIT CARD 3

3.4 THERMAL CONTROL ASSEMBLY

A potted module, containing three temperature sensitive devices, is bonded to the fluidic sensor upper manifold. The first device is a thermo fuse designed to open at 300 ± 2°F and remove all heater power, should a malfunction cause a temperature rise to this level. This level was selected since it is slightly below the KSC safety requirements for equipment operating in a possible hydrogen rich atmosphere.

Secondly, this assembly contains the thermistor used as the control element in the heater control circuit discussed in Paragraph 3.2.

The assembly's third sensor is a thermocouple brought out to a connector J5 within the lower half of the package. This thermocouple is not used during normal operation of the detector, but is provided as a convenience to monitor fluidic sensor block temperature during test and calibration. The couple is an iron-constantan type, which operates the J type pyrometers.

SECTION 4
PACKAGING

The fluidic hydrogen detector packaging concept was selected to meet the basic requirements of: (1) Safety - the system had to be either intrinsically safe or explosion proof; (2) Cost - an inexpensive design was required since a large number are required; and (3) Maintainability - the package must be designed to require minimal and simple maintenance.

4.1 PACKAGE DESCRIPTION

To meet the three requirements, two identical cast aluminum boxes are used as the upper and lower housings. These two boxes are separated by a flat aluminum plate which has two neoprene gaskets bonded to it. The gaskets form a seal between the plate and the upper and lower housings, providing two isolated chambers. Figure 4-1 shows the two housings before the installation of components while Figure 4-2 shows the housings clamped against the center plate and gaskets by four latches. Removal of the upper housing, or cover, as shown in Figure 4-3, allows access to the three printed circuit cards. These cards are installed into slides on each side and an edge connector at the rear. The edge connectors are mounted on a single sided printed circuit card which contains a majority of the package wiring. The center plate and circuit card rack are pictured in Figure 4-4 without the cards installed.

The lower housing contains the fluidic sensor, thermal control assembly, wire harness, and thermocouple connector. A view of the lower housing interior is shown in Figure 4-5. Access into the lower housing is obtained by removing the four screws which mount the center plate to the lower housing. The fluidic hydrogen sensor, shown in Figure 4-6, along with the heater, reluctance transducers, and thermal control assembly, shown in Figure 4-7, are all mounted in a thermally insulated section of the lower housing. Internal temperature of this section is controlled to 245°F. The in/out connector and wire harness shown in Figure 4-7 can be seen installed in Figure 4-5.

The package has a volume of 216 cu. in. and weighs 7.1 pounds.

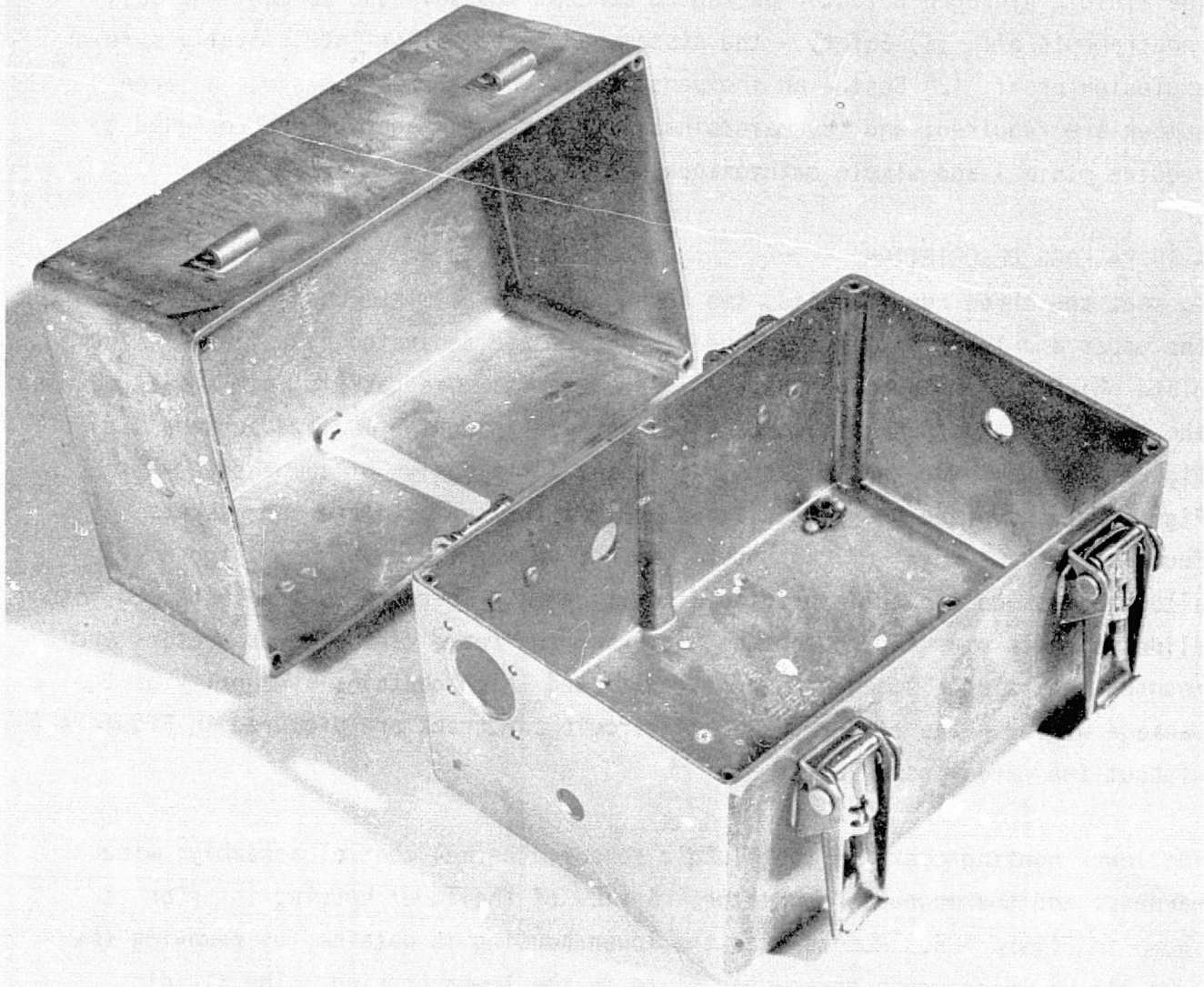

FIGURE 4-1 UPPER AND LOWER HOUSING

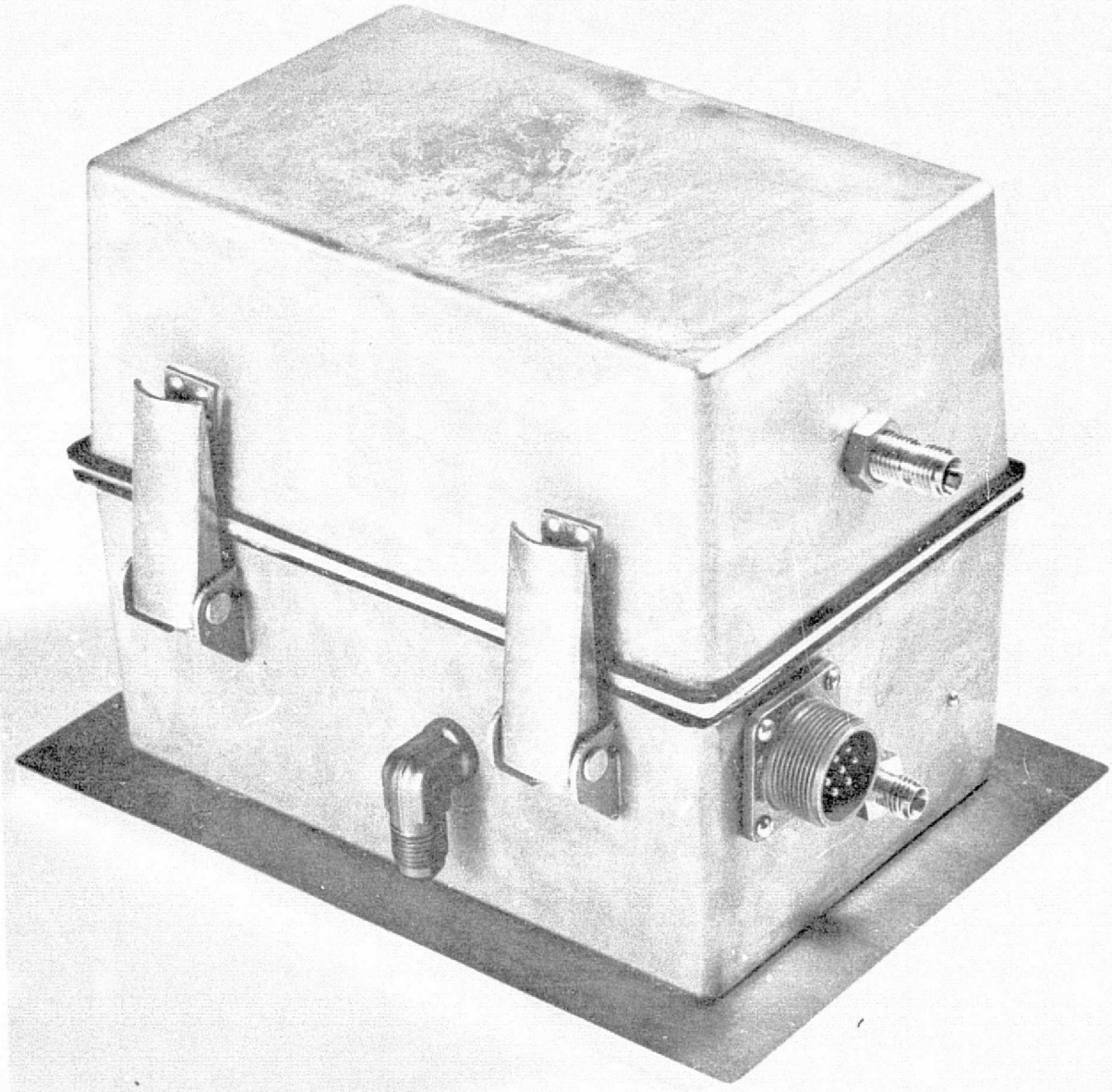

FIGURE 4-2 PACKAGED DETECTOR

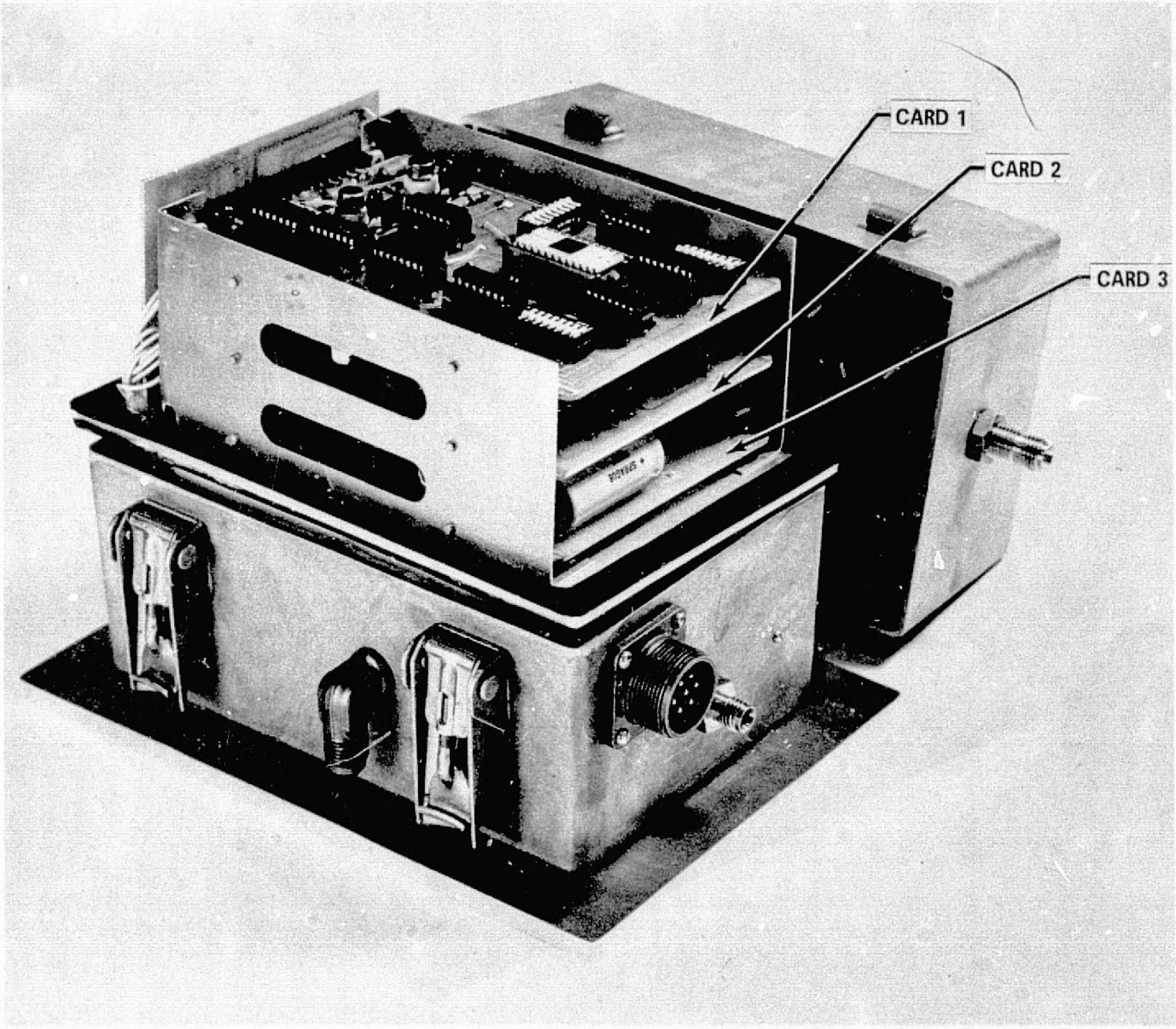

FIGURE 4-3 PACKAGE WITH COVER REMOVED

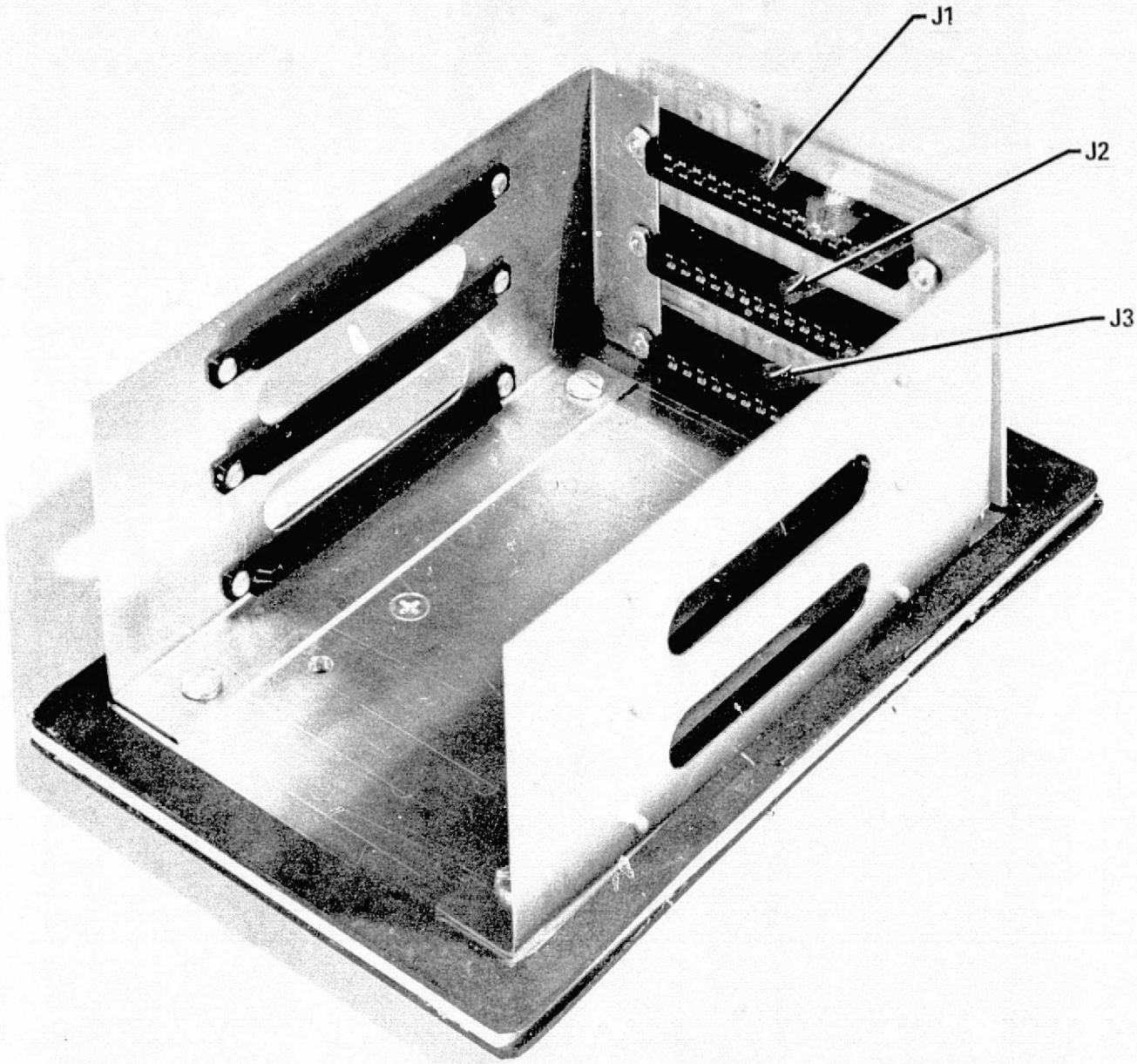

FIGURE 4-4 CIRCUIT CARD RACK

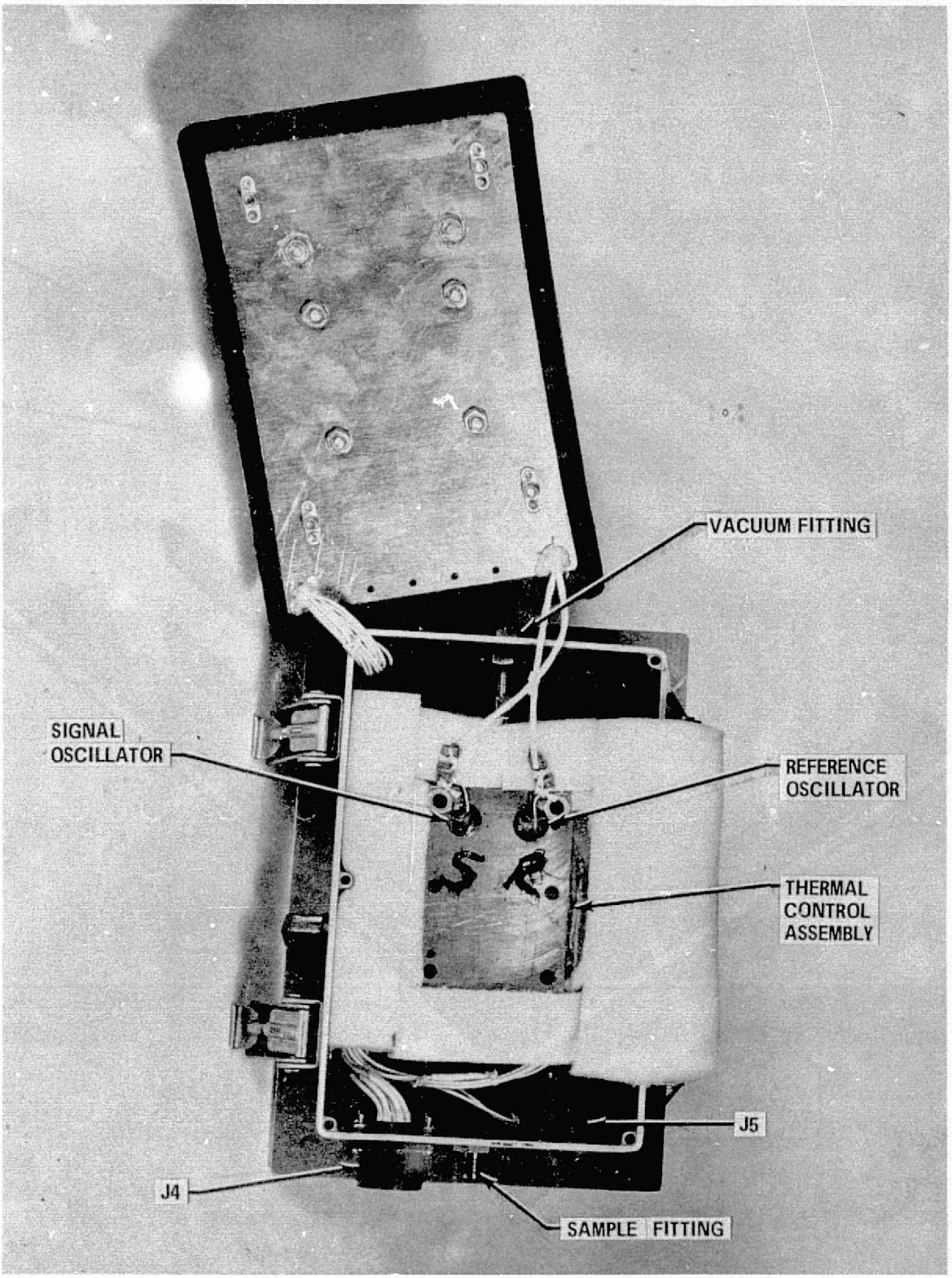

FIGURE 4-5 VIEW INTO LOWER HOUSING

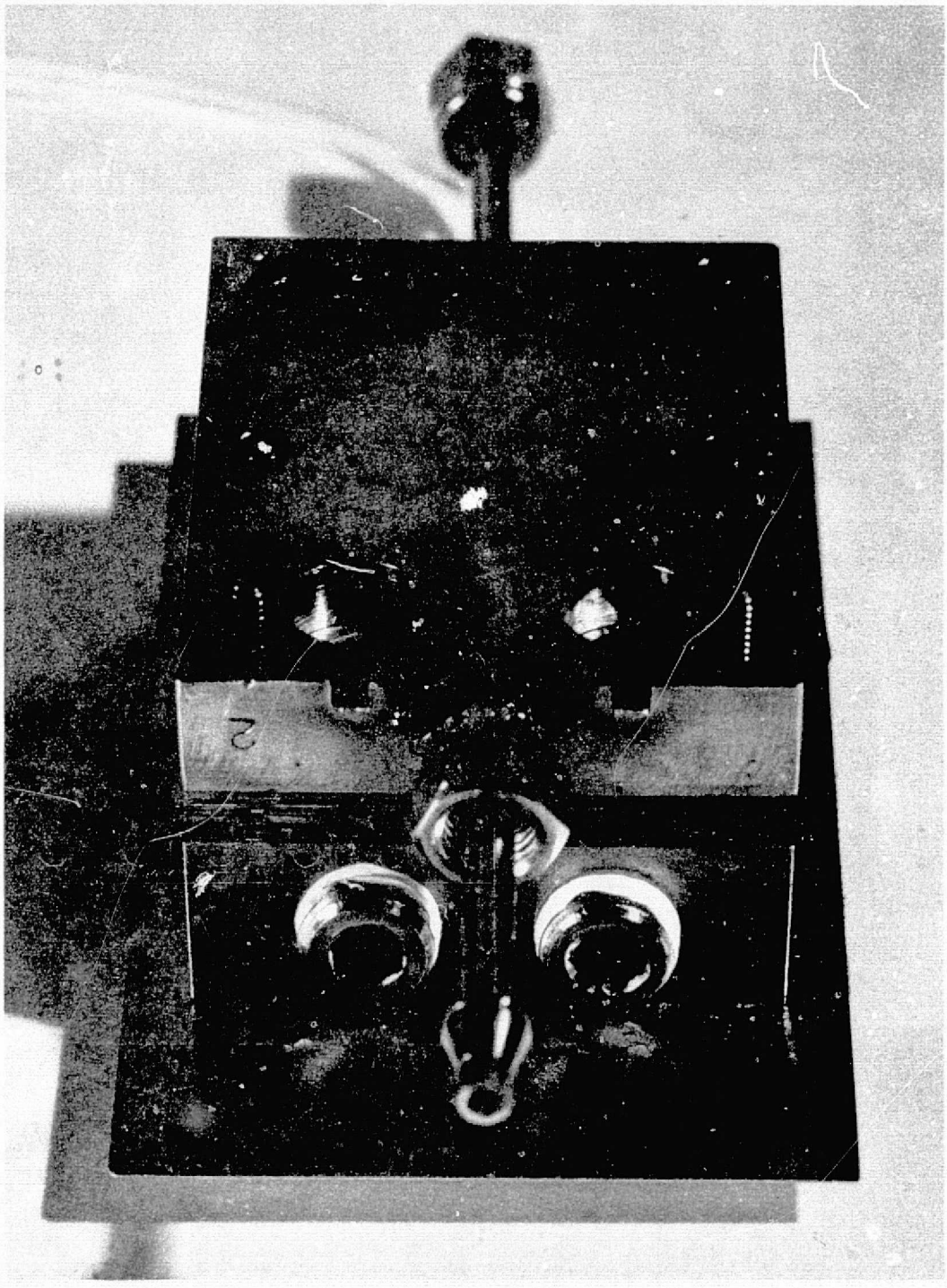

FIGURE 4-6 FLUIDIC HYDROGEN SENSOR

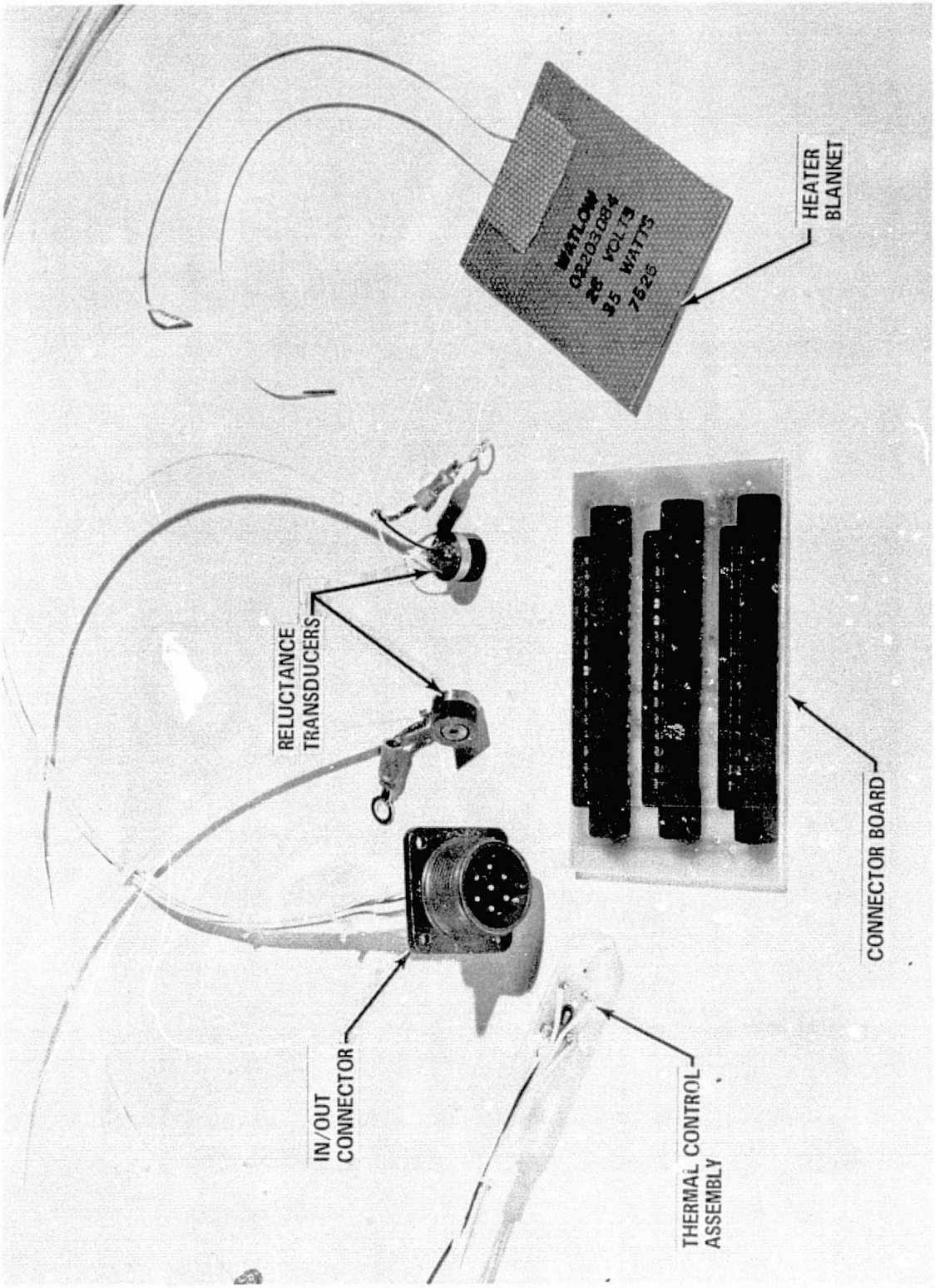

FIGURE 4-7 COMPONENTS

4.2 ACCESSIBILITY AND SERVICE

Access to detector electronics is achieved by the simple removal of the cover. As can be seen in Figure 4-3, the installation and removal of printed circuit card for testing, maintenance or service is extremely easy. Troubleshooting is accomplished, on site, by card substitution and repair by card replacement, requiring only minutes. Card repair can be accomplished in a laboratory where time and equipment are available.

Access to the fluidic hydrogen sensor is not accomplished on site, since the process is more detailed. It is necessary to remove the four screws holding the center plate and the four screws which secure the sensor mounting brackets. The sensor is then held only by the tubing fittings at each end. By removing both fittings, the fluidic sensor can be removed. The entire procedure is detailed in the Operation and Maintenance Manual and requires less than five minutes.

4.3 SAFETY

To insure a safe design that will not trigger an explosion, the package is continually purged with compressed air. The purge air raises the internal package pressure above ambient to eliminate any hydrogen flow from ambient into the package. A purge rate of 0.635 SCFM is used which completely changes the air within the package every 12 seconds. Purge flow is controlled by a 0.031 inch orifice in a voi-shan washer placed in the purge inlet fitting. Purge flow calculations are given in Appendix G.

Purge air enters a fitting in the upper housing, reference Figure 4-2, which is separate and isolated from the lower chamber by four orifices. These orifices provide a flow path for the purge air into the lower chamber. Also shown in Figure 4-2 is the purge vent fitting on the side of the lower housing.

4.4 COST

Budgetary cost estimates for the fluidic hydrogen detector in low volume production is $1500.00 with the cost of materials comprising about half that figure. In high volume production, 500 units or greater, the cost should drop to about $1150.00.

SECTION 5
TEST AND EVALUATION

Testing performed on the hydrogen detector or individual components included long term environmental evaluation of the fluidic sensors, functional testing of each prototype system, and the environmental evaluation of a prototype system. Each of these will be discussed.

5.1 LONG TERM EVALUATION

To determine the effects of the KSC environment on the fluidic hydrogen sensor, five units were built up and operated continuously at a KSC location. The sensors were considered to have three possible areas of susceptibility; i.e., filter clogging due to dirt and dust, poisoning of the catalysts due to salt spray or other contaminants, and degradation of the fluidic elements performance due to contamination.

After build up the sensors were mounted in a temperature controlled enclosure and calibrated on three hydrogen-air mixtures. Actual values for the mixtures, as determined by the manufacturer, were 0.5%, 1.08% and 1.87%. Figure 5-1 shows a typical calibration curve for a sensor with these gas mixtures. Sensor output was determined by using the electronics developed on a previous contract. The curve has been corrected for zero since the oscillators were not initially operating at the same frequency. Curves for the other four units were remarkably similar with the outputs accurate to about ± 0.05% of the actual hydrogen concentration, assuming the gas calibration was accurate. These results were satisfactory, and the sensors were installed at KSC.

After installation at KSC, the sensors were recalibrated using ambient air to establish a zero reference, and sample gas mixtures of 0.55%, 1.03% and 1.98% of hydrogen in air. In each calibration run, the sensor outputs were decoded using the engineering prototype signal processor, and the processor output measured with a digital voltmeter.

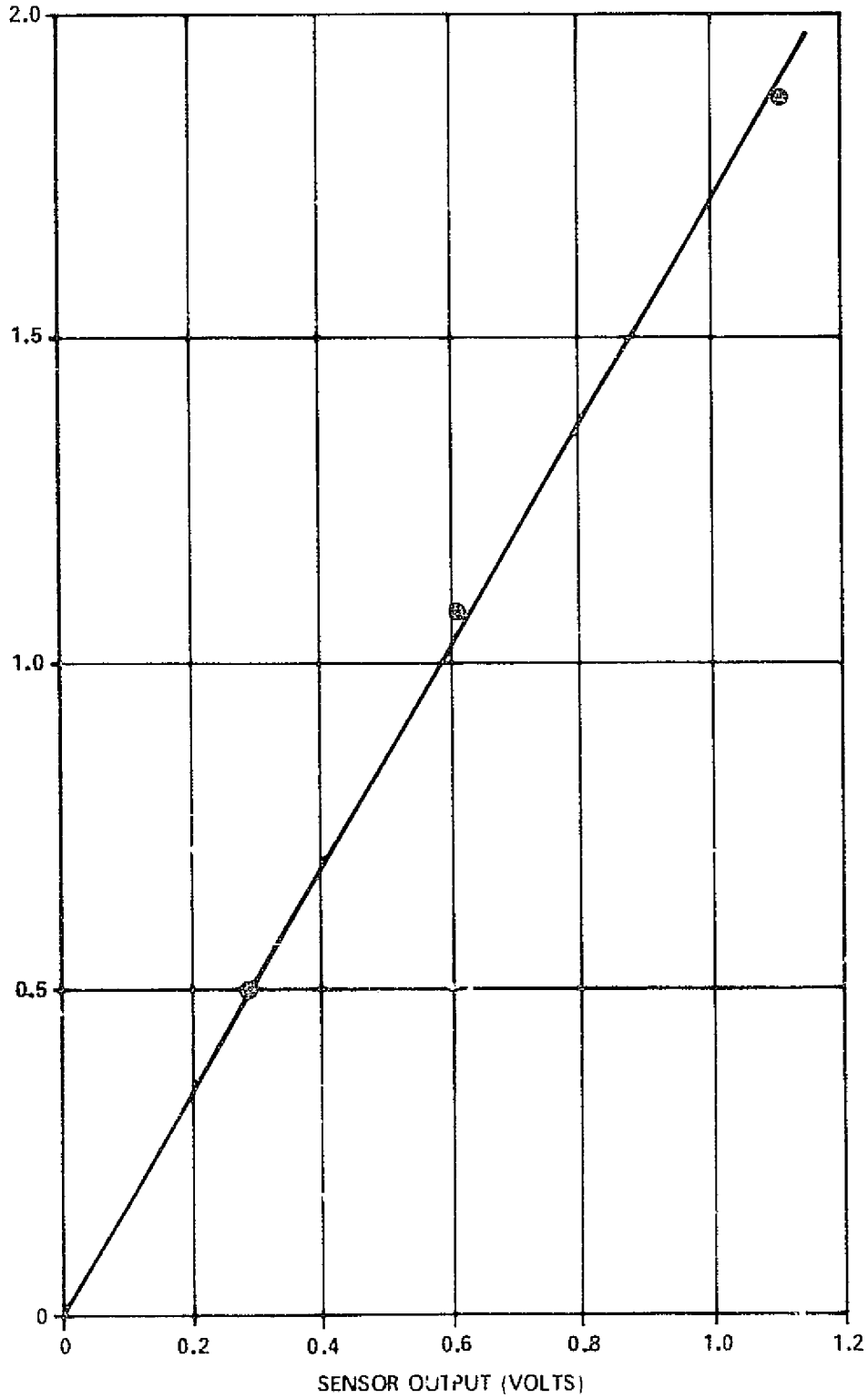

FIGURE 5-1 SENSOR CALIBRATION

The signal processor was not calibrated specifically for any one of the five sensors. Therefore, to establish a consistent method for presenting data, the baseline data was corrected to make the output zero for the ambient air reading of each sensor. The correction factor for each sensor was then applied to all subsequent readings taken on that sensor for both air and hydrogen-air mixtures. This method allows one to observe any drift in sensor output that may occur from one reading to another.

A straight line calibration curve was computed for each sensor between the ambient air zero point and the 1.98% hydrogen-air mixture point. This calibration was based on the initial calibration and assumed the hydrogen concentration values supplied by the manufacturer were absolutely accurate. Output levels were then computed for the 0.55% and 1.03% hydrogen concentrations. These levels are shown by the horizontal dashed lines across each graph which is labeled theoretical output on the right hand side of Figures 5-2 through 5-6.

The outputs are plotted as a function of signal processor output voltage, rather than hydrogen concentration. This was done because the scale factor of the processor is fixed and cannot be changed to accommodate small variations in gain between the sensors. By using the voltage output, a similar scale for all sensors can be used. The sensors were operated continuously from the time of the baseline data reading until data point 6 was plotted, resulting in an operating time of approximately 430 hours. In addition, it is estimated they were operated intermittently for about 240 hours while problems with the installation factilities were being resolved. This represents a total operating time of 670 hours.

Inspection of the data through reading 6 plotted in Figures 5-2 through 5-6 indicates that a large percentage of the data points are within 0.1% of the computed theoretical value. If linearity only is considered, practically all data points are within this tolerance. When zero shifts were experienced, the other data points follow the zero shift pattern. Only with sensor #4 was this problem pronounced, where the worst case zero shift was a value equivalent to 0.25% hydrogen.

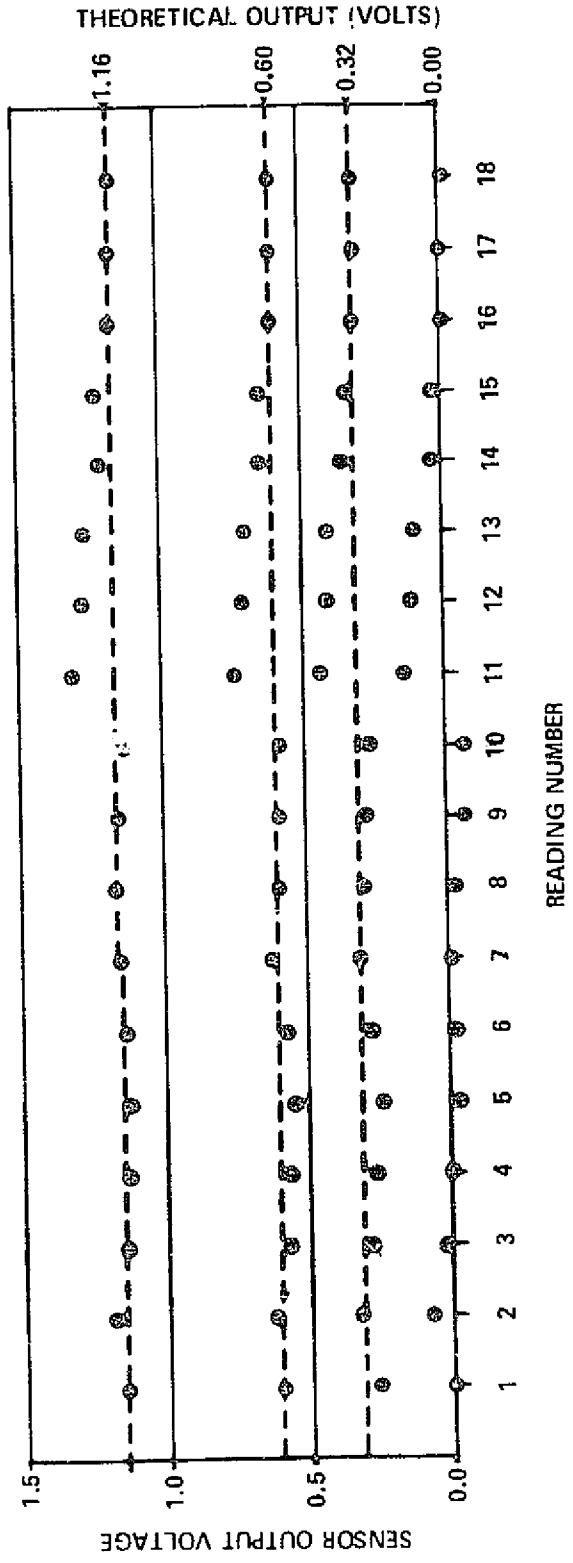

FIGURE 5-2 SENSOR ONE PERFORMANCE

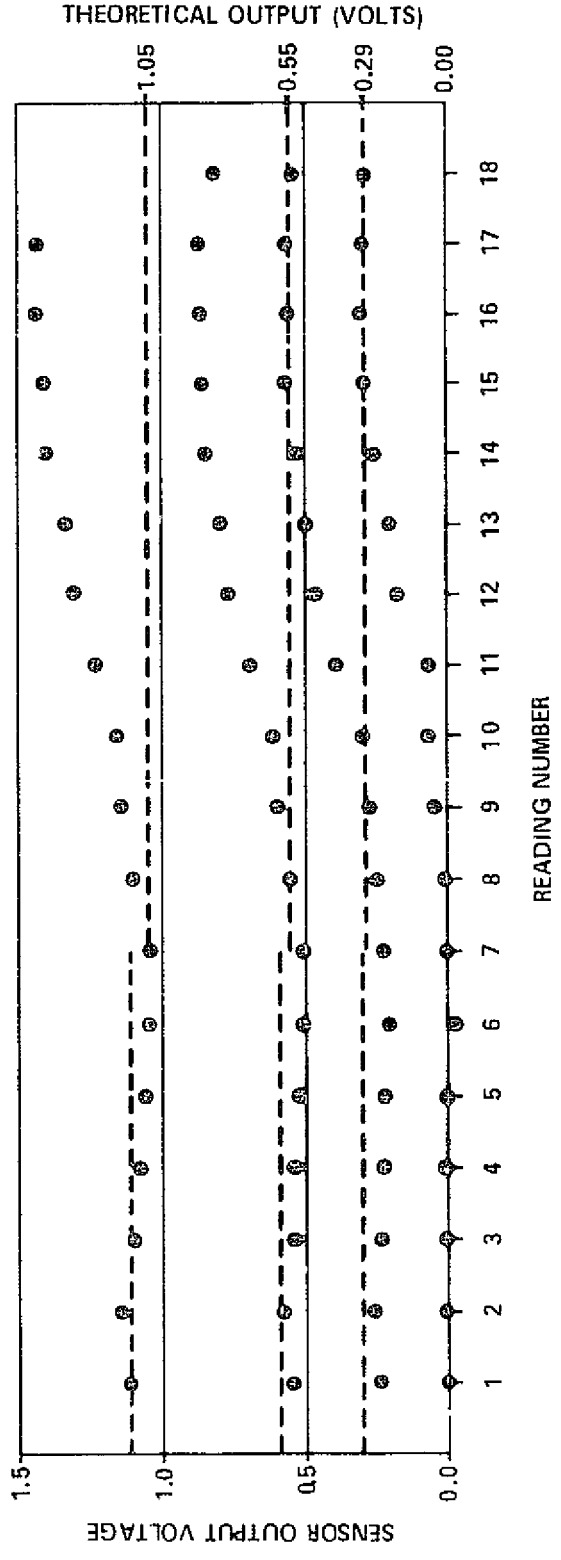

FIGURE 5-3 SENSOR TWO PERFORMANCE

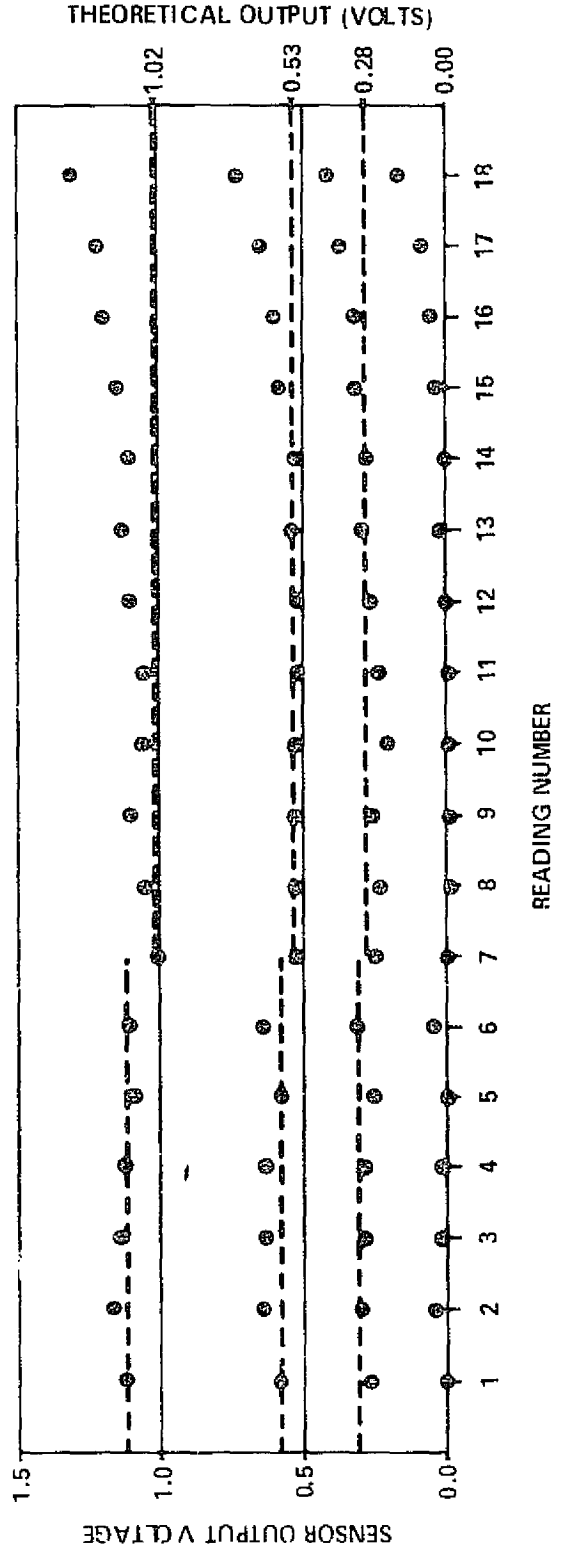

FIGURE 5-4 SENSOR THREE PERFORMANCE

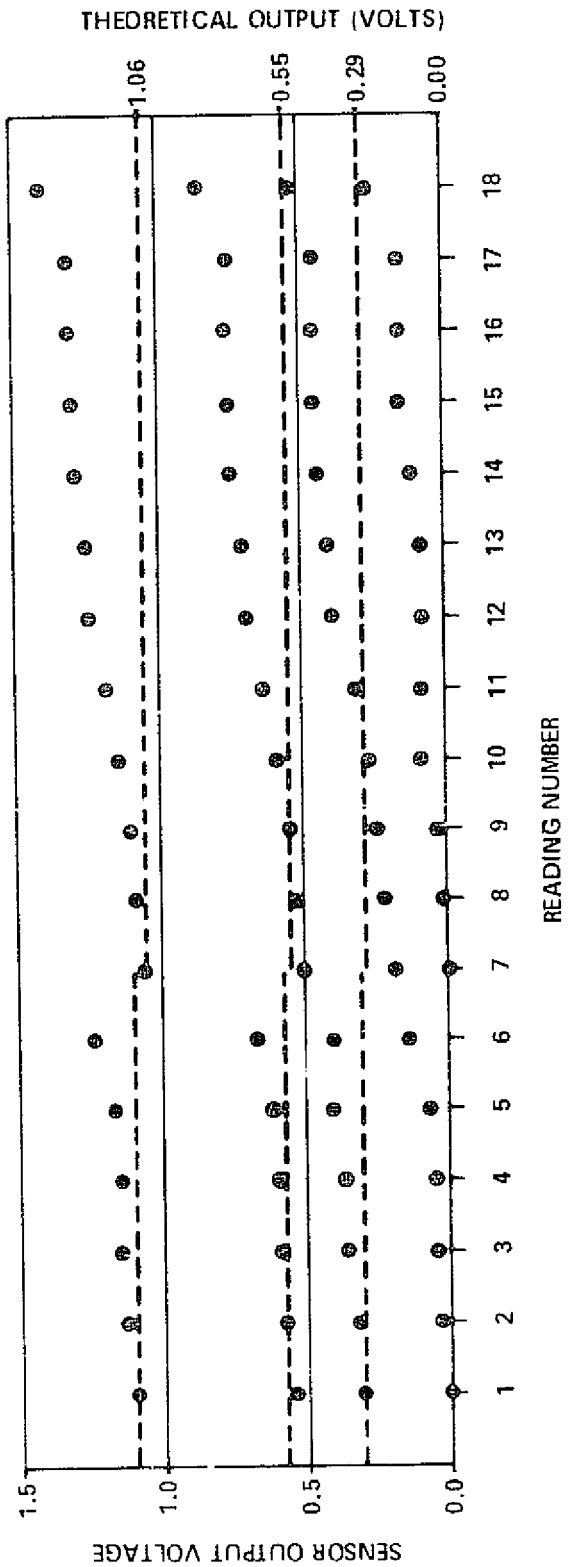

FIGURE 5-5 SENSOR FOUR PERFORMANCE

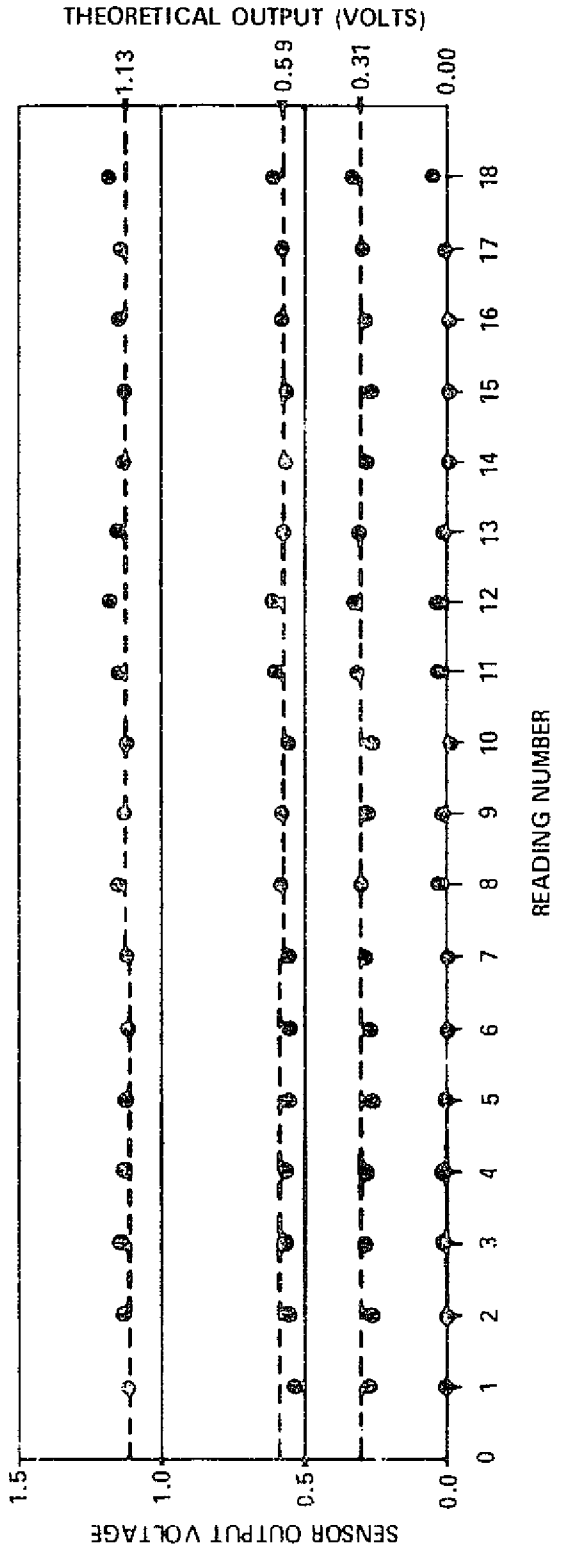

FIGURE 5-6 SENSOR SIX PERFORMANCE

The discontinuity in the theoretical output that appears at reading 7 was caused by the installation of a new vacuum pump. The original vacuum pump required the addition of oil almost daily; therefore, an oilless pump was purchased and installed to eliminate this maintenance problem. The second pump produced a vacuum level which was two inches of mercury lower than the original. This increase in vacuum resulted in a change in sensor performance. Therefore, to provide a fair sensor evaluation, new straight line calibration curves were computed for each sensor between the ambient air zero point and the 1.98% hydrogen-air mixture. This calibration was based on the data of reading 7, taken after the new pump installation. These calibration points for the three hydrogen concentrations are the horizontal dashed lines on each graph from reading 7 on.

Over 2700 hours of operation, or approximately 14 years at the predicted usage rate, was accumulated on the five sensors with no malfunctions. Although zero shift was experienced with four of the sensors, it should be noted that sensor linearity normally varied less than 0.10 percent with a few points being within a 0.15 percent range. This is exemplified best by sensor two. Although this sensor displayed the largest zero drifts, had it been given a zero calibration prior to testing, the output would have remained within a 0.1V band of theoretical values in all cases. Performance of the other sensors is comparable.

No failure of sensor components, no indication of catalyst degradation, and no significant changes in sensor gain or linearity were exhibited by the sensors.

Testing of the five sensors was terminated to investigate the problem of zero shift being experienced in the units. The evaluation started by confirming the sensors operated the same at TICO as they did at KSC. Once this was confirmed, the signal frequency, amplitude, and wave shape of each signal and reference oscillator was checked at three levels of H_2 concentration. All this was done before the enclosure was opened.

After opening, a visual check revealed nothing unusual; however, before the sensors were disconnected, each was flooded externally with H_2 while operating with a pure air input to determine if the sensors had developed any leaks. No leaks were detected. Each lead of the reluctance pickups were flexed to uncover intermittent connections and magnets were checked for proper seating. Tests were made of the thermal gradient across each sensor for uniformity.

At this point, the sensors were disconnected electrically and pneumatically and removed from the enclosure. Torque levels of the six assembly screws of each sensor were checked. All were tight. The sensors were then disassembled and inspected. Contamination was found in both the signal and reference osicllators of all five sensors. Photographs of each oscillator showed the type, coloring, distribution patterns, and quantities of contaminant in each oscillator to be very similar. Figures 5-7 and 5-8 are photographs taken of reference and signal oscillators of system 6. An analysis of the contaminant was performed by the KSC Microchemical Analysis Section to determine its makeup. The Microchemical Analysis Laboratory report is included as Appendix E.

To determine if the observed contaminant had started to clog the three filters used in each sensor, pressure drops and sensor flow requirements were checked. System flow and pressure at the four points shown in the schematic of Figure 5-9 were recorded for each sensor. These values were compared to readings taken previously on new sensors and found to be within the normal variations of a clean system. The three filters were also removed from each sensor and checked individually for clogging. Although contamination was visible on the filters, no increase in pressure drop across the filters could be detected at flow rates five and ten times larger than normal. A summary of the filter tests is presented in Table 5-1, where individual filter pressure drops are shown for a clean sensor and sensors 2 and 6, those with the poorest and best performance, respectively.

The extensive investigation of system pressure drops and flow requirement was conducted to determine if a change in mass flow had occurred in the sensors which displayed a zero shift. Any change in mass flow through either the reference or signal oscillator will manifest itself as sensor zero shift. If this zero shift was caused by partially clogged filters, there should be a detectable difference

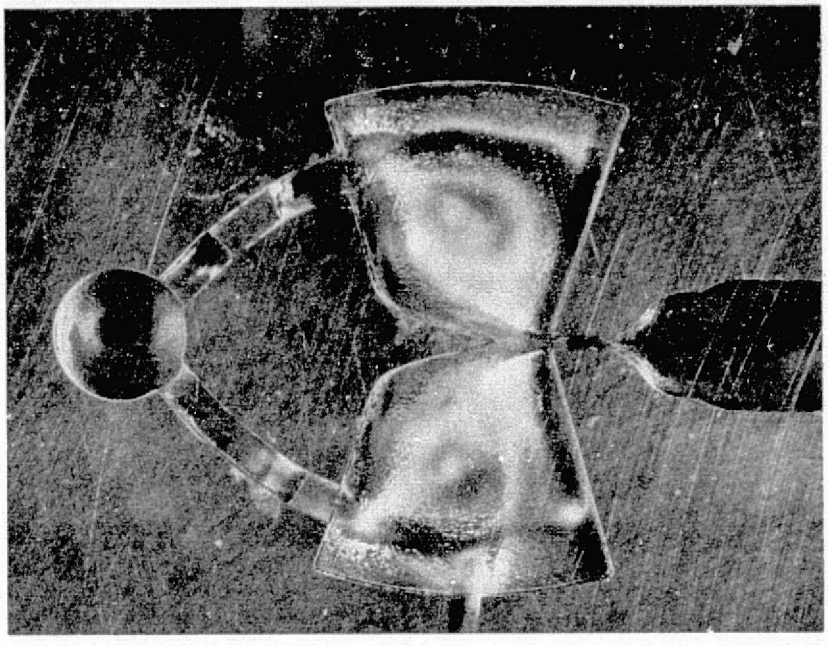

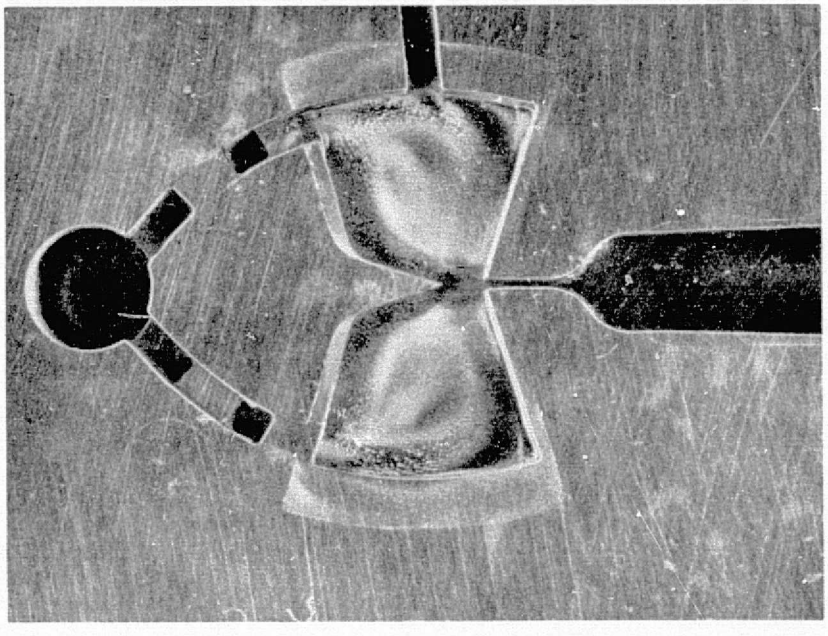

FIGURE 5-7 REFERENCE OSCILLATOR

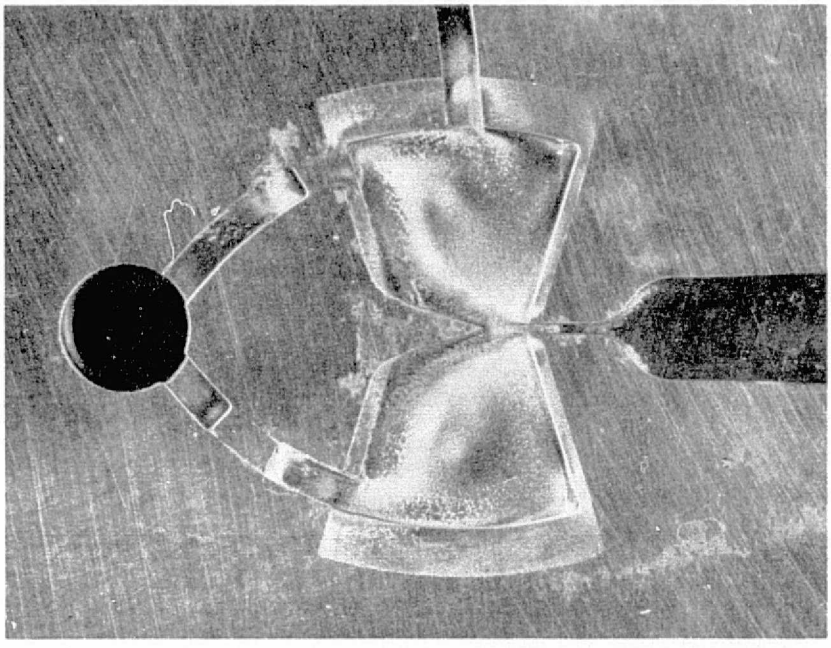

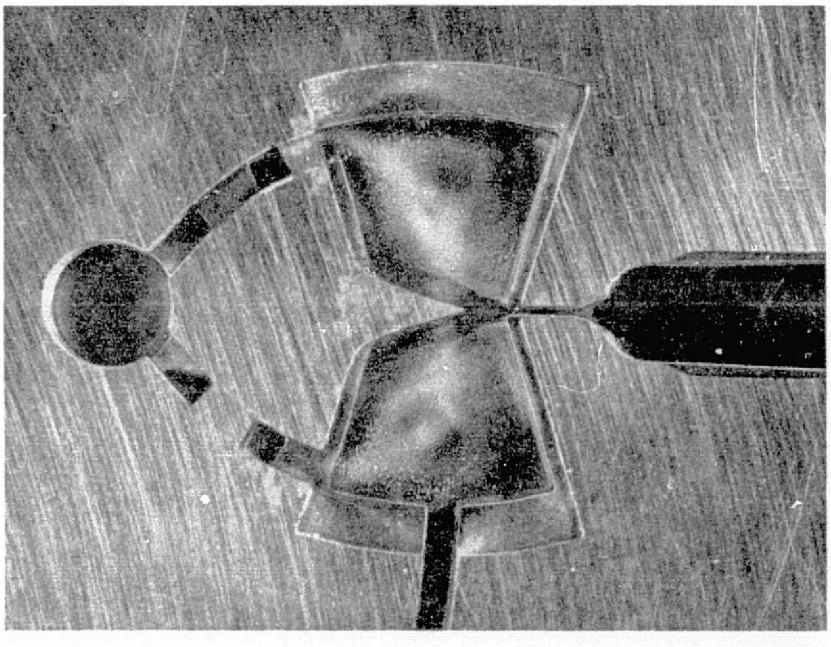

FIGURE 5-8 SIGNAL OSCILLATOR

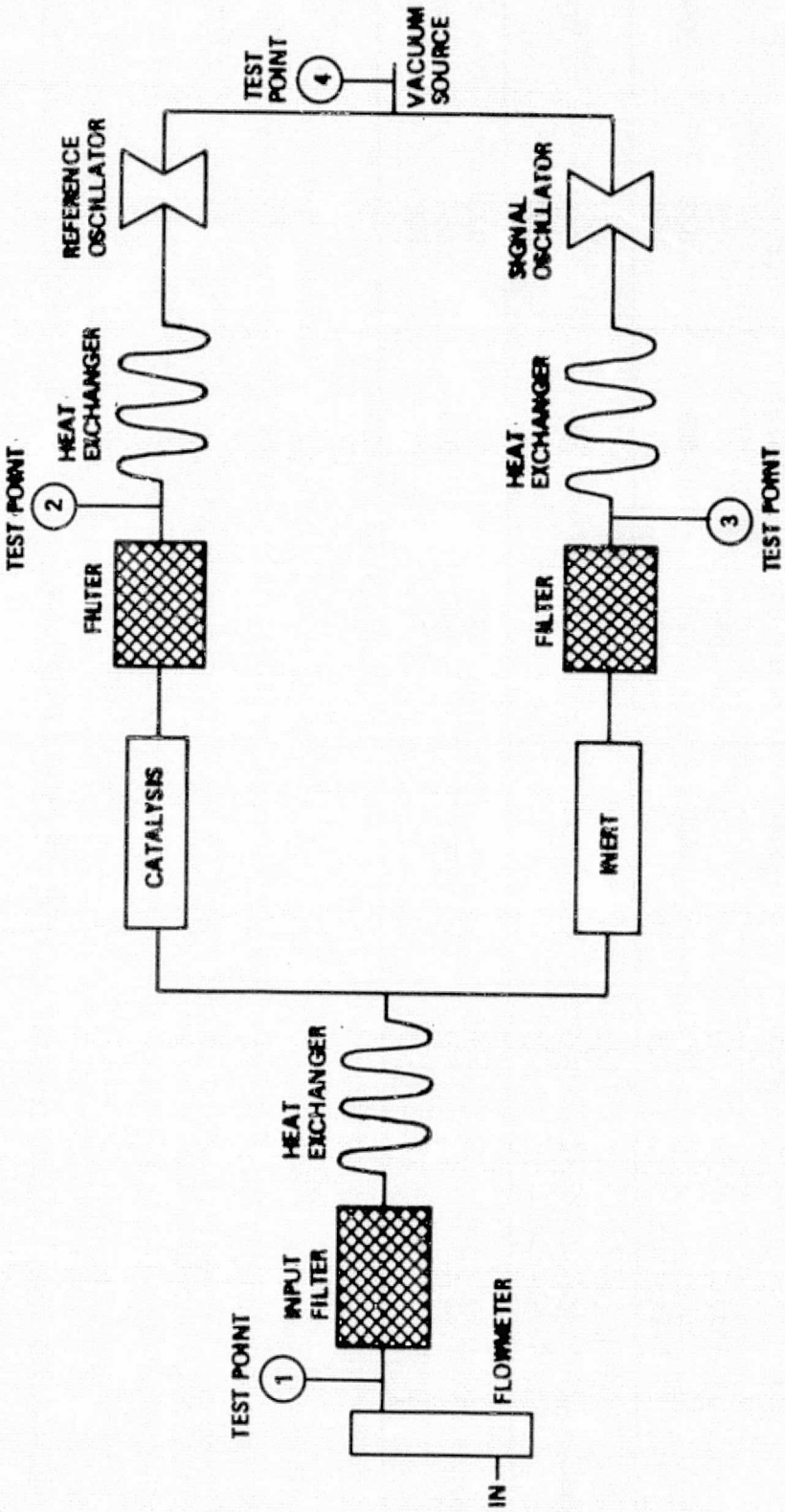

FIGURE 5-9 SYSTEM TEST POINTS

FLOW [SCCM]	FILTER POSITION	SENSOR					
		2 POOREST PERFORMANCE		6 BEST PERFORMANCE		7 CLEAN	
		PRESSURE (PSIG)	DIFF (PSIG)	PRESSURE (PSIG)	DIFF (PSID)	PRESSURE (PSIG)	DIFF (PSID)
5800	Input Signal Reference	.027 .026 .029	.003	.032 .027 .031	.004	.035 .028 .024	.004
8550	Input Signal Reference	.045 .043 .047	.004	.054 .045 .052	.007	.057 .046 .040	.006
11250	Input Signal Reference	.065 .064 .069	.005	.077 .064 .077	.013	.082 .064 .059	.005

TABLE 5-1

FILTER FLOW EVALUATION

between the flow capabilities of the signal and reference oscillator filters. However, an examination of Table 5-1 shows that sensor 6, which displayed virtually no zero shift, had the greatest difference in pressure or flow impedance between the two filters; and sensor 2, which displayed maximum zero shift, had a better pressure balance between the signal and reference filters

Although the contaminant buildup in each oscillator appeared to be the same, the exact amount deposited in each is unknown, and even if the quantities were known and equal, their effect on each oscillator would not necessarily be the same. This contaminant buildup was, however, suspected to be the primary factor contributing to sensor zero shift.

5.2 FUNCTIONAL EVALUATION

Each hydrogen detector was functionally evaluated after buildup for proper operation. The units were tested for fluidic sensor scale factor, processor electronics linearity, complete detector linearity, output scale factor, operation of the self test circuit, and performance and adjustment of the heater control circuit. Performance of the following tests is described in the Operation and Maintenance Manual.

5.2.1 Fluidic Sensor Linearity

Three air-hydrogen mixtures were used to establish the scale factor of each fluidic sensor. This was accomplished by determining the fluidic sensor difference frequency for pure air and the three mixtures. These mixtures were certified standards with concentrations of 0.50, 0.99 and 1.98%. First, the difference frequency (Δf) between the signal and reference oscillators for pure air and the three hydrogen concentrations was recorded. Then the value of Δf at 0% H_2 was subtracted from each reading giving the actual Δf change from zero due to each concentration. These Δf changes were then normalized and averaged to find the scale factor value of each sensor to be used in switch setting calculations.

5.2.2 Processor Electronics Linearity

Processor electronics linearity was established by applying simulated reference and difference frequencies to the processor from signal generators. First, a simulated reference oscillator frequency of 15 kHz was applied to the processor and the divide by M switches set to 3000. This forced the maximum gate time; i.e., if $\tau_g = \tau_{g2}$, to become one second. The zero switches were set to 255, or $\tau_{g1} = 0$; this makes $\tau_g = \tau_{g2}$ and allows all Δf pulses generated to pass through the gate. In this mode of operation, a simulated difference frequency applied to the processor will appear at the D/A input as a binary number equal to that frequency. Therefore, full scale output can be attained with a Δf of 250 Hz, half scale with 125 Hz, etc. Six points were checked on each processor from 0 to 5 volts output in one volt increments. Differences of less than 5 millivolts were experienced on all units.

5.2.3 Self Test Circuit

Operation of the self test circuit was insured by disabling the signal to each detector in the circuit. The input from each reluctance transducer to their respective amplifiers was shorted to ground sequentially and the output signal monitored. The heater circuit oscillator output was then shorted to ground and the self test signal output again monitored.

5.2.4 Heater Control Circuit

Heater circuit operation was monitored from initial turn on of each detector until operating temperature was reached and stability achieved. The pulse duration of heater power was monitored along with fluidic sensor block temperature during warm up. The oscillator frequency and pulse width modulator output signal were checked under both cold and hot conditions. As the proper temperature was reached (245°F) potentiometer R-1 on circuit board 3 was adjusted to maintain this temperature. Temperature was monitored throughout the remainder of testing to detect any shift in operating point. No changes were observed.

5.2.5 Detector System

After checkout of the electronics and fluidic sensor, the detector was evaluated as a system. This entailed the calculation of the values to be set into the zero offset and M switches and the operation of the detectors on three hydrogen concentrations. The same air-hydrogen mixtures of 0.50, 0.99 and 1.98% H_2 were used. Since the detector output scale factor is 1 volt per percent hydrogen, the output voltages ideally would be 0.50, 0.99 and 1.98 Vdc, respectively. Results of the functional evaluation of each system along with a varying number of additional checks on each detector are given in Figures 5-10 through 5-15. These figures show the turn on to turn on stability for six of the seven delivered detectors. Detector number 3 was used for environmental evaluation and its performance curve is shown in Paragraph 5.3.

Performance curves of Figures 5-10 through 5-15 are plotted from data taken by reading detector output with a digital voltmeter. While taking these readings, output drift was observed when the detector was operated for 30 or 40 seconds at a given H_2 level. To better visualize what was happening, traces were made on an X-Y recorder. The Y axis was made to sweep at a fixed rate, while detector output was applied to the X axis. Results are given in Figures 5-16 through 5-19 for three of the sensors evaluated. Hydrogen concentrations in air of 0.00, 0.50, 0.99 and 1.98 percent were used with each level being applied for 100 seconds. The smallest incremental change in output voltage in these figures is equal to 20 mVdc, which is the minimum D/A output voltage change. Also, the smallest duration of voltage change is the duration of minimum system sampling time. Evaluations were made with both increasing and decreasing hydrogen concentration levels.

Since the drifts could be caused by either the fluidics or electronics, additional curves were made to evaluate only the electronics. The detectors were operated with simulated inputs, as described in Paragraph 5.2.2, for linearity checkout, so the output voltage was controlled by the Δf signal generator. A simulated Δf of 100 Hz was applied, which gives an output voltage of 2.00 volts. Figure 5-20 shows the variations in two system outputs. The single step changes observed in these curves can be caused by either the D/A, whose output is accurate to within

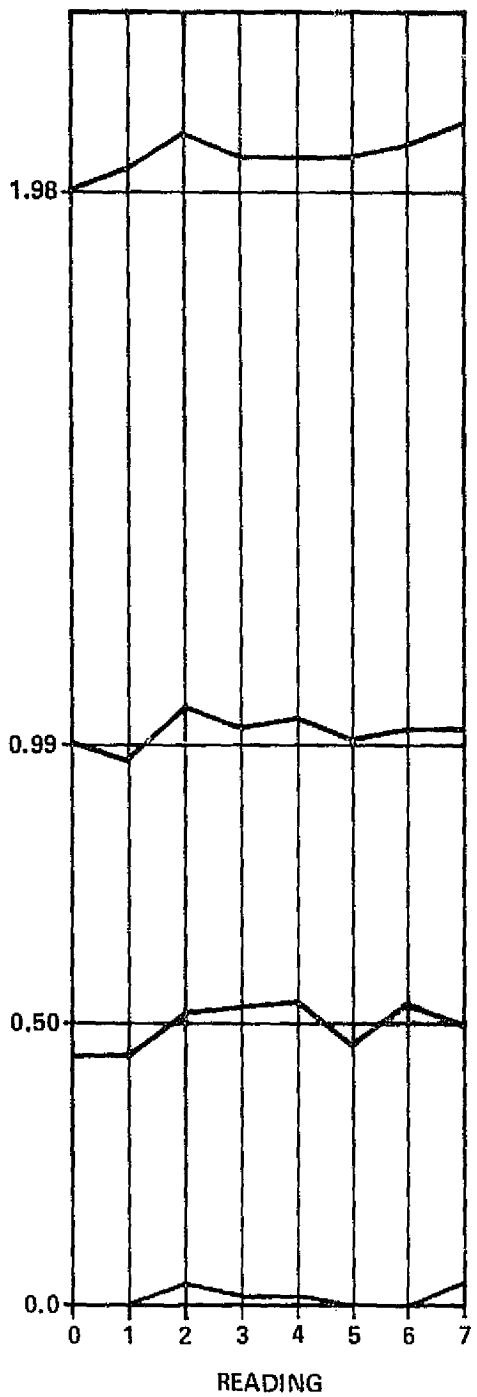

FIGURE 5-10 SYSTEM 1 PERFORMANCE CURVE

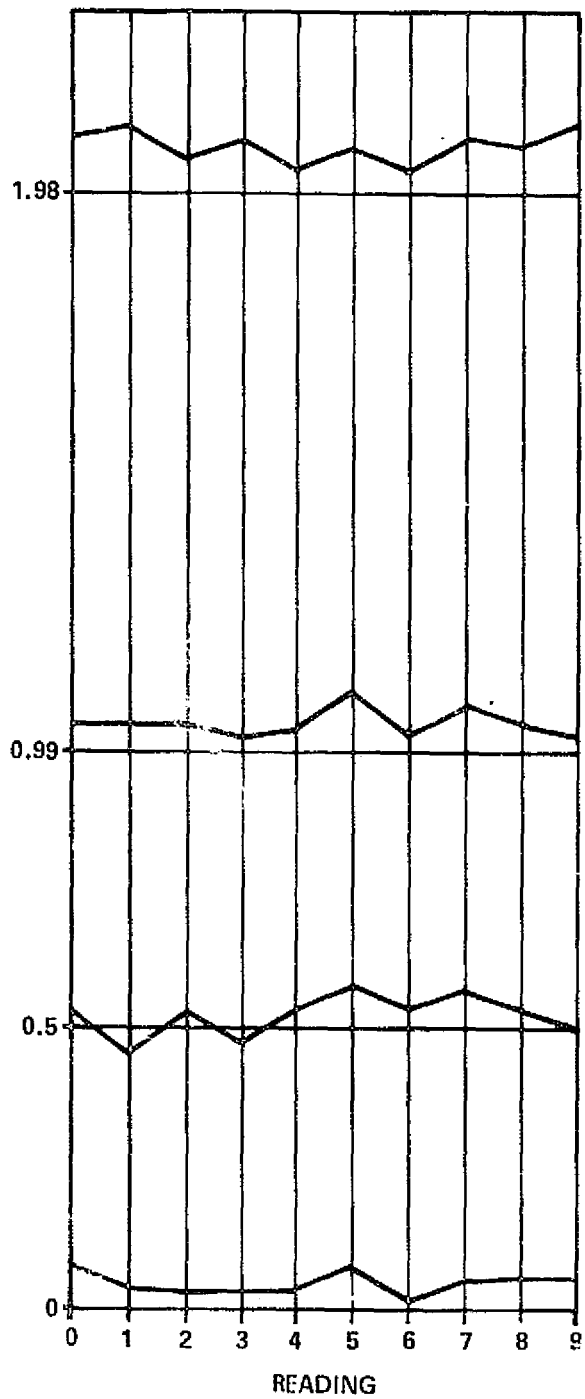

FIGURE 5-11 SYSTEM 2 PERFORMANCE CURVE

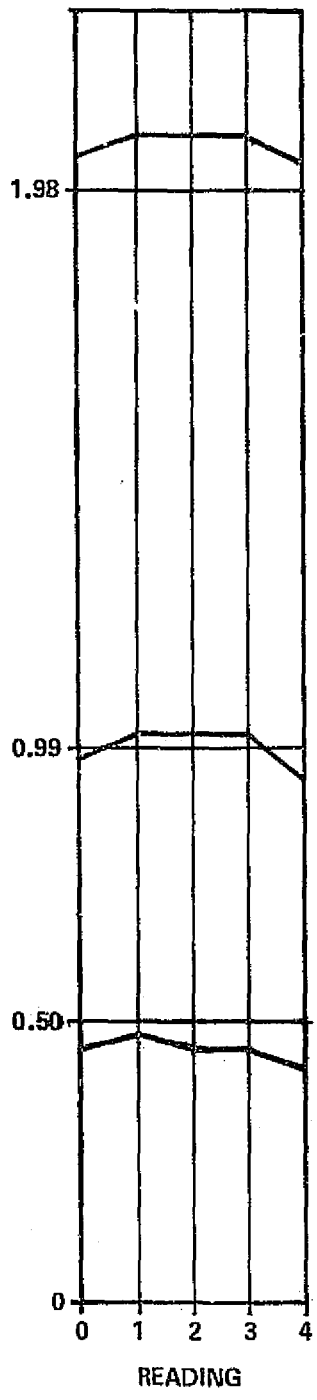

FIGURE 5-12 SYSTEM 4 PERFORMANCE CURVE

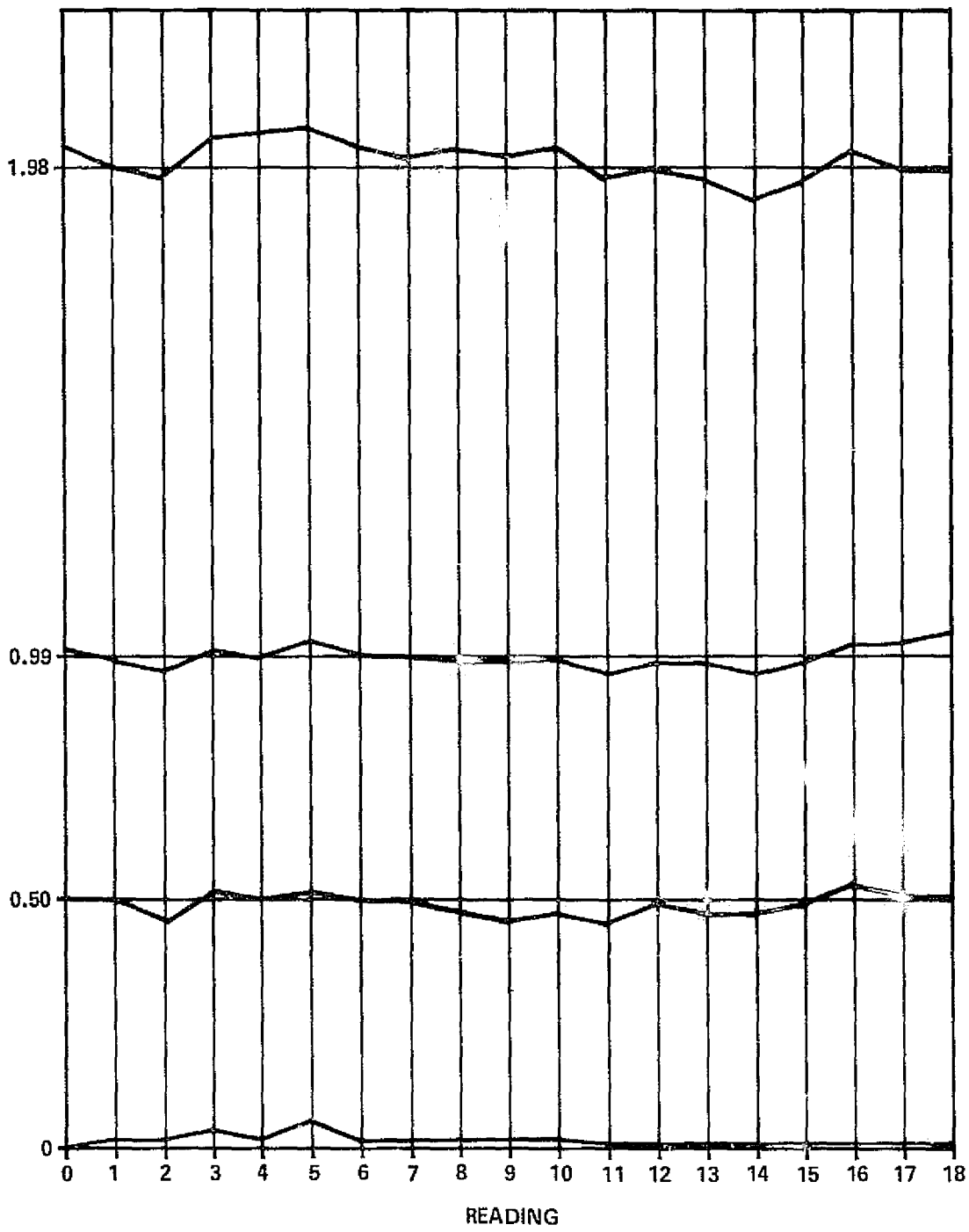

FIGURE 5-13 SYSTEM 6 PERFORMANCE CURVE

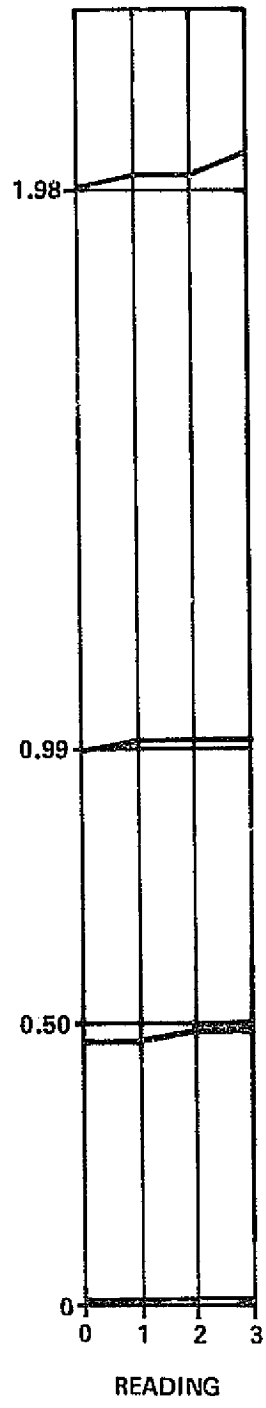

FIGURE 5-14 SYSTEM 7 PERFORMANCE CURVE

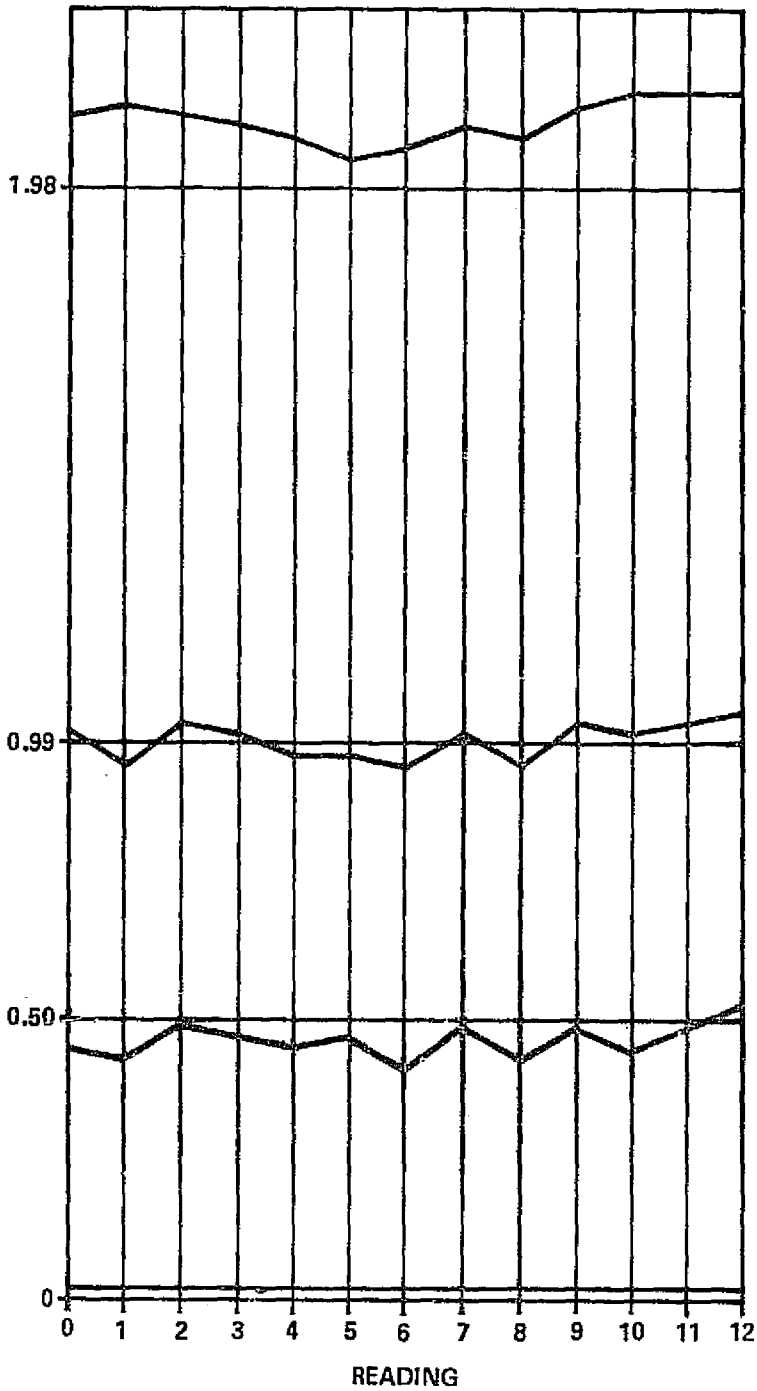

FIGURE 5-15 SYSTEM 8 PERFORMANCE CURVE

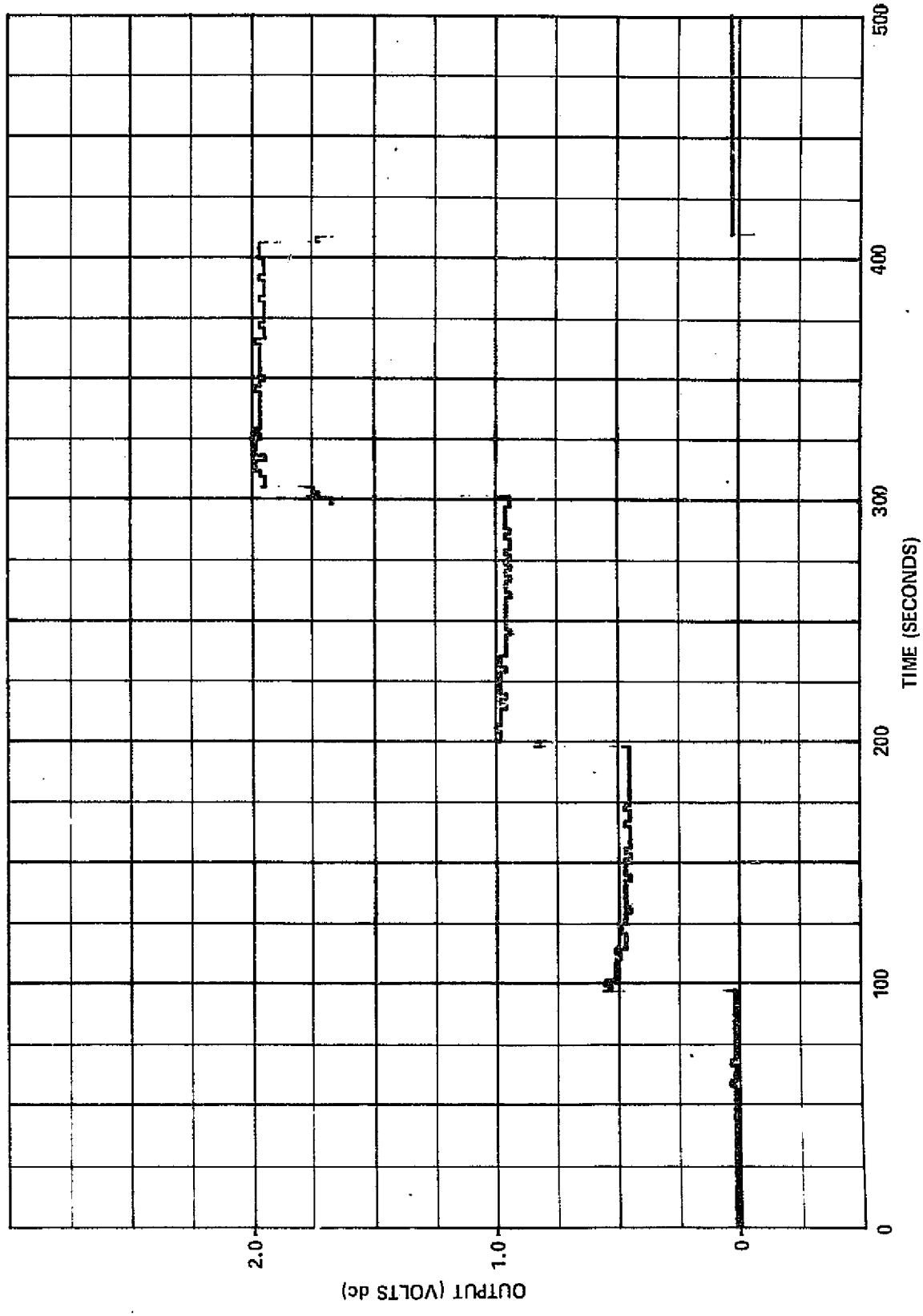

FIGURE 5-16 SYSTEM 6 STABILITY

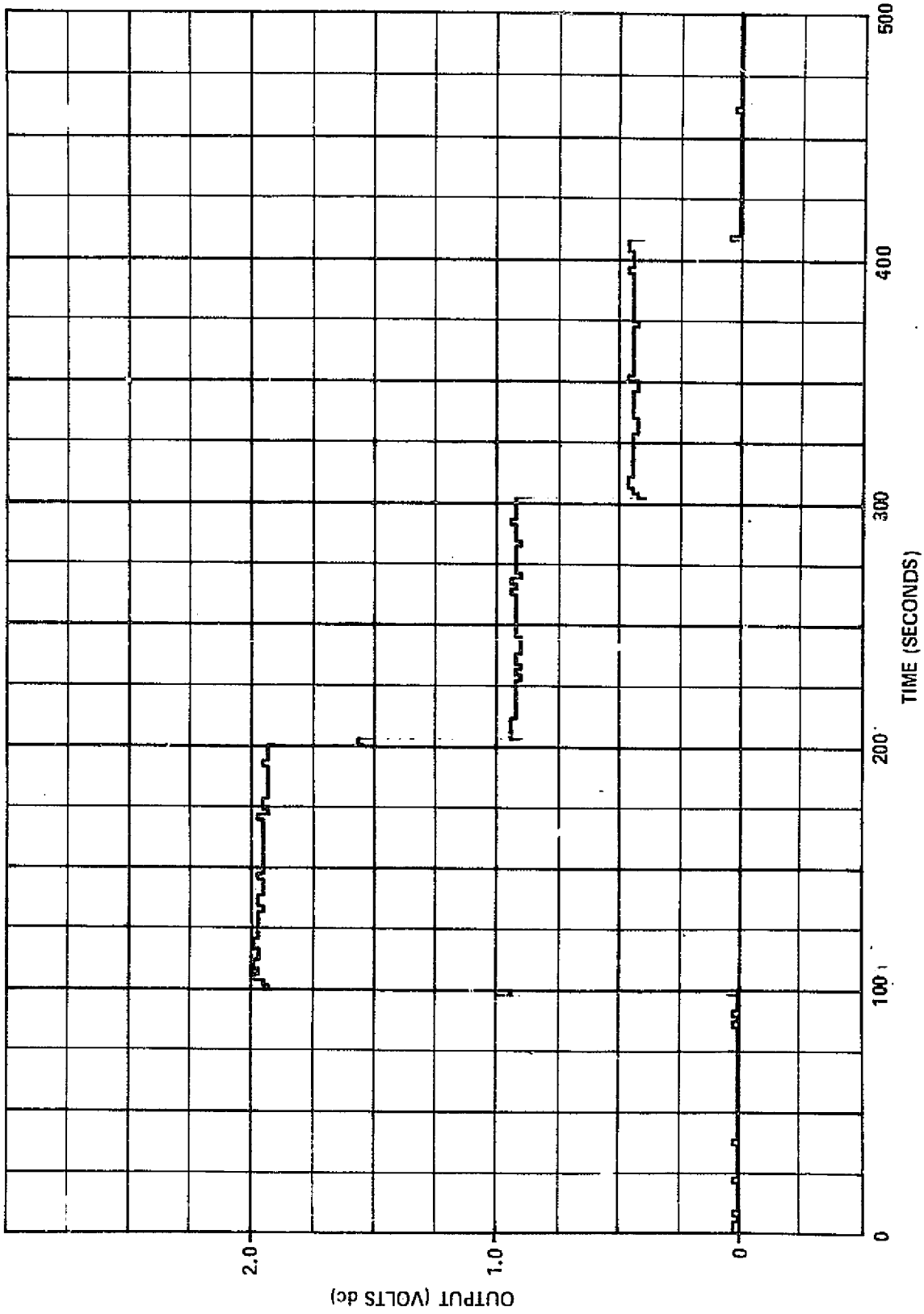

FIGURE 5-11 SYSTEM 6 STABILITY

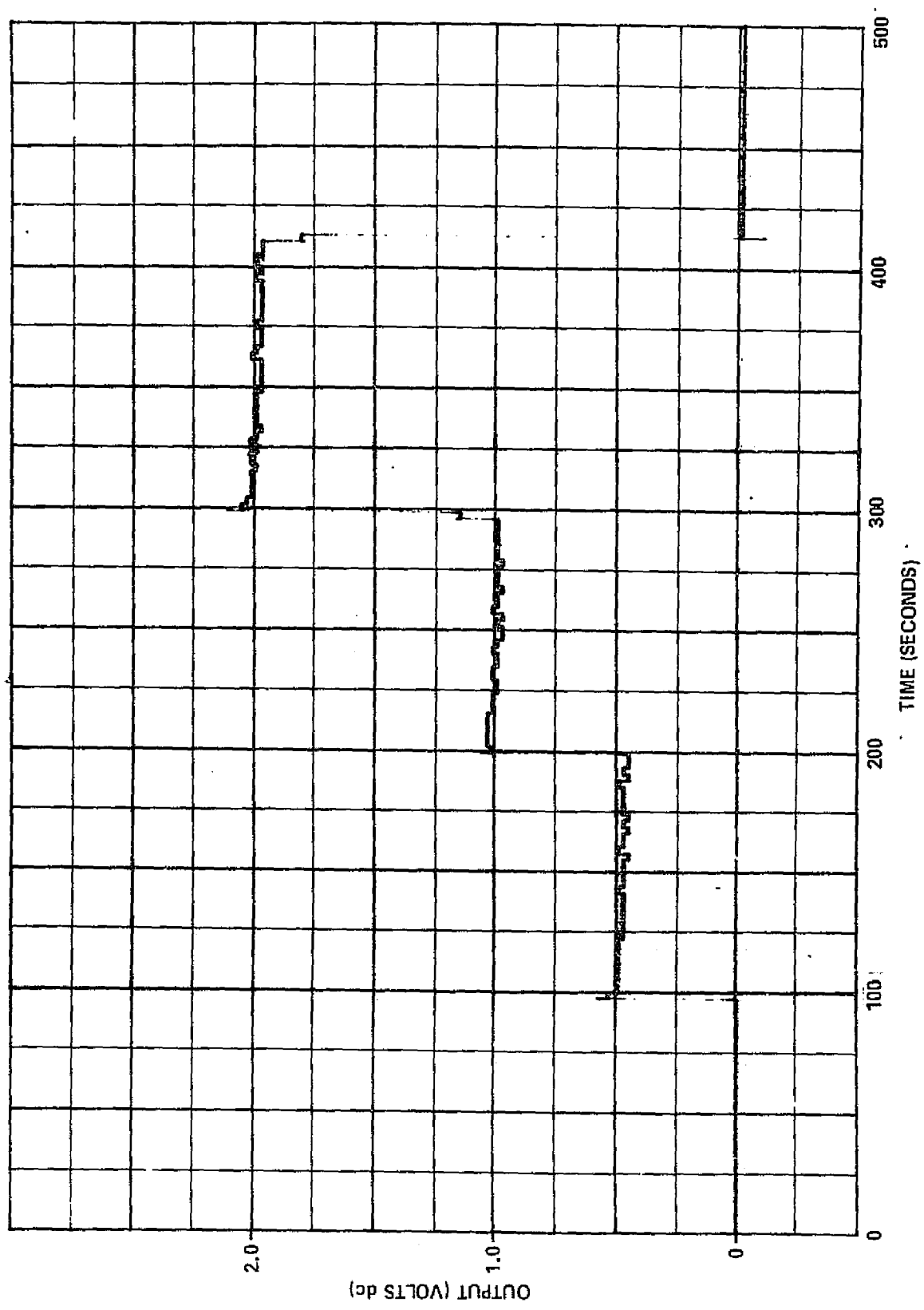

FIGURE 5-18 SYSTEM 7 STABILITY

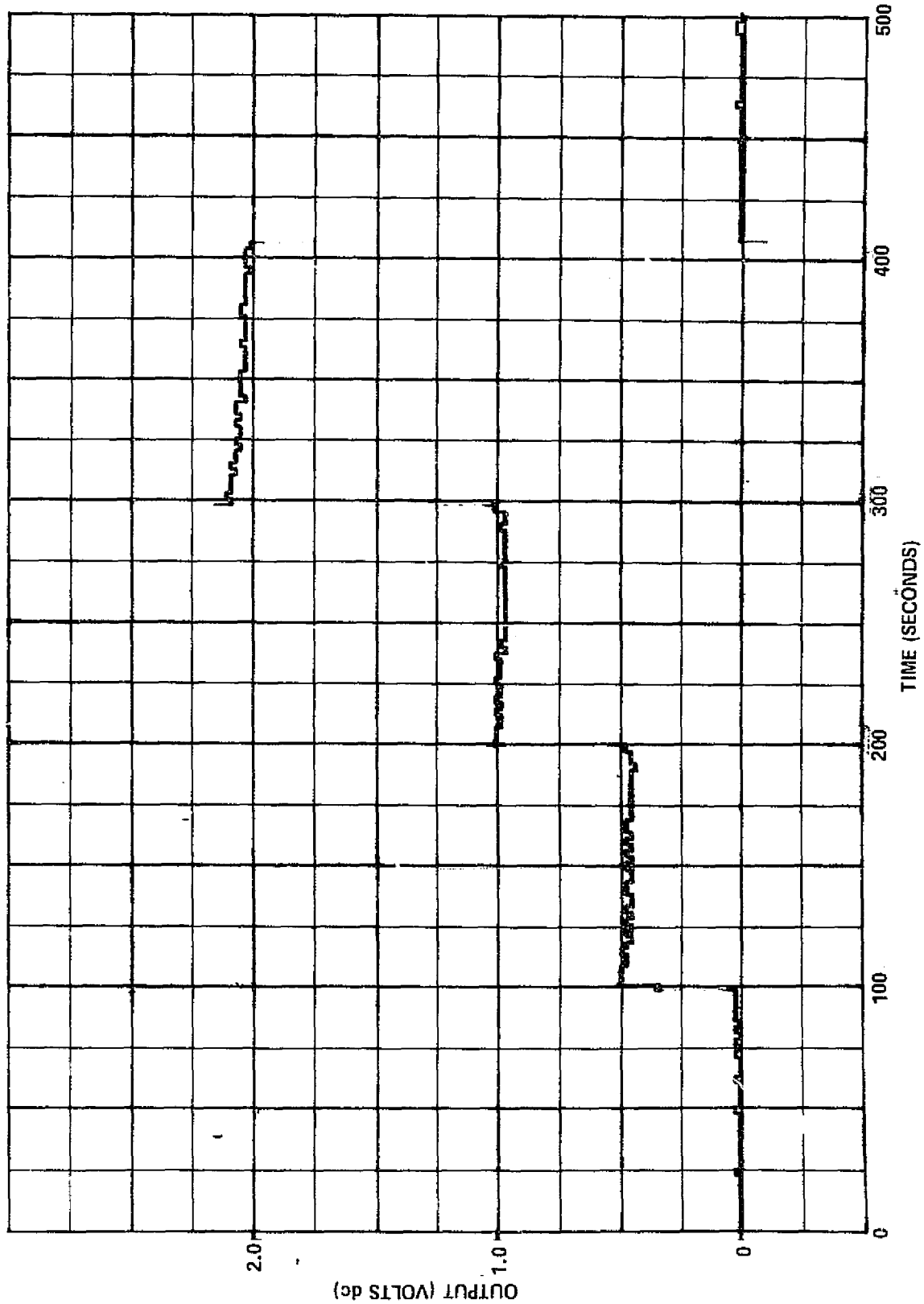

FIGURE 5-19 SYSTEM 8 STABILITY

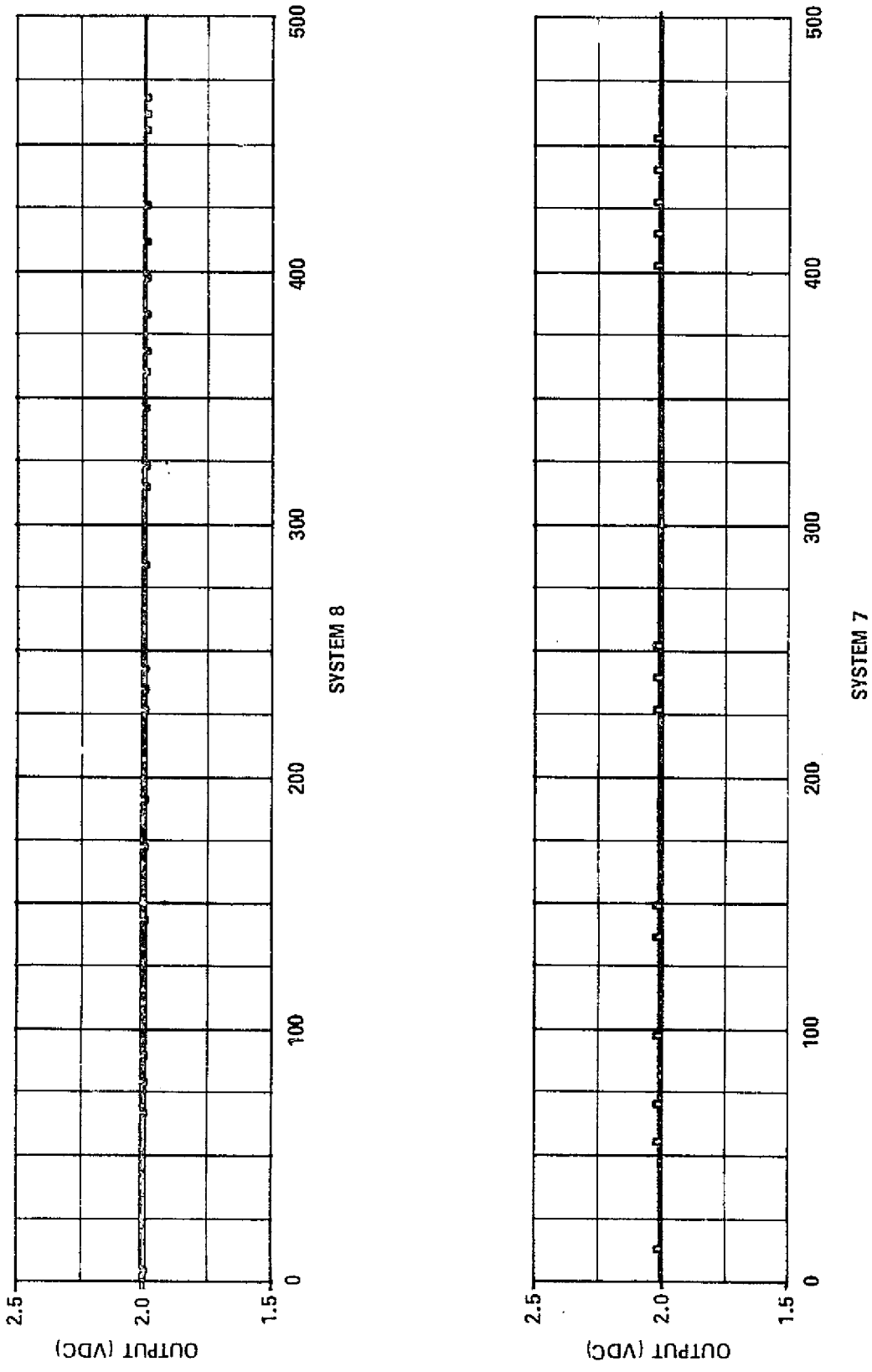

FIGURE 5-20 PROCESSOR DRIFT EVALUATION

one input bit or by instability in the signal generator simulating Δf. The slow drift shown in the upper curve of Figure 5-17 was caused by improper alignment of the paper on the X-Y recorder, since the digital voltmeter used to monitor the voltage read 2.020 Vdc at the start and finish of this curve. These curves place the primary cause of output voltage drift on the fluidic sensors.

5.3 ENVIRONMENTAL TESTING

An environmental evaluation was performed on the hydrogen detector production prototype design to establish system susceptibility to a KSC environment. Units were exposed to temperature, pressure, humidity, salt spray, sand and dust, and a helium background. Test descriptions, setups, sequences and data sheets filled out during each test are included in Appendix F.

Detector serial number 3 was exposed to the environments of temperature, pressure, humidity, and salt spray. To expedite testing, detector number 4 was exposed to sand and dust, and system number 6 was used in the helium background tests. Two problems were encountered during environmental testing; i.e., the selection of detector number 3 and the use of a particular hydrogen-air mixture.

The tests were conducted using certified air-hydrogen mixtures of 0.50, 0.99 and 1.87 percent. However, the 1.87% mixture proved to be questionable. During environmental testing, output voltages indicating that the 1.87% gas mixture was 2.0% or greater were consistently being observed. An investigation of this showed the mixture to be in error. A total of 24 tests were conducted on different detectors using air-hydrogen mixtures of 0.50, 0.99, 1.87 and 1.98%. In all cases, the 1.87% mixture and the 1.98% mixture gave the same, or very close to the same, output values. And in each case, when the data was plotted for the four mixtures and pure air, linearity between the mixtures of 0.00, 0.50, 0.99 and 1.98% was very good, while the 1.87% mixture always fell away from a straight line through the other points. To make the data which was recorded during environmental testing usable, an average was taken of the 24 indicated hydrogen levels from the above tests. This average was 1.99925 percent, which was rounded off to 2.00 percent. Therefore, in the performance curves of system number 3, given in Figure 5-21, a hydrogen level of 2.00 percent is used to present the results.

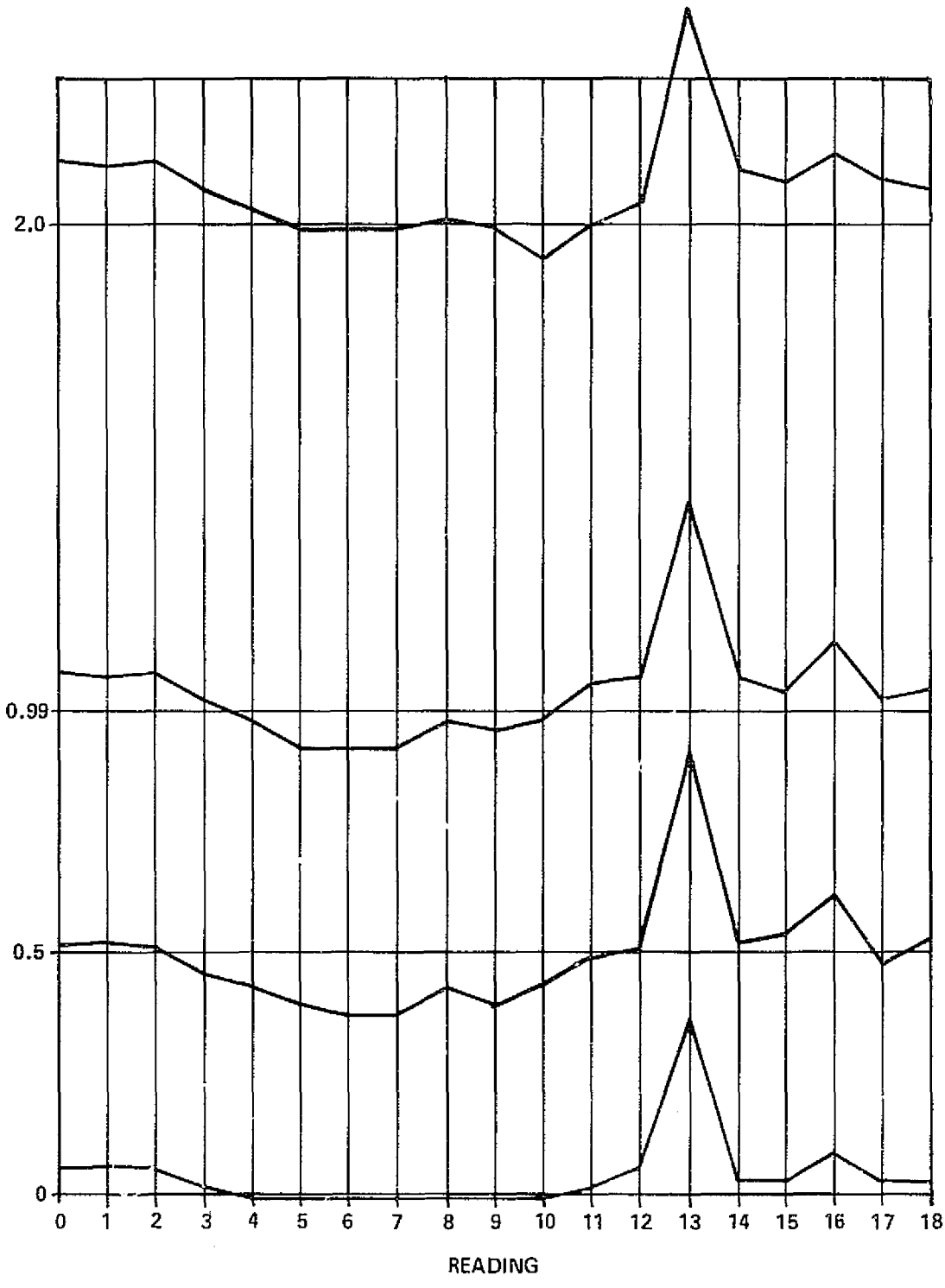

FIGURE 5-21 SYSTEM 3 PERFORMANCE CURVE

The second problem encountered during environmental testing could not be easily rectified. During checkout of detector number 3, prior to environmental testing, system performance appeared normal; however, as environmental testing proceeded, a null shift problem became apparent. Examination of Figure 5-21 shows the problem to be null shift since at any individual set of readings, the linearity is acceptable. During testing when the changes were observed and conditioning did not require hours of chamber time, i.e. high and low pressure, the unit was conditioned and operated on air from within the chamber, then alternately from air external of the chamber and in both cases, the null shift was observed. This indicated that the shift was not environmentally caused. Further support of this was verified with the post salt spray readings. These readings have the greatest deviation from normal and they showed a change in Δf of 19 from the value obtained in detector checkout prior to environmental testing. This was the first time since original detector checkout that the system was back into the laboratory where Δf readings could be verified. There is little doubt that the variations observed during environmental evaluation are the result of null shifts experienced in the fluidic hydrogen sensor and not caused by the environment. To further check this, detector number 3 was operated under ambient conditions each day for four days after the final environmental test, readings 15 through 18 of Figure 5-21, and a null shift was again observed during reading 16. Performance of detector number 3 on an average was within specification as shown in Table 5-2.

Exposure of detector number 4 to a sand and dust environment caused no degradation in performance. System performance before and after the environment is shown in readings 3 and 4, respectively, of Figure 5-12. This testing was performed by an outside laboratory under the procedure given in Appendix F.

Operation of the hydrogen detector with helium background was performed on system 6. This system was selected since it had demonstrated better null stability than detector 3. The detector was subjected to five helium background levels and four hydrogen concentrations at each level. The flow requirements for each gas at the different concentration levels was calculated. To accurately produce these flow rates, a group of orifices were calibrated. This was done by applying a known upstream pressure to an orifice and collecting the output flow

TABLE 5-2

SYSTEM 3 PERFORMANCE

H_2 Concentration (%)	Specification Range (Volts dc)	Mean (Volts dc)	Standard Deviation
0.00	0.000 ± 0.050	0.020	0.030
0.50	0.500 ± 0.050	0.469	0.068
0.99	0.990 ± 0.050	1.010	0.066
2.00	2.000 ± 0.100	2.067	0.059

Compiled from the readings taken during environmental testing of System 3.

in a 400 cc cylindrical flask that was suspended over water. Initially, the flask was filled with water and submerged to the water level. When flow was initiated, the flask was withdrawn so the water level inside the flask was the same as the surrounding water level. This procedure insured that the pressure inside the flask was atmospheric. The time required to fill the flask was timed with a stop watch. Three runs were made for each data point, and the results were averaged to determine the flow rate.

During conduction of these tests, a reduction in output voltage was observed at the higher helium concentrations. At first, it was thought that with larger percentages of helium, there was not enough oxygen present to support complete hydrogen reduction. The amount of air needed for complete reduction was calculated to be less than that present with the maximum helium level. Another consideration was the molecular weight of the gas mixture at high helium concentrations would be less than normal and therefore the fluidic oscillator frequency will increase. This increase in frequency can affect a detector in two areas.

First, if the two fluidic oscillators are not extremely well matched they will not track, or maintain a constant Δf at 0% H_2, as the level of helium increases. To check on this, the signal and reference oscillator frequencies were recorded for the five helium levels with 1.98% H_2 present. Under perfect conditions, the output voltage should remain at 1.98 Vdc; however, with 70% H_e background the output had dropped to 1.466 Vdc. In checking the variations in Δf at the different helium levels, it was found that Δf had changed 11 Hz over an oscillator frequency change of over 6700 Hz. This was considerably better than expected, but did not explain the problem.

The second effect of an increase in oscillator frequency is the resulting change in basic system timing when the reference frequency is changed. From equation (2), Appendix D, it can be seen that as f_r increases, τ_r decreases and therefore, the length of time the timing gate is left open is reduced while all other processor times remain constant. This results in early gate closing and therefore a decrease in output voltage. To verify this, changes in f_r and detector output voltage were

plotted as shown in Figure 5-22. Although these curves do not coincide, they do have considerable similarity, implying that variations in f_r were the primary cause of loss in output. Additional confirmation of this was found by calculating the theoretical output voltage at each helium level for f_r values recorded with a 2% H_2 concentration present. These results are given in Table 5-3. The initial increase in output voltage at five and ten percent helium, in Figure 5-22 and Table 5-3, were caused by the change in Δf. Change in Δf occurred simultaneously with changes in f_r and had a greater effect on output, since the decrease in total gas mass per unit volume was small at the low helium concentrations. To check this, the theoretical f_r was calculated and plotted with the actual f_r, as given in Figure 5-23. Actual f_r increase was slightly lower than theoretical; however, the calculations were based on perfect gas conditions of constant temperature and pressure, which may account for this difference.

These tests demonstrate the hydrogen detector can identify H_2 in an atmosphere with 70% H_e present. At this level, however, the detector experiences a loss in scale factor of approximately 25%. If high helium concentrations are anticipated, this loss can be compensated by the selection of alarm levels.

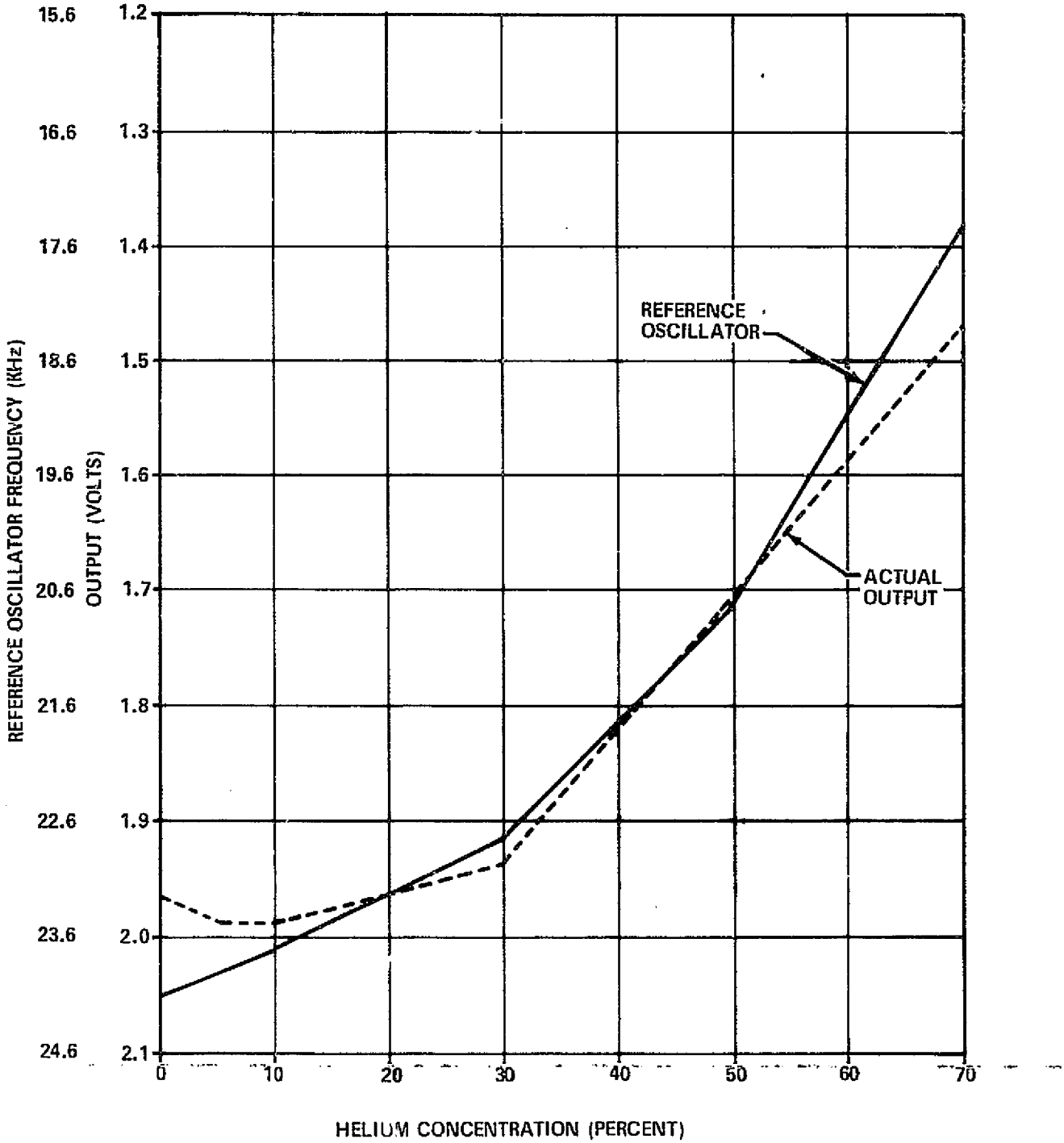

FIGURE 5-22 HELIUM SENSITIVITY

TABLE 5-3
DETECTOR THEORETICAL OUTPUT

H_e Concentration (%)	Recorded f_r (Hz)	Δf (Hz)	$\frac{1}{2}\tau_{g2}$ (Sec)	$37\,\tau_{\Delta f}$ (Sec)	τ_g (Sec)	Number Into D/A	Theoretical Output (VDC)	Actual Output (VDC)
0	16099	127	1.0985	0.2913	0.8072	102.5	2.050	1.964
5	16313	129	1.0835	0.2868	0.7967	1 2.8	2.055	1.983
10	16497	130	1.0714	0.2846	0.7868	102.2	2.046	1.986
30	17429	132	1.0141	0.2803	0.7338	96.9	1.937	1.937
50	19442	134	0.9091	0.2761	0.6330	84.8	1.696	1.700
70	22800	138	0.7752	0.2861	0.5071	69.9	1.399	1.466

Given: $\tau_g = \frac{1}{2}\tau_{g2} - \tau_{g1}$

and $\frac{1}{2}\tau_{g2} = 5M\tau_r$

$\tau_{g1} = JX\tau_{\Delta f}$

and $JX = 37$; $M = 3537$

$\tau_g = \frac{1}{2}\tau_{g2} - 37\tau_{\Delta f}$

The number into the D/A is quantity of Δf pulses which occur in the time of τ_g.

The theoretical output is the number into the D/A times 0.020 volts the D/A scale factor.

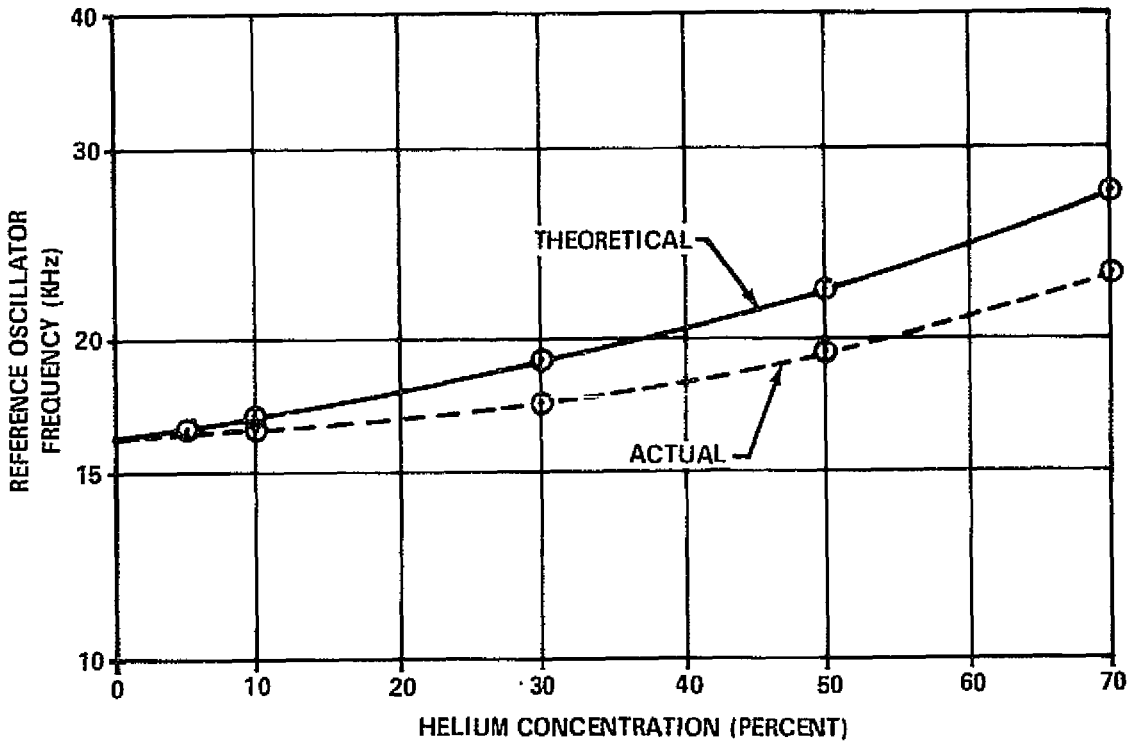

FIGURE 5-23 REFERENCE OSCILLATOR FREQUENCY

SECTION 6
CONCLUSIONS & RECOMMENDATIONS

6.1 CONCLUSIONS

The basic program objective to advance the hydrogen detector development from the engineering prototype stage to the production prototype stage has been achieved. A detector system has been developed which meets the accuracy requirements, is inexpensive to manufacture, easily maintained, insensitive to the KSC environment, relatively unaffected by a helium background, and has demonstrated a long term operational capability.

A detector accuracy of 500 ppm has been demonstrated at hydrogen concentrations up to one percent and within five percent of reading above that level. This accuracy has been repeatable in day-to-day stability evaluation and over long term continuous operation. When produced in large quantities, the system cost will be approximately $1150. Detector maintenance is minimal; i.e., periodic calibrations and annual input filter replacement. These are both accomplished without removing the package cover or disturbing the package installation. Environmental testing demonstrated the hydrogen detector capability to perform in a KSC environment. Evaluation in an atmosphere with a high concentration of helium revealed a small degradation in performance at concentrations above 30 percent.

6.2 RECOMMENDATIONS

If further effort is to be expended on the fluidic hydrogen detector, two primary tasks should be accomplished. First, a method should be developed to bond the eight laminae that comprise each fluidic oscillator. Second, a small sintered metal input filter should be developed which has an absolute rating of 10 microns or less.

During the etching process of the active fluidic elements, which make up the oscillators, tolerances of 0.0002 inch are maintained. These tolerances are necessary to provide a stable oscillator. Oscillator stability is required since only a relatively small change in oscillator frequency is experienced per

percent of hydrogen. Therefore, a change of only a few cycles in one oscillator can produce a relatively large erroneous indication of hydrogen. For example, if a fluidic sensor provides a difference of 40 Hz per percent hydrogen, then a 4 Hz change in one oscillator gives a 0.1% error in the hydrogen level detected. In this sensor where the error is to be less than 500 ppm, or 0.05%, that means the two oscillator frequencies cannot change, relative to each other, more than 2 Hz. This extremely tight tolerance demands stable oscillators. It is believed the zero shift, experienced with some detectors, would be minimized if the oscillator laminae were bonded. Bonding would eliminate minute creeping or slippage between laminae which can now occur primarily during the thermal cycling from turn on to turn on.

Investigations to establish the cause of null shift experienced with five sensors used for long term environmental evaluation revealed a contamination deposit in all fluidic oscillators. From numerous studies on the effect of contamination within fluidic elements, performed by MDAC TICO, it is known that a contamination buildup affects oscillator frequency. Extreme cases have displayed an increase in frequency of 800 percent. Again, in our application a relative frequency change of only 2 Hz is acceptable. Therefore, any method to reduce the contamination rate will extend the operational life.

During evaluation of the filters used in the five sensors the manufacturer of these filters was contacted and the filtration level established at a nominal rating of 50 microns. A general rule of thumb for most filters is an order of magnitude increase in rating from nominal to absolute; therefore, the filters were considered to be 500 micron absolute filters. Further investigation indicated that two to five micron nominal filters were the smallest sintered metal filters available.

To minimize contaminant buildup rate in the fluidic oscillators, it is recommended that a sintered metal filter be developed which has an absolute rating between 5 and 10 microns.

Interest in a hydrogen detector which did not require a vacuum source was expressed late in the program. If this becomes a requirement, a small vacuum pump could be utilized in each detector to provide pneumatic power. This pump should be capable of maintaining 6.125 psia at a flow rate of 2200 sccm.

APPENDIX A
HYDROGEN SENSOR THEORY

The development of the hydrogen sensor theory will be based on inviscid flow since it has been shown that this is a valid and reasonably accurate assumption which also considerably simplifies the mathematics without sacrificing an understanding of the principles.

It has been shown that the frequency of a fluidic oscillator is proportional to the speed of sound in the working gas. This can be stated as:

(1) $F = C\sqrt{K/M}$

Where: F = oscillator frequency
K = ratio of the specific heats of the gas
M = molecular weight of the gas
C = constant, of proportionality, depending upon the oscillator physical parameters and the temperature

For hydrogen and air:

$K_{H_2} \approx K_{air} = 1.4$

Therefore, for a given oscillator at a specific temperature:

(2) $F_{air} = C_1\sqrt{\frac{1}{M_{air}}}$ where $C_1 = \sqrt{1.4}\ C$

(3) $F_{(air + H_2)} = C_1\sqrt{\frac{1}{M_{(air + H_2)}}}$

(4) $F_{(air + H_2)} = F_{air}\sqrt{\frac{M_{air}}{M_{(air + H_2)}}}$

which can be restated for the signal oscillator as:

(5) $F_s = F_{so}\sqrt{\frac{M_{air}}{M_{(air + H_2)}}}$

Where: F_s = frequency of the signal oscillator on any air + hydrogen mixture
F_{so} = frequency of the signal oscillator on air only

In this application the reference oscillator operates on the exhaust products of a catalytic converter. Therefore, the equation for the reference oscillator can be written as:

$$(6) \quad F_r = F_{ro}\sqrt{\frac{M_{air}}{M_{exh.\ gas}}}$$

Where: F_r = frequency of the reference oscillator for any air + hydrogen mixture entering the catalytic converter
F_{ro} = frequency of the reference oscillator on air only

$$(7) \quad \frac{F_s}{F_r} = \frac{F_{so}}{F_{ro}}\sqrt{\frac{M_{exh.\ gas}}{M_{(air + H_2)}}}$$

Since the mass of the gas passing through the catalytic converter does not change, a mass balance equation can be written as:

$$(8) \quad M_{exh.\ gas} = \frac{Mass_{(exh\ gas)}}{Moles_{(exh\ gas)}} = \frac{Mass_{(air + H_2)}}{Moles_{(exh\ gas)}}$$

If a mole of an air and hydrogen mixture enters the system, then CH_2 moles of H_2 enter the catalytic converter, where CH_2 is the concentration of hydrogen by volume. The reaction in the converter is:

$$(9) \quad H_2 + 1/2\ O_2 \rightarrow H_2O$$

which, when expressed in terms of molar concentrations, becomes:

$$(10) \quad CH_2(H_2) + 1/2\ CH_2(O_2) \rightarrow CH_2(H_2O)$$

Therefore, the number of moles of exhaust gas is $1/2\ CH_2$ less than the one mole of the air and hydrogen mixture that entered the system. Then:

$$(11) \quad M_{exh\ gas} = \frac{Mass_{(air + H_2)}}{1-1/2\ CH_2}$$

Since the mass is equal to the molecular weight for 1 mole, one can state:

$$(12)\quad M_{exh\ gas} = \frac{M_{(air + H_2)}}{1\text{-}1/2\ CH_2}$$

Substituting this value in Eq. (7):

$$(13)\quad \frac{F_r}{F_s} = \frac{F_{ro}}{F_{so}} \sqrt{1\text{-}1/2\ CH_2}$$

Thus, the frequency ratios are related by the function $\sqrt{1\text{-}1/2\ CH_2}$ and are independent of the composition of the input gas. Therefore, additional gases in the input mixture, such as helium, should not affect the accuracy of the instrument as long as there is sufficient air (oxygen) in mixture to support reaction of Eq. (9). If this function is plotted against the hydrogen concentration, as in Figure A-1, an approximately linear function results. From this figure, it can be seen that:

$$\sqrt{1\text{-}1/2\ CH_2} = \frac{\%H_2 + K}{K} \qquad \text{Where } K = -397.48155$$

Substituting in Eq. (13) the following relationship is obtained:

$$\frac{F_r}{F_s} = \frac{F_{ro}}{F_{so}} \left(\frac{\%H_2 + K}{K}\right)$$

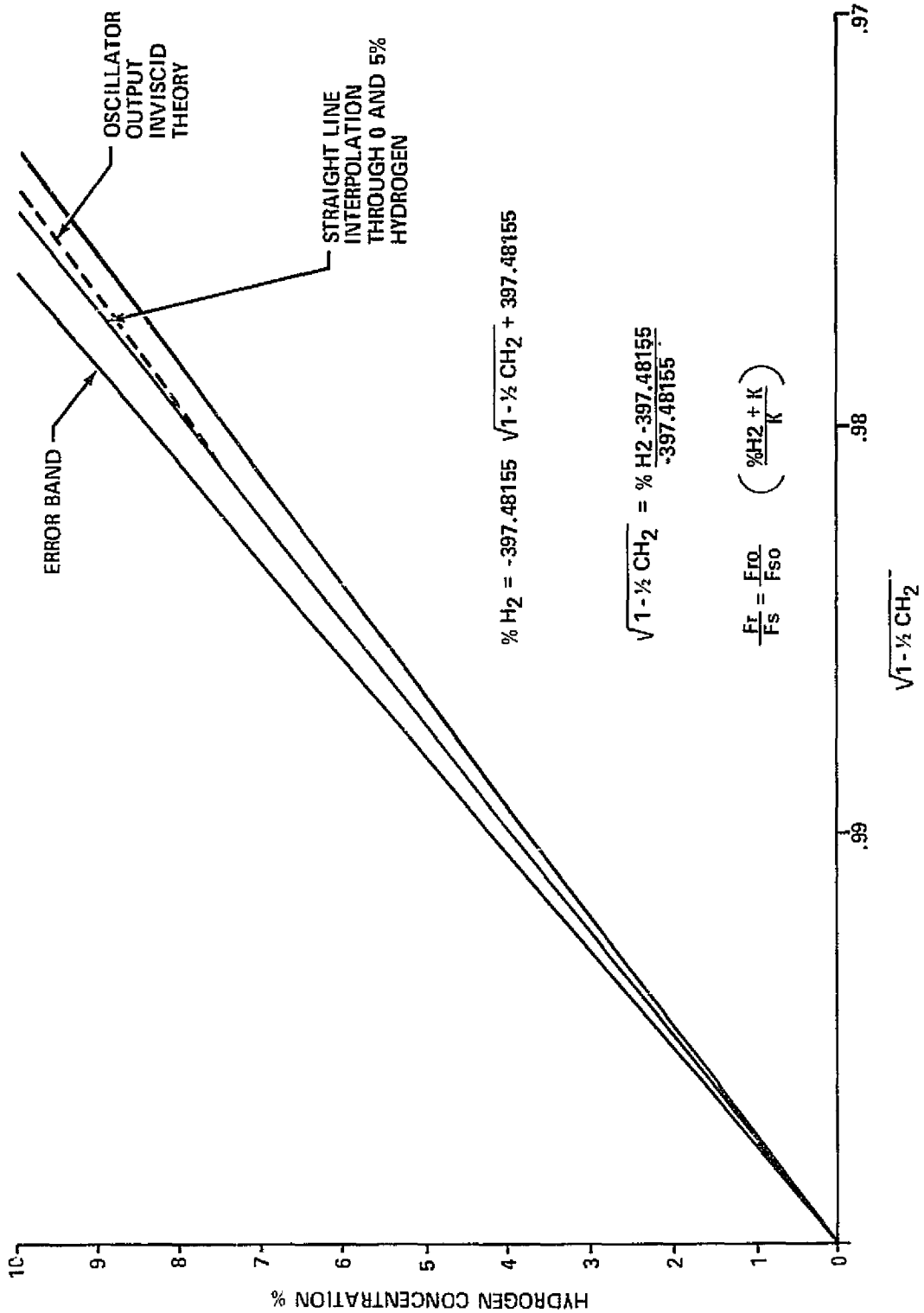

FIGURE A-1 LINEAR APPROXIMATION FOR OSCILLATOR OUTPUT

APPENDIX B
MANIFOLD DRAWINGS

Drawings of the fluidic hydrogen sensor manifold blocks are presented in this appendix to provide a complete understanding of flow paths and component locations.

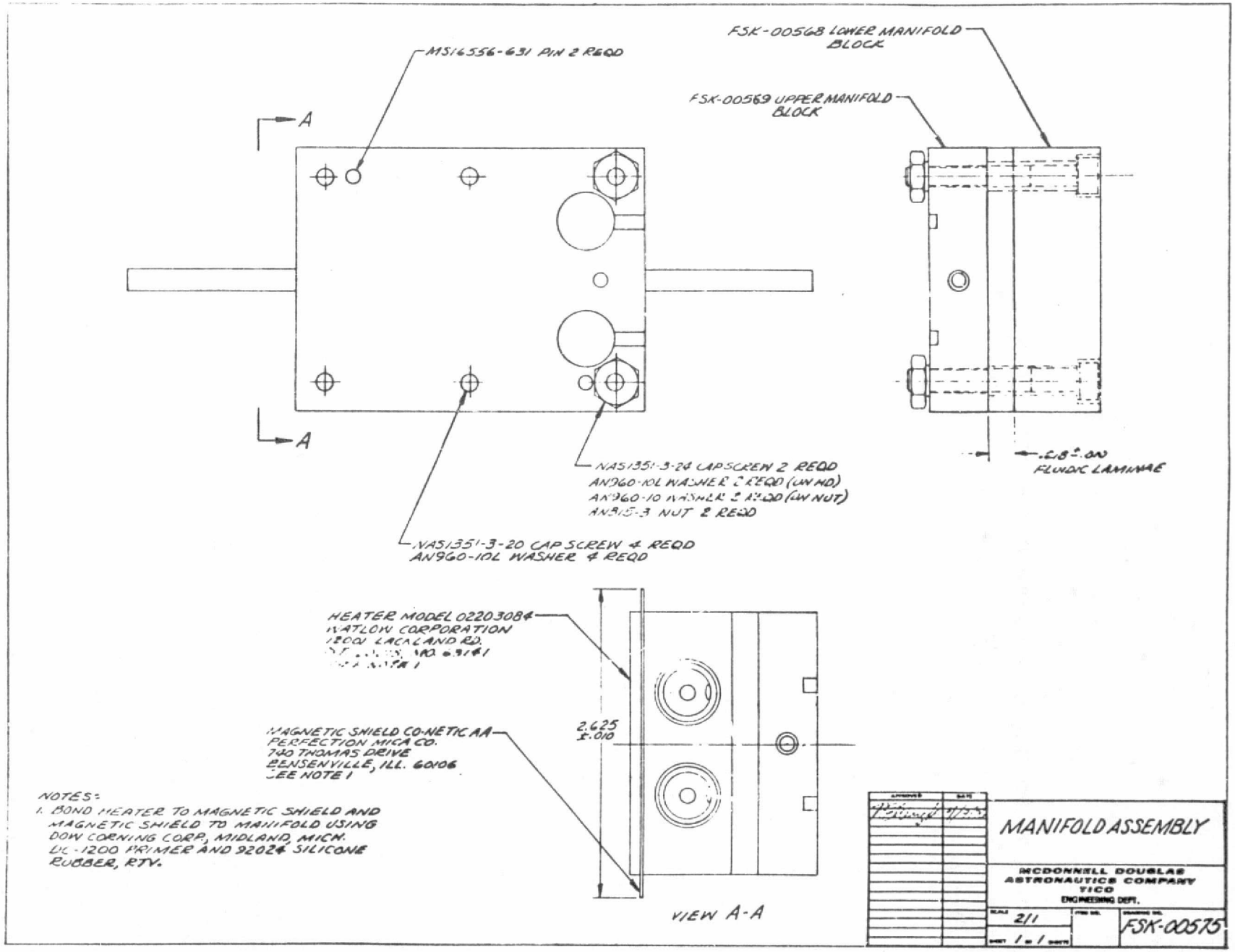

FIGURE B-1

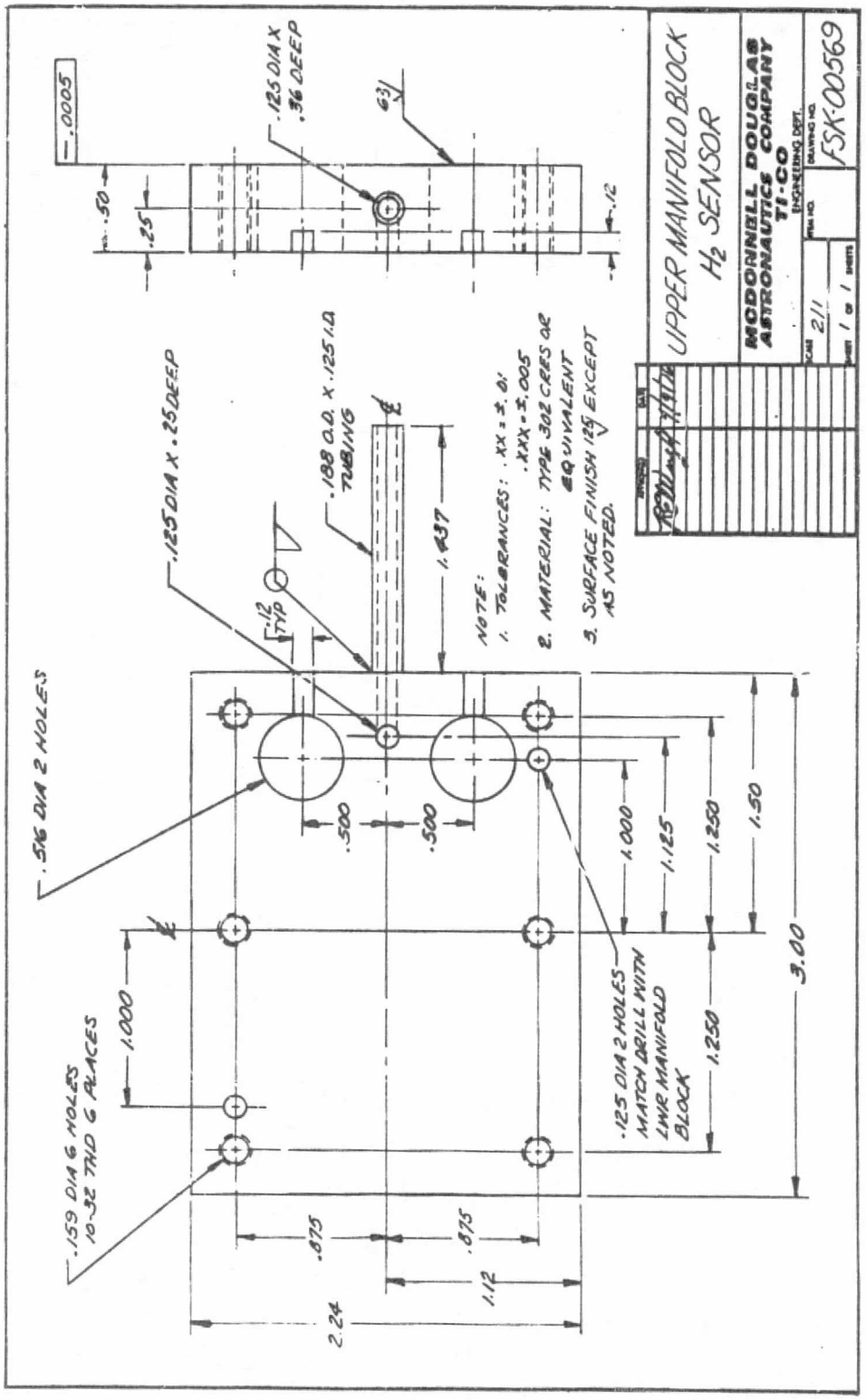
UPPER MANIFOLD BLOCK
H2 SENSOR
MCDONNELL DOUGLAS ASTRONAUTICS COMPANY ST-CO
FSK-00569
.125 DIA X .36 DEEP
.188 O.D. X .125 I.D TUBING
.125 DIA X .25 DEEP
.56 DIA 2 HOLES
.159 DIA 6 HOLES 10-32 THD 6 PLACES
.125 DIA 2 HOLES MATCH DRILL WITH LWR MANIFOLD BLOCK
NOTE:
1. TOLERANCES: .XX = ±.01
.XXX = ±.005
2. MATERIAL: TYPE 302 CRES OR EQUIVALENT
3. SURFACE FINISH 125 EXCEPT AS NOTED.

FIGURE B-2

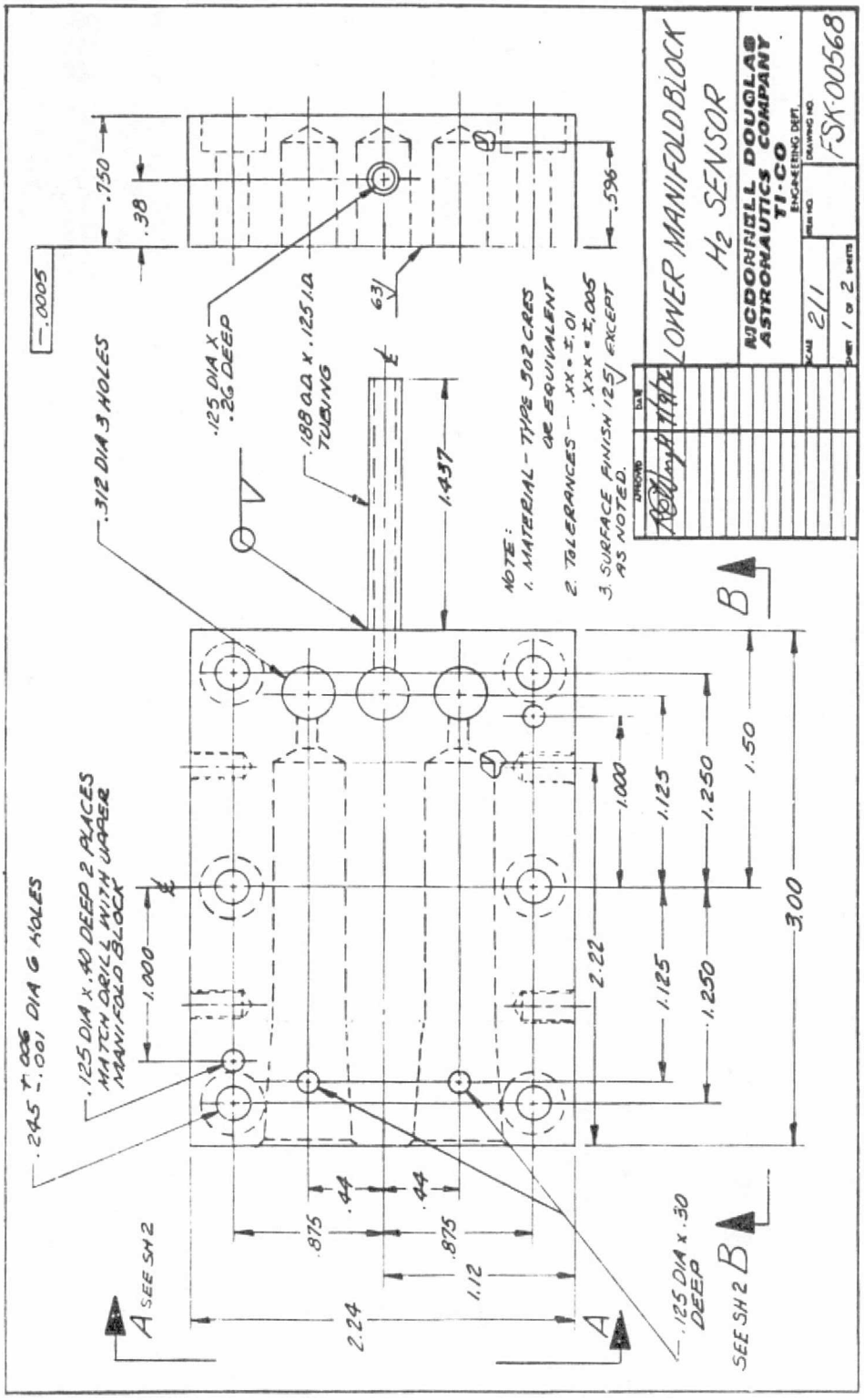
LOWER MANIFOLD BLOCK
H2 SENSOR
MCDONNELL DOUGLAS ASTRONAUTICS COMPANY
TI·CO
FSK-00568
.750
.38
.0005
.125 DIA X .26 DEEP
.188 OD X .125 ID TUBING
.312 DIA 3 HOLES
1.437
63
.596
NOTE:
1. MATERIAL - TYPE 302 CRES OR EQUIVALENT
2. TOLERANCES - .XX = ±.01 .XXX = ±.005 EXCEPT AS NOTED.
3. SURFACE FINISH 125 EXCEPT
.245 +.006 -.001 DIA 6 HOLES
.125 DIA X .40 DEEP 2 PLACES MATCH DRILL WITH MANIFOLD BLOCK
1.000
2.22
1.000
1.125
1.250
1.50
3.00
1.125
1.250
.875
.44
.44
.875
1.12
2.24
A
SEE SH 2
B
.125 DIA X .30 DEEP
SEE SH 2

FIGURE B-3

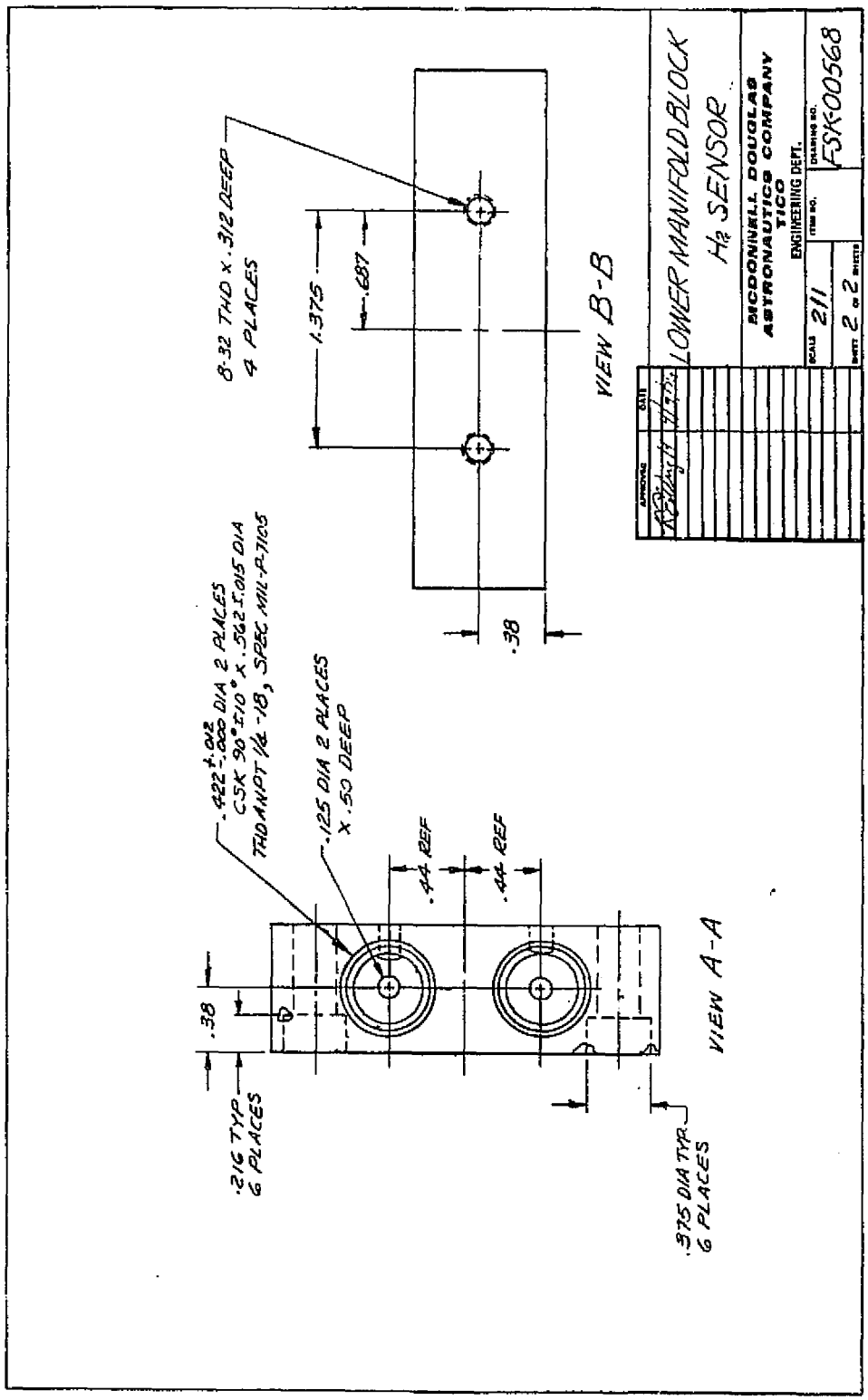
8-32 THD x .312 DEEP
4 PLACES
1.375
.687
VIEW B-B
.38
.422 +.002 -.006 DIA 2 PLACES
CSK 90° ±10° x .562 ±.015 DIA
THD ANPT ½-18, SPEC MIL-P-7105
.125 DIA 2 PLACES
X .50 DEEP
.44 REF
.44 REF
.38
.216 TYP
6 PLACES
.375 DIA TYP
6 PLACES
VIEW A-A
LOWER MANIFOLD BLOCK
H2 SENSOR
MCDONNELL DOUGLAS
ASTRONAUTICS COMPANY
TICO
ENGINEERING DEPT.
SCALE 2/1
SHEET 2 OF 2 SHEETS
FSK00568

FIGURE B-4

APPENDIX C
SCHEMATICS

Schematics of each printed circuit card and package wiring are given in this appendix. Photographs of each printed circuit card are provided with active circuit components identified. The photographs are included to aid in the translation from schematic to hardware when locating components.

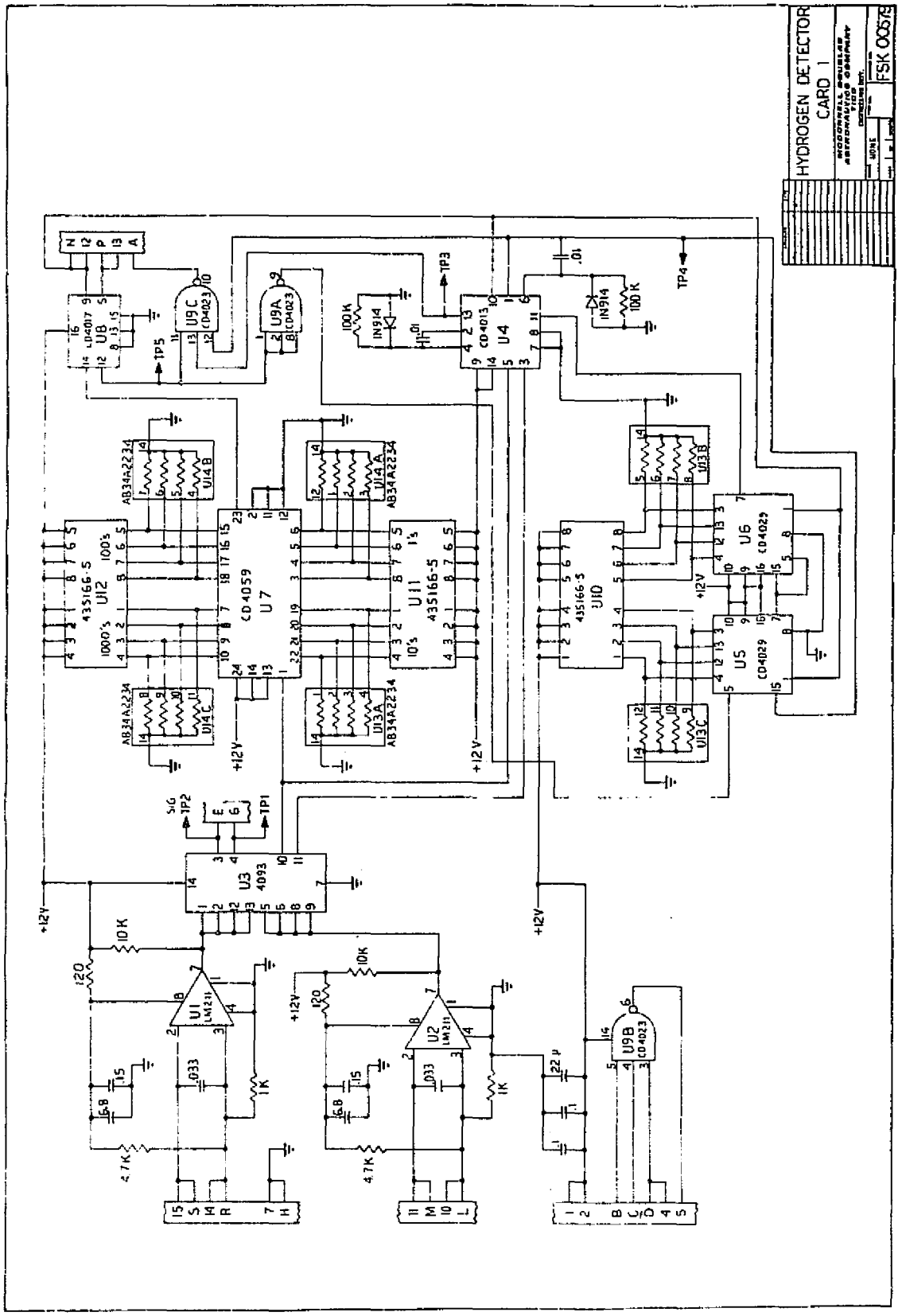
HYDROGEN DETECTOR
CARD 1
FSK 00575
U1
U2
U3
4093
U4
CD4013
U5
CD4029
U6
CD4029
U7
CD4059
U8
CD4017
U9A
CD4023
U9B
CD4023
U9C
CD4023
U10
U11
U12
U13A
U13B
U13C
U14A
U14B
U14C
AB34A2234
435166-5
IN914
100K
10K
1K
4.7K
.033
.15
.68
.01
22 µ
+12V
TP1
TP2
TP3
TP4
TP5
SIG

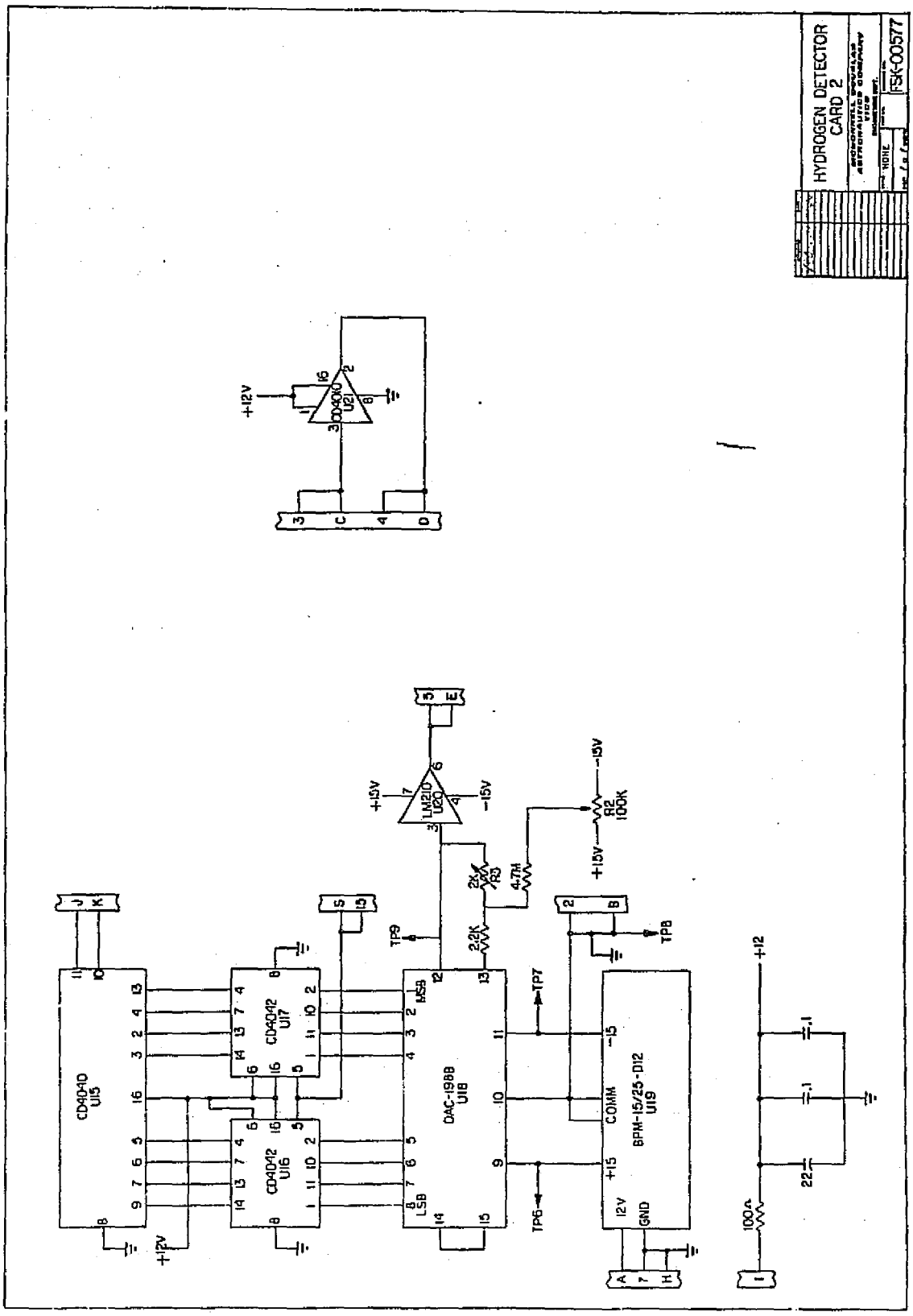

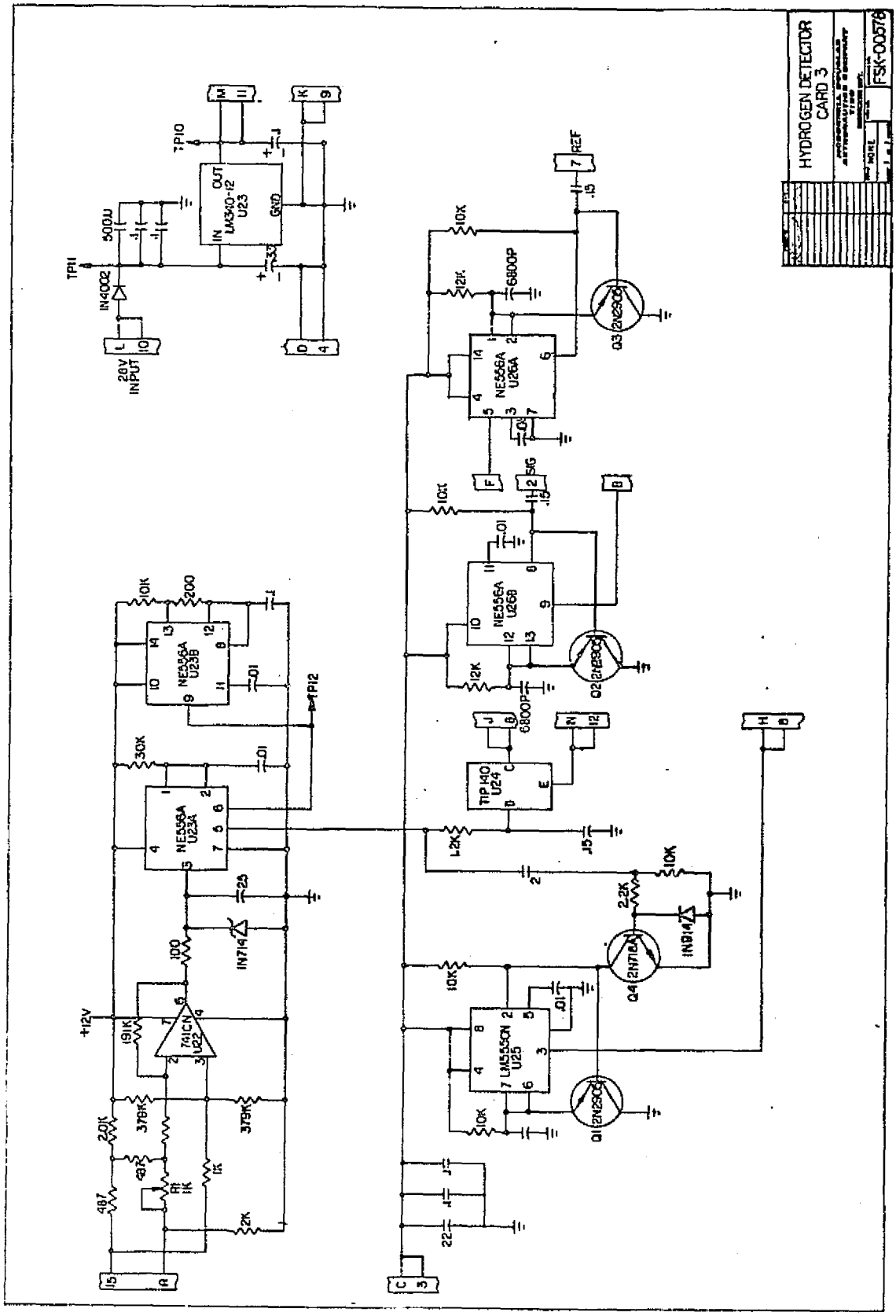
HYDROGEN DETECTOR
CARD 3
FSK-00578
TP10
TP11
TP12
500U
IN4002
28V
INPUT
LM340-12
U23
OUT
IN
GND
REF
10K
12K
6800P
Q3 (2N2907)
NE556A
U26A
.01
.15
5K
Q2 (2N2907)
U26B
200
30K
2.5K
TIP140
U24
Q4 (2N718A)
IN914
25
100
IN714
+12V
191K
741CN
U22
LM555CN
U25
Q1 (2N2907)
2.01K
378K
49K
1K
487
22

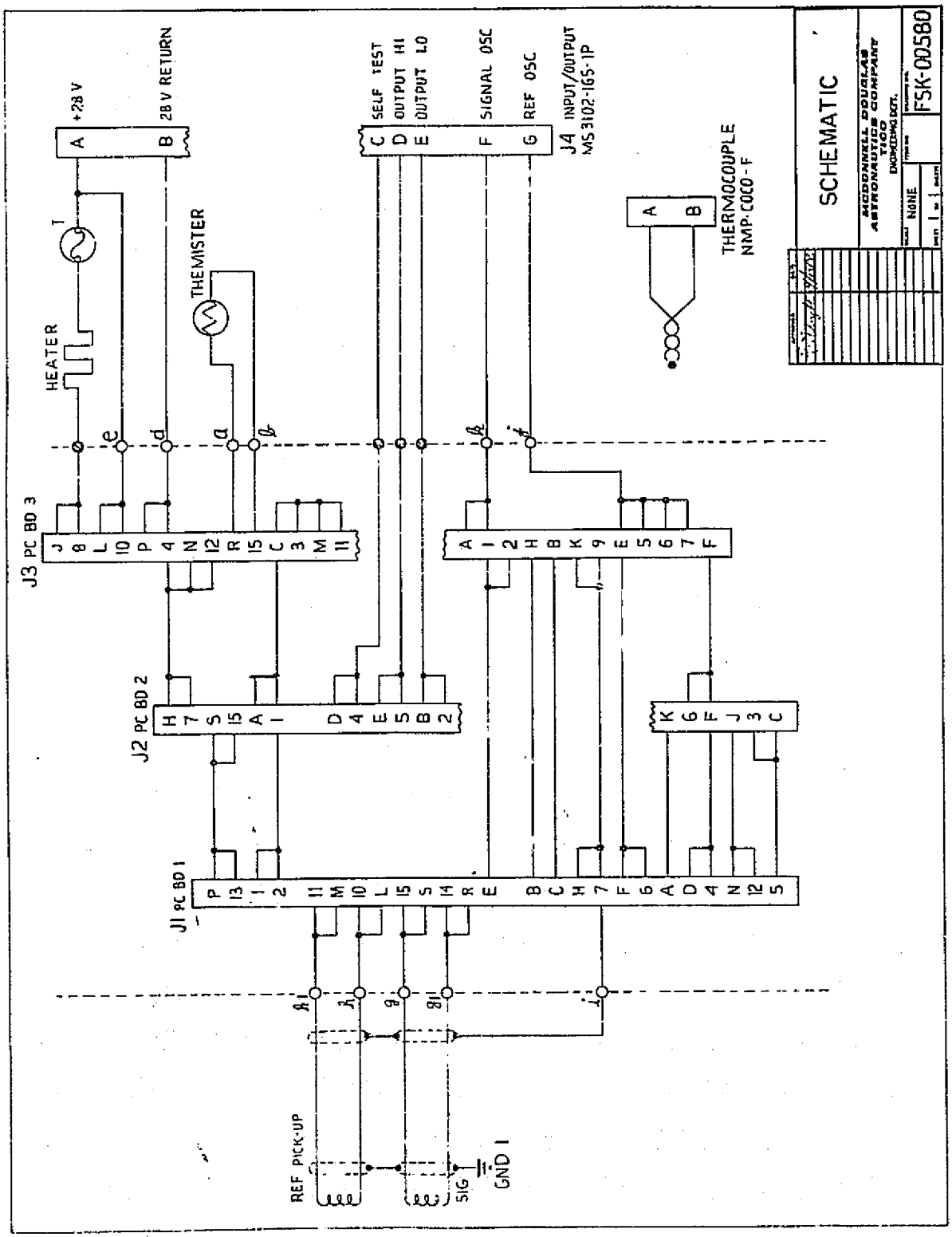
SCHEMATIC
FSK-00580
+28 V
28 V RETURN
SELF TEST
OUTPUT HI
OUTPUT LO
SIGNAL OSC
REF OSC
J4 INPUT/OUTPUT
MS 3102-16S-1P
THERMOCOUPLE
NMP-COCO-F
HEATER
THERMISTER
J3 PC BD 3
J2 PC BD 2
J1 PC BD 1
REF PICK-UP
SIG
GND 1

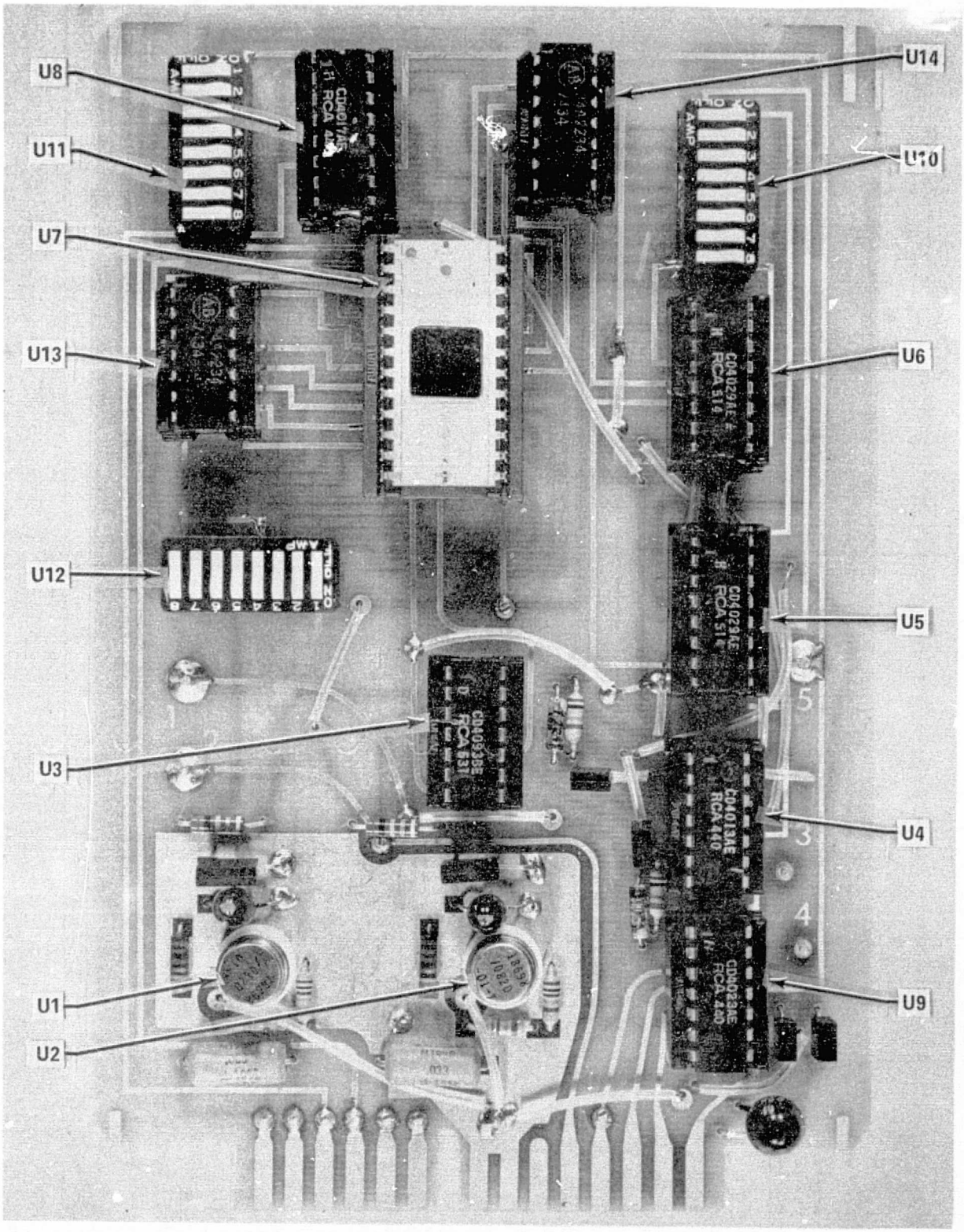

CARD 1

CARD 2

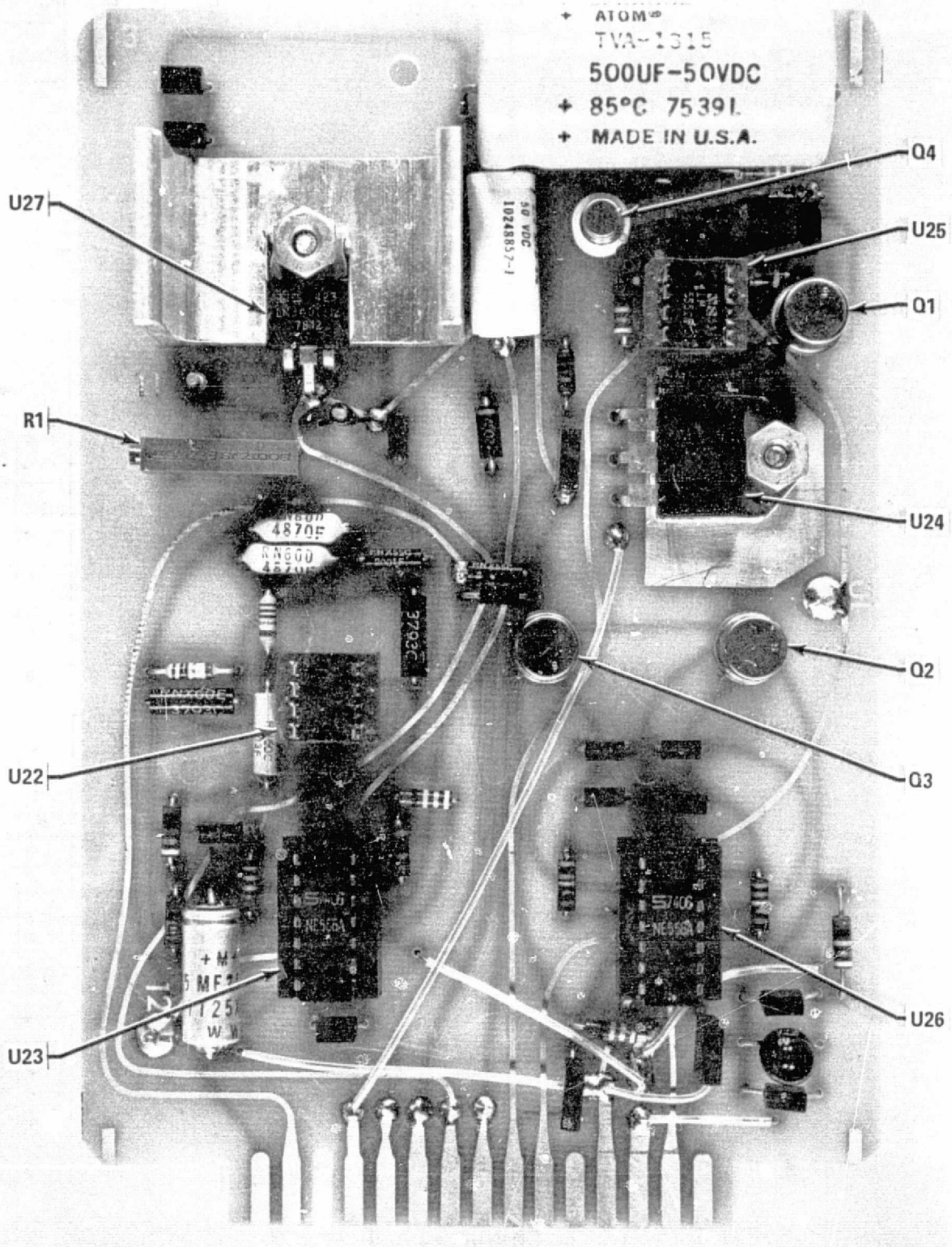
+ ATOM®
TVA-1315
500UF-50VDC
+ 85°C 75391
+ MADE IN U.S.A.
50 VDC
U27
Q4
U25
Q1
R1
U24
Q2
U22
Q3
U26
U23

CARD 3

APPENDIX D
PROCESSOR ELECTRONICS OPERATION

Operation of the timing gate, used to control the quantity of difference frequency (Δf) pulses reaching the output digital to analog convertor (D/A), is the heart of the processor electronics. System requirements for an output voltage of 1 Vdc per 1% H_2 coupled with the selected D/A dictate that the D/A input scale factor must be a binary value of 50 per 1% H_2. Therefore, the timing gate control signals must open the gate for a time equal to 50 times the period of one Δf cycle, times the percent of hydrogen present, or:

$$\tau_g = 50H\tau_{\Delta f} \qquad (1)$$

where: τ_g = time gate is open

H = percent hydrogen concentration

$\tau_{\Delta f}$ = period of Δf

The duration of τ_g is a function of both τ_{g1} and τ_{g2} control signals, as shown in Figure D-1. The expression for τ_{g2} is:

$$\tau_{g2} = 10M\tau_r \qquad (2)$$

where: τ_{g2} = period of one cycle of control 2 input frequency

τ_r = period of reference frequency

M = number selected by M switches

The expression for the delay in τ_{g1} coming on is:

$$\tau_{g1} = JX\tau_{\Delta f} \qquad (3)$$

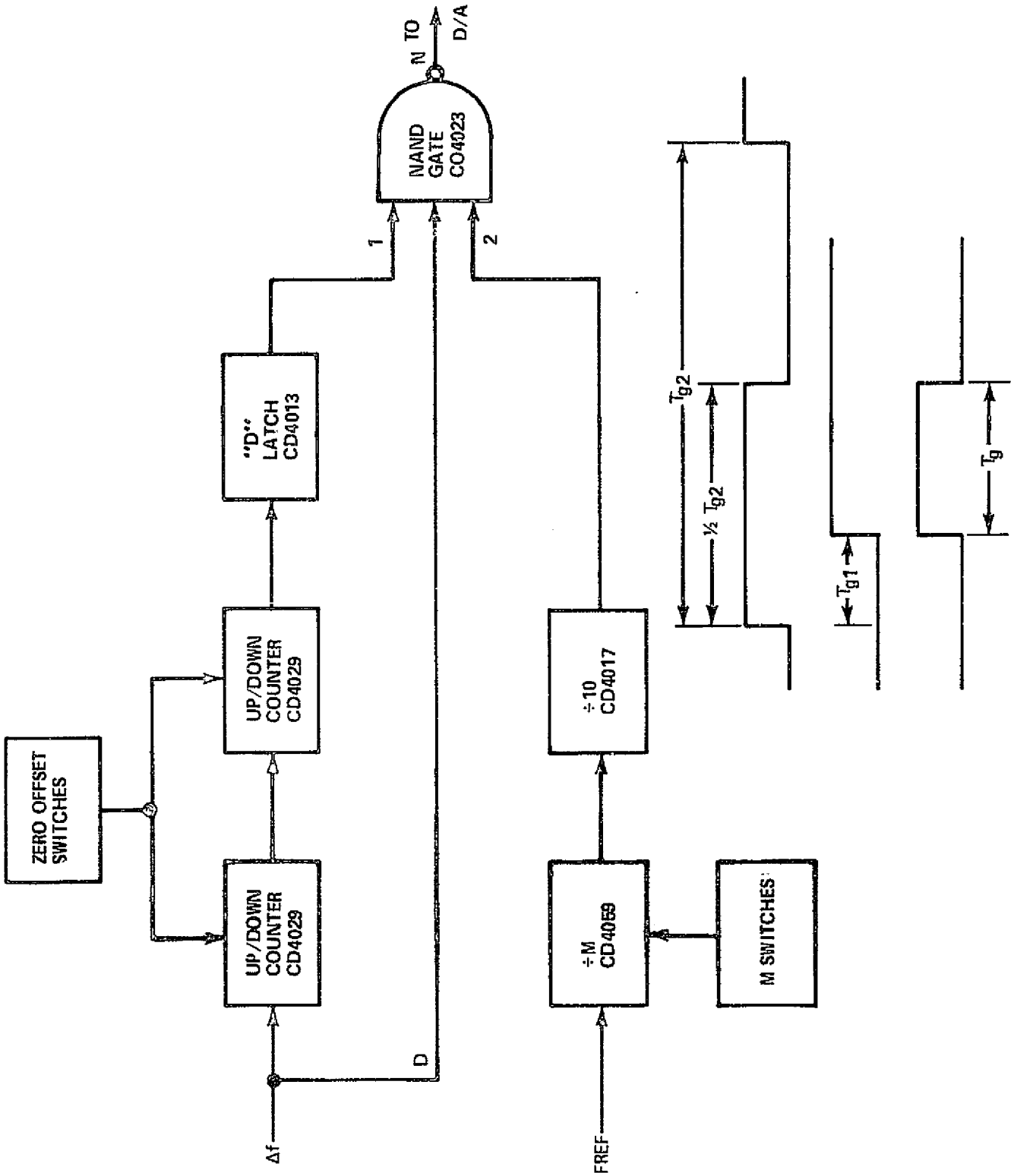

FIGURE D-1 TIMING GATE

where: τ_{g1} = delay period from rise of τ_{g2} to rise of τ_{g1}

$\tau_{\Delta f}$ = period of Δf

X = Δf at 0% H_2

J = system gain factor

Gain factor (J) is the ratio between the scale factor of the D/A input (N) and the scale factor of the fluidic sensor output (D) or:

$$J = \frac{N}{D} \tag{4}$$

where: N = binary number into the D/A/1% H_2 to achieve proper output, in present application N = 50

D = Δf/1% H_2 from the fluidic sensor

System gain is achieved in the processor by applying this gain factor to the difference frequency signal. The weighting of Δf pulses by the factor J causes the gate control times to be increased such that J times D Δf pulses pass through the timing gate. This means the electronics has made the fluidic hydrogen scale factor (D) equal to the D/A input scale factor (N).

From the timing diagram:

$$\tau_g = \frac{1}{2}\tau_{g2} - \tau_{g1} \tag{5}$$

where: τ_g = time gate is open

Substituting equations (1) (2) and (3) in (5):

$$50H\tau_{\Delta f} = 5M\tau_r - JX\tau_{\Delta f} \tag{6}$$

At 0% H_2, H = 0

$$0 = 5M\tau_r - JX\tau_{\Delta f}$$

or $$5M\tau_r = JX\tau_{\Delta f}$$

Solving for M:

$$M = \frac{JX\tau_{\Delta f}}{5\tau_r}$$

Also at 0% H_2, X = Δf by definition, $\tau_r = \frac{1}{f_r}$ and $\tau_{\Delta f} = \frac{1}{\Delta f}$

Substituting $$M = \frac{J\Delta f\ f_r}{5\Delta f}$$

or $$M = \frac{Jf_r}{5} \qquad (7)$$

Equation (7) becomes the method of determining the M switch settings when calibrating a system.

Equation (3) was introduced earlier; however, implementation was not discussed. Figure D-1 shows Δf pulses entering two up/down counters, which also have an input from the zero set switches. These counters, used in the count up mode, will provide an output level change when switch inputs plus some quantity of Δf pulses total 255. The function of this circuit is to delay the start of τ_g for a period of time equal to the period of $X\Delta f$ pulses, times the system gain factor, or:

$$\tau_{gl} = JX\tau_{\Delta f}$$

The zero offset switches are connected to the up counter jam inputs, and each time the counters are reset the switch values are preset into them. Mathematically, the output goes high when:

$$Z + JX = 255 \qquad (8)$$

where: Z = number selected by zero offset switches,

and the time it takes for this to occur is $JX\tau_{\Delta f}$. Rewriting equation (7) gives the method of selecting the zero offset switch values.

$$Z = 255 - JX \qquad (9)$$

To show how equations (7) and (9) are used to calibrate a system, typical system parameters will be assumed. From initial testing of a system the reference frequency, difference frequency at 0% H_2 and change in difference frequency per percent hydrogen are known. Therefore:

Let, $f_r = 16$ kHz
$X = 60$
$D = 45$

And from the chosen D/A and output scale factor

$$N = 50$$

From equation (4)

$$J = \frac{N}{D} = \frac{50}{45} = 1.1111$$

From equation (7) the ÷M switch values are:

$$M = \frac{J\, f_r}{5} = \frac{1.1111 \times 16{,}000}{5}$$

$$M = 3556$$

From equation (9) the zero offset switch values are:

$$Z = 255 - JX$$
$$Z = 255 - 1.1111 \times 60$$
$$Z = 188$$

Eight switches are provided in component U10 where the values for Z are inserted as a binary number, with switch no. 8 the most significant bit. Values of M are inserted in the switches of components U11 and U12. These values are entered as a binary coded decimal as follows:

Component	Switches	LSB	MSB	Value
U12	5,6,7,8	5	8	1000
U12	1,2,3,4	1	4	100
U11	5,6,7,8	5	8	10
U11	1,2,3,4	1	4	Units

TABLE D-1
M SWITCH FUNCTIONS

To demonstrate the effect of different hydrogen concentrations on system timing, Table D-2 has been developed using the assumed values from above.

TABLE D-2 SYSTEM TIMING TABLE

$\%H_2$	Signal Frequency	Reference Frequency	Δf	Pulses Required at D/A	$\frac{1}{2}\tau_{g2}$ [Sec]	τ_{gl} [Sec]	τ_g [Sec]	$\tau_{\Delta f}$ [Sec]	Pulses Reaching D/A
0	16060	16000	60	0	1.11125	1.11110	0.00015	0.01667	0.009
1	16105	16000	105	50	1.11125	0.63491	0.47634	0.009524	50.01
2	16150	16000	150	100	1.11125	0.44444	0.66681	0.006667	100.02

Given or calculated constants:

X = 60

D = 45

J = 1.1111

M = 3556

Z = 188

The number of pulses passing through the a gate to reach the D/A will be:

$$\frac{\tau_g}{\tau_{\Delta f}}$$

APPENDIX E
CONTAMINANT ANALYSIS

MICROCHEMICAL ANALYSIS SECTION
SO-LAB-32, Room 1274, O&C Building
NASA/KSC
Oct. 8, 1975

SUBJECT: Analysis of Contaminants on Oscillator Plates

LABORATORY REQUEST NO: MAS-6734

RELATED DOCUMENTATION: DAAH01-68-C-0282

1.0 Foreword

1.1 Requester: R. Wright/MDAC/267-4100 Ext. 7467

1.2 Requester's Sample Description: Dirt on oscillator plates
(1) Top, #1 and #4 (2 Plates Each)
(2) Bottom, #1 and #4 (2 Plates Each)

1.3 Requested: (1) Chemical analysis of contaminant
(2) SEM for rough estimate of particle size

2.0 Chemical Analysis and Results

2.1 Procedure

(1) The contaminant on each of the plates was noted to consist of dark and light zones.

A composite sample of each of these zones was randomly selected from the contaminated surface region of each pair of plates and was analyzed by an electron microprobe technique.

(2) X-Ray diffraction analysis was performed on a composite sample of light and dark zone contaminant from the Top #4 Plates.

(2) SEM was performed on the Top #4 Plates.

2.2 Results

2.2.1 Electron Microprobe Analysis

(1) Four Composite Samples of Contaminant From Light Zone:

Top #1 Plates, Top #4 Plates, Bottom #1 Plates, Bottom #4 Plates

All four samples generally similar, containing heterogeneous major S, Si; low major to strong minor Ca, Cl, Fe, K; low minor to strong traces Cr, Ni; traces Cu, Zn, Ti; and possible traces of Pd.

(2) Four Composite Samples of Contaminant From Dark Zone:

Top #1 Plates, Top #4 Plates, Bottom #1 Plates, Bottom #4 Plates.

All four samples generally similar; containing heterogeneous major S, Fe, Si, Ca; low major to strong minor K; minor to trace Cr, Ni; traces Cu, Zn, Ti, Cl; and possible traces of Pd.

A comparison of element relative concentrations in the light and dark contaminant zones reveals the following differences:

Light Zones: Relatively greater Cl concentration; lower Fe, Cr, Ni concentrations.

Dark Zones: Relatively greater Fe, Cr, Ni concentrations; lower Cl concentration.

2.2.2 X-Ray Diffraction Analysis

(1) Composite sample of light and dark zone contaminants, Top #4 Plates.

A computer search of the X-ray data suggests the following possibilities:

1. FeS_2
2. $(NH_4)_2Fe(SO_3)_2 \cdot H_2O$

2.2.3 SEM Examination of Contaminant on Top #4 Plate

(1) The single particles range in size from approximately 0.5 microns to 3.0 microns.

(2) Particle clusters range in size from approximately 3.0 microns to 20.0 microns in their longest dimension.

(3) The bulk of the particles measure between 0.5 and 3.0 microns.

(Photomicrographs are attached to report)

3.0 Conclusions

3.1 The oscillator plate contaminants are speculated to consist primarily of an aggregate of environmental debris and steel corrosion products. The observed element distributions and relative concentrations in the contaminant suggest the following:

(a) Principal Environmental Debris: Sand (SiO_2), Salt (NaCl), Coquina ($CaCO_3$).

(b) Principal Steel Corrosion Products: Iron oxides, iron sulfides.

3.2 The bulk of the particles comprising the contaminant range in size from approximately 0.5 microns to 3.0 microns.

Particles clusters, ranging in size from approximately 3.0 microns in their longest dimension, were also observed in the contaminant population.

Chemist: _____
R. Burton

Approved: _____
J. F. Jones

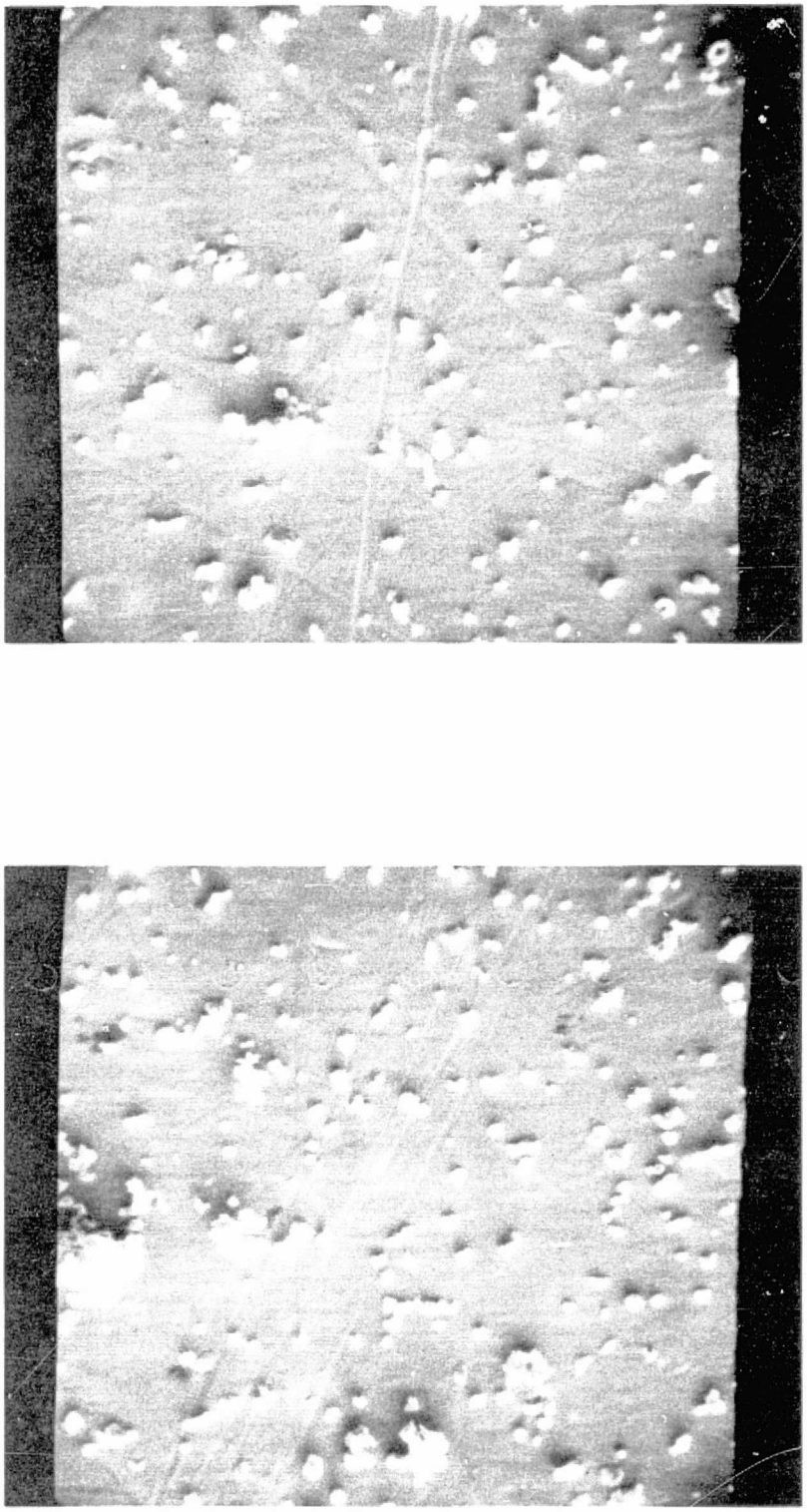

FIGURE E-1 1090 MAGNIFICATION

APPENDIX F
ENVIRONMENTAL TEST PROGRAM

Environmental testing was conducted to demonstrate the ability of the design verification detector to sense the required range of hydrogen concentrations in a simulated launch environment.

Prior to each environmental test described below the design verification sensor was subjected to a baseline performance test. In this test the unit was supplied with calibrated mixtures of air and hydrogen of 0.5, 0.99 and 1.87% H_2 and the output recorded.

The environments to which the design verification sensor was subjected and the procedure used for each environment are:

1. Temperature
   a) Place the test item in the test chamber with applicable instrumentation.
   b) Raise the test chamber to 150°F and maintain until temperature stabilization is attained; run the unit at a minimum of three hydrogen levels and record performance.
   c) Return the test item, nonoperating, to standard ambient conditions and restabilize.
   d) Repeat baseline test.
   e) Place the test item in the test chamber with applicable instrumentation.
   f) Lower the test chamber to 0°F and maintain until temperature stabilization is attained, run the unit at a minimum of three hydrogen levels and record performance.
   g) Return test chamber to ambient conditions and stabilize.
   h) Repeat baseline test.

2. Pressure
   a) Place the test item in the test chamber with applicable instrumentation.
   b) Increase pressure in chamber to 31 in. Hg absolute, operate unit at a minimum of three hydrogen levels and record performance. Return chamber to ambient.
   c) Repeat baseline test.

d) Return test item to test chamber with applicable instrumentation.

e) Lower pressure in test chamber to 29 in. Hg absolute, operate unit at a minimum of three hydrogen levels and record performance. Return chamber to ambient.

f) Repeat baseline test.

3. Humidity

a) Place test item in humidity chamber with applicable instrumentation.

b) Gradually raise internal chamber temperature to 100°F and the relative humidity to 95% over a period of two hours.

c) Maintain condition for not less than six hours.

d) Maintain 80% relative humidity, or greater, and reduce internal chamber temperature to 80°F for 16 hours.

e) Operate unit at a minimum of three hydrogen concentrations, record data. Return chamber to ambient.

f) Repeat baseline test.

4. Dust

The dust test will be performed using equivalent 140 mesh silica flour.

a) Place test unit in test chamber at 75°F and less than 22% relative humidity. Adjust air velocity to 1750 $\pm$ 250 feet per minute. Adjust dust feeder to control dust concentration to 0.3 $\pm$ 0.2 grams per cubic foot. Maintain conditions for six hours. Unit nonoperating.

b) Turn off all controls; allow chamber to return to ambient conditions. Remove accumulated dust from test item by brushing, wiping, or shaking; care should be taken to avoid introduction of additional dust into the test item.

c) Operate unit at a minimum of three hydrogen concentrations, record data.

d) Repeat baseline test.

5. Various Gas Backgrounds

Performance of the design verification sensor will be determined for gas mixtures containing H_2, H_e and air as specified in the following table. Percents are by volume.

Test	Air	H_e	H_2
1	Balance	5	0.5
	Balance	5	1.0
	Balance	5	2.0
2	Balance	10	0.5
	Balance	10	1.0
	Balance	10	2.0
3	Balance	30	0.5
	Balance	30	1.0
	Balance	30	2.0
4	Balance	50	0.5
	Balance	50	1.0
	Balance	50	2.0
5	Balance	70	0.5
	Balance	70	1.0
	Balance	70	2.0

After the five tests outlined above, the unit will be subjected to a baseline test as before and the results compared to determine the effect of helium in the atmosphere. The test setup is shown in Figure F-1.

6. Salt Spray

In the salt spray test the solution shall be a 5% salt solution prepared by dissolving five pounds of salt in 95 pounds of distilled water. The fog rate shall be 0.5 to 3 milliliters of solution per hour for each 80 square centimeters of horizontal collecting area.

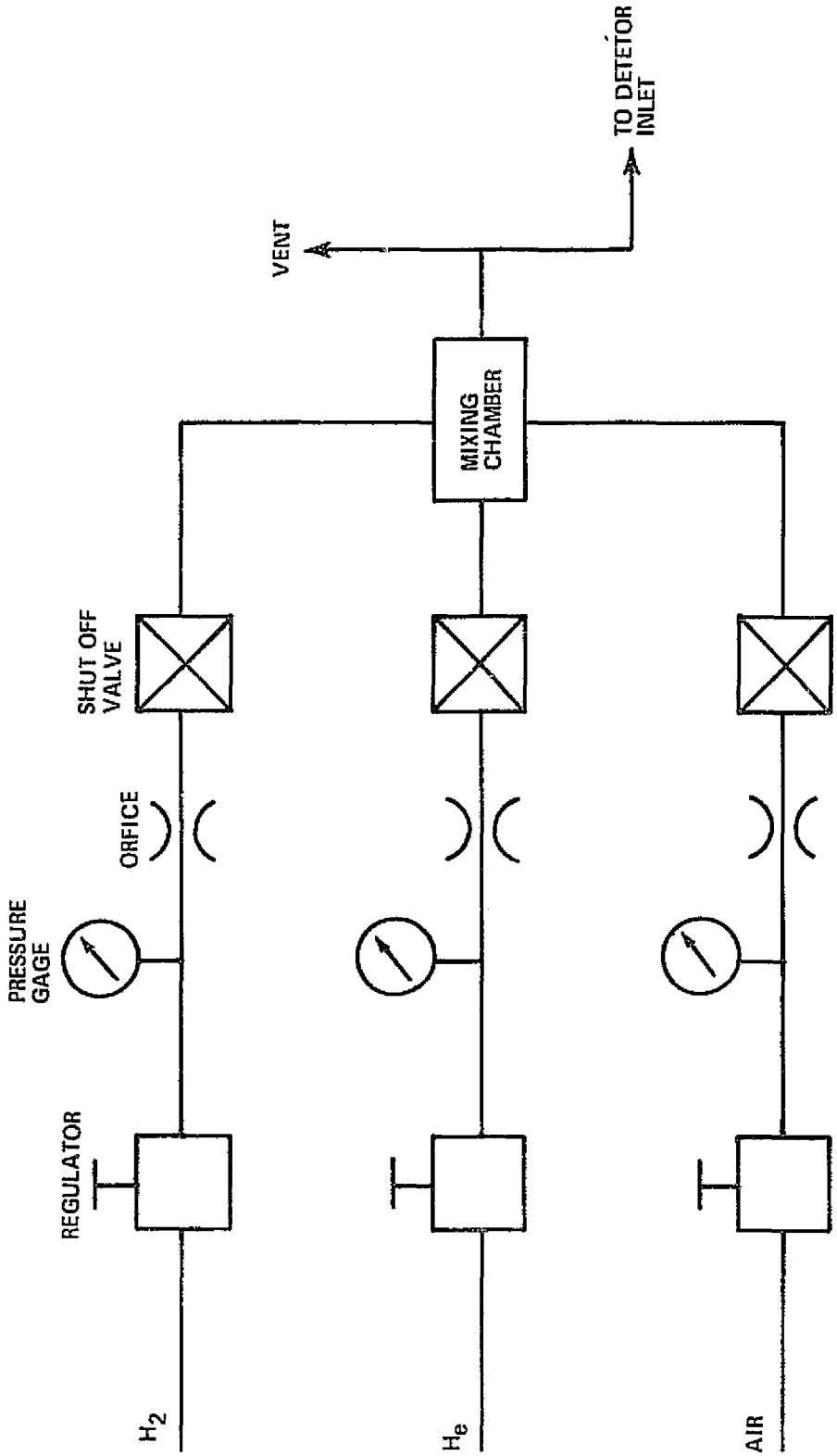

FIGURE F-1 HELIUM BACKGROUND TEST SET UP

a) Place the test unit in the salt spray chamber.
b) Establish salt fog and stabilize flow conditions. Expose the test unit for 48 hours.
c) Remove test unit and operate at a minimum of three hydrogen concentrations; record data.
d) Allow unit to air dry for 48 hours. Repeat step c.
e) Repeat baseline data.

The testing sequence and system exposed to each environment is shown in Figure F-2. Results of each test are contained in the data sheets on the following pages of this Appendix. The detectors were connected in the test chamber as shown in Figure F-3 for the environments of temperature, pressure and humidity. The connections for salt spray and sand and dust are given in Figure F-4.

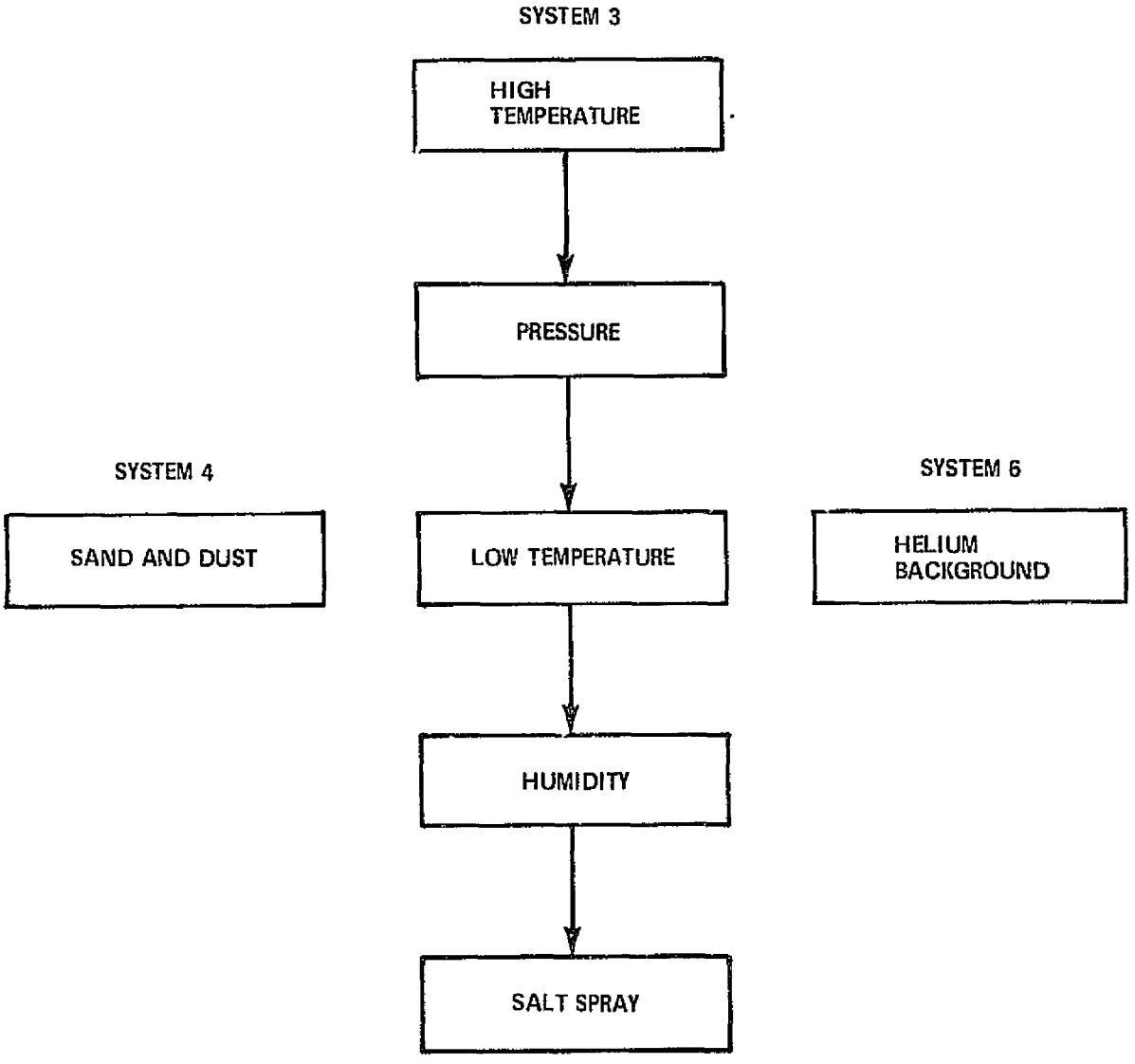

FIGURE F-2 ENVIRONMENTAL TESTING

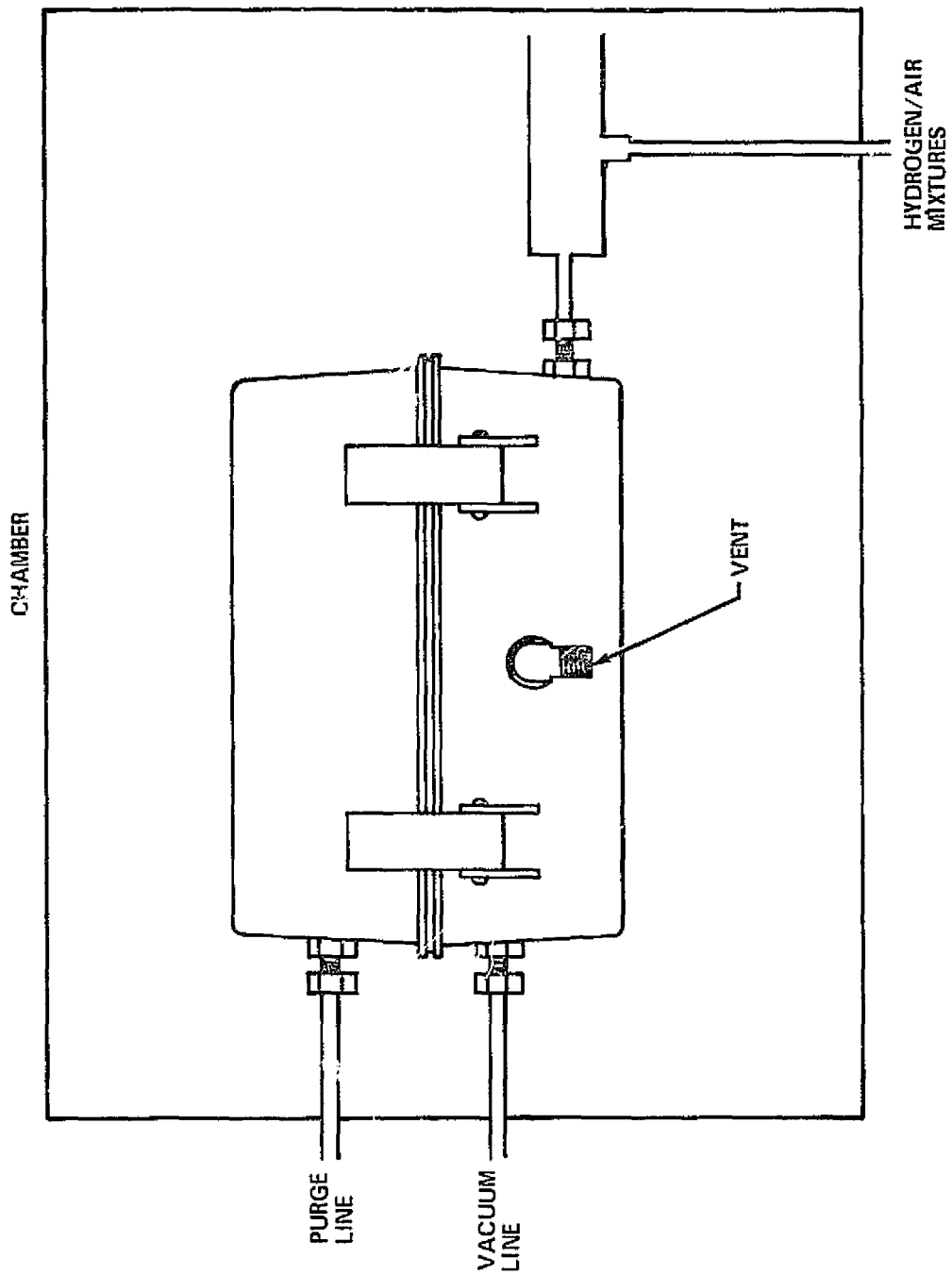

FIGURE F-3 OPERATIONAL TEST SET UP

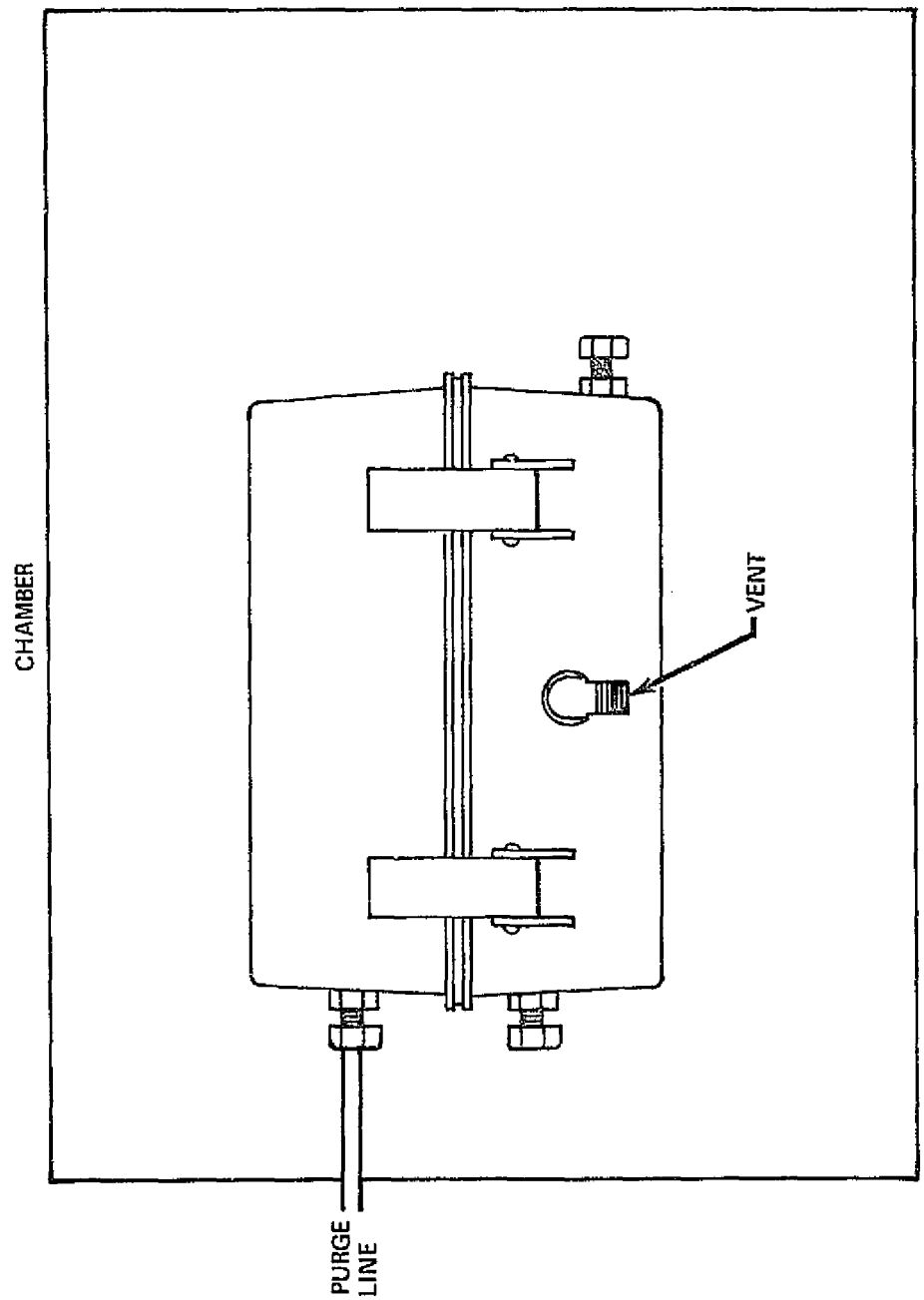

FIGURE F-4 NON-OPERATIONAL TEST SET UP

HYDROGEN SENSOR
ENVIRONMENTAL EVALUATION

DATE 3/3/76

SYSTEM NO. 3

ENVIRONMENT Temperature

VACUUM LEVEL 17.5 in. Hg

TEMPERATURE 245 °F

% H_2	OUTPUT VOLTAGE				
	Pre-test Ambient	150°F	Post Hi Temp Ambient	* 0°F	Post Lo Temp Ambient
0	0.053	0.057	0.053	-0.010	-0.008
0.50	0.512	0.517	0.511	0.429	0.391
0.99	1.072	1.062	1.072	0.969	0.951
1.87	2.132	2.123	2.131	2.008	1.989
DATE	3/3/76	3/3/76	3/4/76	3/5/76	3/5/76
TIME	14:20	18:30	01:30	13:05	17:30

COMMENT:

*Chamber would not operate properly at low temperature. Proceeded to pressure test between hi and lo temperature. Therefore, pre-lo temp ambient test results are post-lo pressure ambient readings.

HYDROGEN SENSOR
ENVIRONMENTAL EVALUATION

DATE 3/4/76

SYSTEM NO. 3

ENVIRONMENT Pressure

VACUUM LEVEL 17.5 in. Hg

TEMPERATURE 245 °F

	OUTPUT VOLTAGE				
% H_2	Pre-Test Ambient	31" Hg	Post Hi Press. Ambient	29" Hg	Post Lo Press. Ambient
0	0.013	-0.007	-0.007	-0.007	-0.007
0.50	0.452	0.432	0.393	0.373	0.372
0.99	1.013	0.973	0.912	0.911	0.912
1.87	2.072	2.032	1.992	1.992	1.992
DATE	3/4/76	3/4/76	3/4/76	3/4/76	3/4/76
TIME	15:20	15:45	15:55	16:30	16:40

COMMENT:

HYDROGEN SENSOR
ENVIRONMENTAL EVALUATION

DATE 3/8/76

SYSTEM NO. 3

ENVIRONMENT Humidity

VACUUM LEVEL 17.5 in. Hg

TEMPERATURE 245 °F

% H_2	OUTPUT VOLTAGE				
	Pre-Test Ambient	80% Rel. Hum. 80°F	Post-Test Ambient		
0	-0.007	+0.012	+0.051		
0.50	0.430	0.489	0.508		
0.99	0.969	1.047	1.066		
1.87	2.025	2.101	2.140		
DATE	3/8/76	3/9/76	3/9/76		
TIME	08:10	09:25	13:30		

COMMENT: System shut off for 12 hours between low temp. 3/5 and humidity 3/8.

HYDROGEN SENSOR
ENVIRONMENTAL EVALUATION

DATE 3/9/76

SYSTEM NO. 3

ENVIRONMENT Salt Fog

VACUUM LEVEL 17.5 in. Hg

Started 13:30 - 3/9/76

TEMPERATURE 245 °F

	OUTPUT VOLTAGE				
% H_2	Pre-Test Ambient	Post Test Wet	Post Test Dry		
0	+0.051	+0.374	+0.025		
0.50	0.508	0.910	0.521		
0.99	1.066	1.429	1.060		
1.87	2.140	2.444	2.115		
DATE	3/9/76	3/11/76	3/13/76		
TIME	13:30	14:35	14:30		
		Δf ≈ 82	Δf ≈ 65		

COMMENT: Post Test Wet; Temp. 230°F, cannot analyze until after Post Test Dry on 3/13. (3/11)

Problem may be just wet thermocouple wire since power supply current is correct. (3/11)

3/12 Temperature reads correct today; suspect wire was wet.
3/12 Δf today ≈ 100.
3/13 System looked good today; temp. was correct, problem was thermocouple wire since it is double cloth covered.

HYDROGEN SENSOR
ENVIRONMENTAL EVALUATION

DATE 3/15/76

SYSTEM NO. 3

ENVIRONMENT Ambient

VACUUM LEVEL 17.5 in. Hg

Check of system drift with heater

TEMPERATURE 245 °F

left on continually.

	OUTPUT VOLTAGE				
% H_2					
0	+0.024	+0.086	+0.025	+0.027	
0.50	0.540	0.621	0.481	0.523	
0.99	1.039	1.139	1.019	1.042	
1.87	2.093	2.153	2.093	2.077	
DATE	3/15/76	3/16/76	3/17/76	3/18/76	
TIME	12:00	14:05	10:10	15:00	
	$\Delta f \approx 65$	$\Delta f = 67$	$\Delta f \approx 65$	$\Delta f \approx 65$	

COMMENT: 3/19 Sent to lab for cleaning. When returned insure switch settings are correct.

HYDROGEN SENSOR
ENVIRONMENTAL EVALUATION

DATE 3/5/76

SYSTEM NO. 4 ENVIRONMENT Sand & Dust

VACUUM LEVEL 17.5 in. Hg

TEMPERATURE 245 °F

	OUTPUT VOLTAGE				
% H_2	Pre-Test	Post-Test			
0	+0.012	+0.013			
0.50	0.453	0.416			
0.99	1.016	0.934			
1.87	2.081	2.024			
DATE	3/2/76	3/12/76			
TIME		10.20			

COMMENT:

HYDROGEN SENSOR
ENVIRONMENTAL EVALUATION

DATE 3/23/76

SYSTEM NO. 6

ENVIRONMENT He Background

VACUUM LEVEL 17.5 in. Hg

TEMPERATURE 245 °F

% H_e / % H_2	OUTPUT VOLTAGE				
	0	5	10	30	50
0	0.012	0.033	0.011	0.010	0.012
0.5	0.456	0.519	0.523	0.445	0.465
1.0	0.968	1.018	0.987	0.948	0.872
2.0	1.964	1.983	1.986	1.937	1.700

Check at 2% Hz

SIG	16226	16442	16627	17561	19576
REF	16099	16313	16497	17429	19442
DIFF	127	129	130	132	134

COMMENT:

Due to loss in gain at high H_e concentrations made check of f_s & f_r at 2% H_2.

HYDROGEN SENSOR
ENVIRONMENTAL EVALUATION

DATE 3/23/76

SYSTEM NO. 6

ENVIRONMENT H_e Background (Continued)

VACUUM LEVEL 17.5 in. Hg

TEMPERATURE 245 °F

% H_e / % H_2	OUTPUT VOLTAGE				
	70				
0	0.011				
0.5	0.326				
1.0	0.740				
2.0	1.466				
SIG	22938				
REF	22600				
DIFF	138				

COMMENT:

APPENDIX G
GAS DYNAMICS

HELIUM BACKGROUND CALCULATIONS

It was mentioned in Appendix A that the frequency of a fluidic oscillator is proportional to the speed of sound in the fluid flowing through it. Thus,

$$f = c$$

$$c = \sqrt{kgRT}$$

where f = frequency
c = speed of sound in fluid
where k = ratio of specific heats of gas flowing
g = acceleration of gravity
R = gas constant for gas flowing
T = temperature of gas flowing

It is assumed that temperature remains constant; the speed of sound is proportional to the product kR which is a function of the mixture of gases flowing.

Figure G-1 presents a graphical representation of the five test mixtures used when H_2 = 2%.

Table G-1 summarizes the calculations made for frequency variation for the five mixtures.

A sample calculation for gas mixture 3 is included herein.

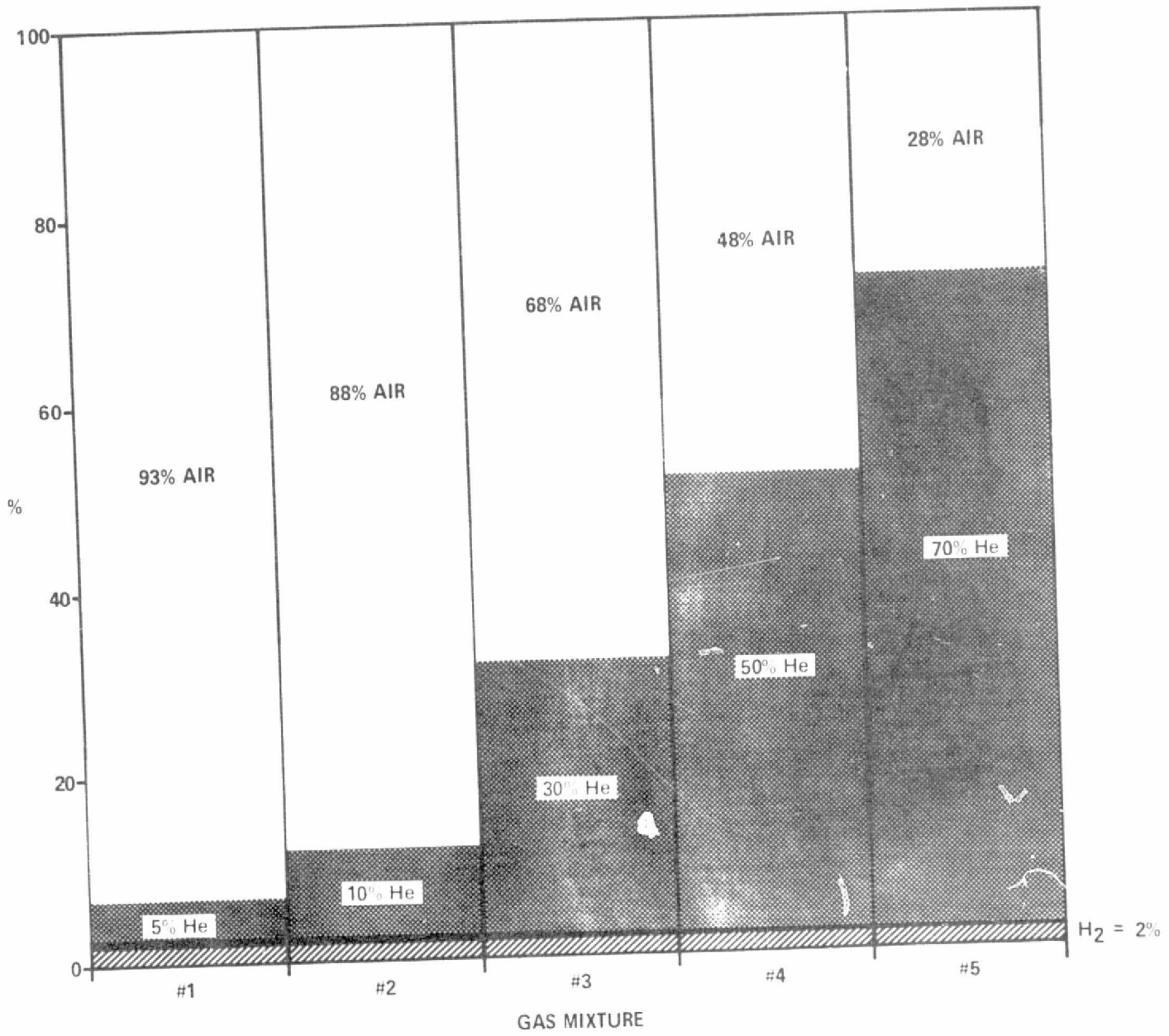

FIGURE G-1 TEST MIXTURES

TABLE G-1
SUMMARY

Mixture #	B_{H_2} % by Vol.	B_{H_e} % by Vol.	B_{air} % by Vol.	R_{mix} ft lb_f/lb_m °R	k_{mix}	$\sqrt{k_{mix}R_{mix}}$	% Increase In Frequency*
1	2	5	93	56.797	1.411	8.952	2.57
2	2	10	88	59.52	1.419	9.190	5.29
3	2	30	68	73.73	1.455	10.357	18.66
4	2	50	48	96.64	1.499	12.036	37.9
5	2	70	28	141.01	1.552	14.79	69.45

*Based on frequency of a mixture of 2% H_2 and 98% air by volume.

Sample Calculation for Gas Mixture #3

Given: The gas mixture consists of 2% by volume hydrogen, 30% by volume helium, and 68% by volume air.

The following data is taken from Young's "Basic Engineering Thermodynamics", McGraw-Hill.

Gas	Mol. Wt.	Gas Const.	C_p	C_v	k
Hydrogen	2	766.6	3.42	2.43	1.41
Helium	4.002	386.0	1.25	0.755	1.66
Air	28.97	53.3	0.240	0.171	1.40

where C_p = specific heat at constant pressure
C_v = specific heat at constant volume
k = ratio if specific heats = C_p/C_v

The first step is to convert from percents by volume (B) to percents by weight (G).

$$G_{H_2} = \frac{B_{H_2} M_{H_2}}{B_{H_2} M_{H_2} + B_{H_e} M_{H_e} + B_{air} M_{air}}$$

$$G_{H_e} = \frac{B_{H_e} M_{H_e}}{B_{H_2} M_{H_2} + B_{H_e} M_{H_e} + B_{air} M_{air}}$$

$$G_{air} = \frac{B_{air} M_{air}}{B_{H_2} M_{H_2} + B_{H_e} M_{H_e} + B_{air} M_{air}}$$

where B_{H_2} = % by volume hydrogen

G_{H_2} = % by weight hydrogen

M_{H_2} = molecular weight hydrogen

$$G_{H_2} = \frac{0.02(2)}{.02(2) + .3(4.002) + .68(28.97)} = 0.00191 = .191\%$$

$$G_{H_e} = \frac{0.3(4.002)}{.02(2) + .3(4.002) + .68(28.97)} = 0.0573 = 5.73\%$$

$$G_{air} = \frac{0.68(28.97)}{.02(2) + .3(4.002) + .68(28.97)} = 0.9408 = 94.08\%$$

$$R_{mix} = G_{H_2}R_{H_2} + G_{H_e}R_{H_e} + G_{air}R_{air}$$

$$= 0.00191(766.6) + 0.0573(386) + 0.9408(53.3) = 73.73$$

$$C_{p_{mix}} = G_{H_2}C_{p_{H_2}} + G_{H_e}C_{p_{H_e}} + G_{air}C_{p_{air}}$$

$$= 0.00191(3.42) + 0.0573(1.25) + 0.9408(.24) = 0.3039$$

$$C_{v_{mix}} = G_{H_2}C_{v_{H_2}} + G_{H_e}C_{v_{H_e}} + G_{air}C_{v_{air}}$$

$$= 0.00191(2.43) + 0.0573(0.755) + 0.9408(.171) = 0.2088$$

$$k_{mix} = \frac{C_{p_{mix}}}{C_{v_{mix}}} = \frac{0.3039}{0.2088} = 1.455$$

$$\sqrt{k_{mix}R_{mix}} = \sqrt{1.455 \times 73.73} = 10.357$$

$$\% \text{ increase in } f = \frac{10.357}{8.728} = 18.66\%$$

PURGE CALCULATIONS

KSC safety requirements dictate that enclosures containing possible ignition sources in a possible explosive atmosphere must be subjected to a continuous purge during hazardous operations, ref. DTI-M-23.

Purge Requirement:

Flow Rate - 0.5 to 1.0 SCFM through enclosure to atmosphere
Min. Pressure - 0.5"H_2O positive pressure, enclosure to atmosphere

Calculation based on purge source being a regulated supply (50 psig) of nitrogen with 10°F dewpoint.

The purge philosophy chosen has the purge flow (50 psig dry N_2) entering the purge inlet fitting, which incorporates a flow control orifice, into the electronics half of the detector assembly which will be maintained at 2.0"H_2O gage with respect to ambient. From the electronics side of detector purge flow will enter the sensor half via flow orifices; the sensor side will be controlled to 1.0"H_2O gage with respect to ambient. Finally, the purge flow will exit the detector via the vent outlet orifice to ambient. Thus, the pressure differentials are such that infiltration of ambient gases into detector is precluded as is infiltration of gases from sensor side of the detector to the electronics side.

A schematic of this system is given in Figure G-2.

Flow Conditions for Orifice "A"

P_1 = 50 psig P_2 = 2.0"H_2O gage
Q = 0.5 - 1.0 SCFM
Orifice Size Selected D = 0.031"
Q = 0.635 SCFM

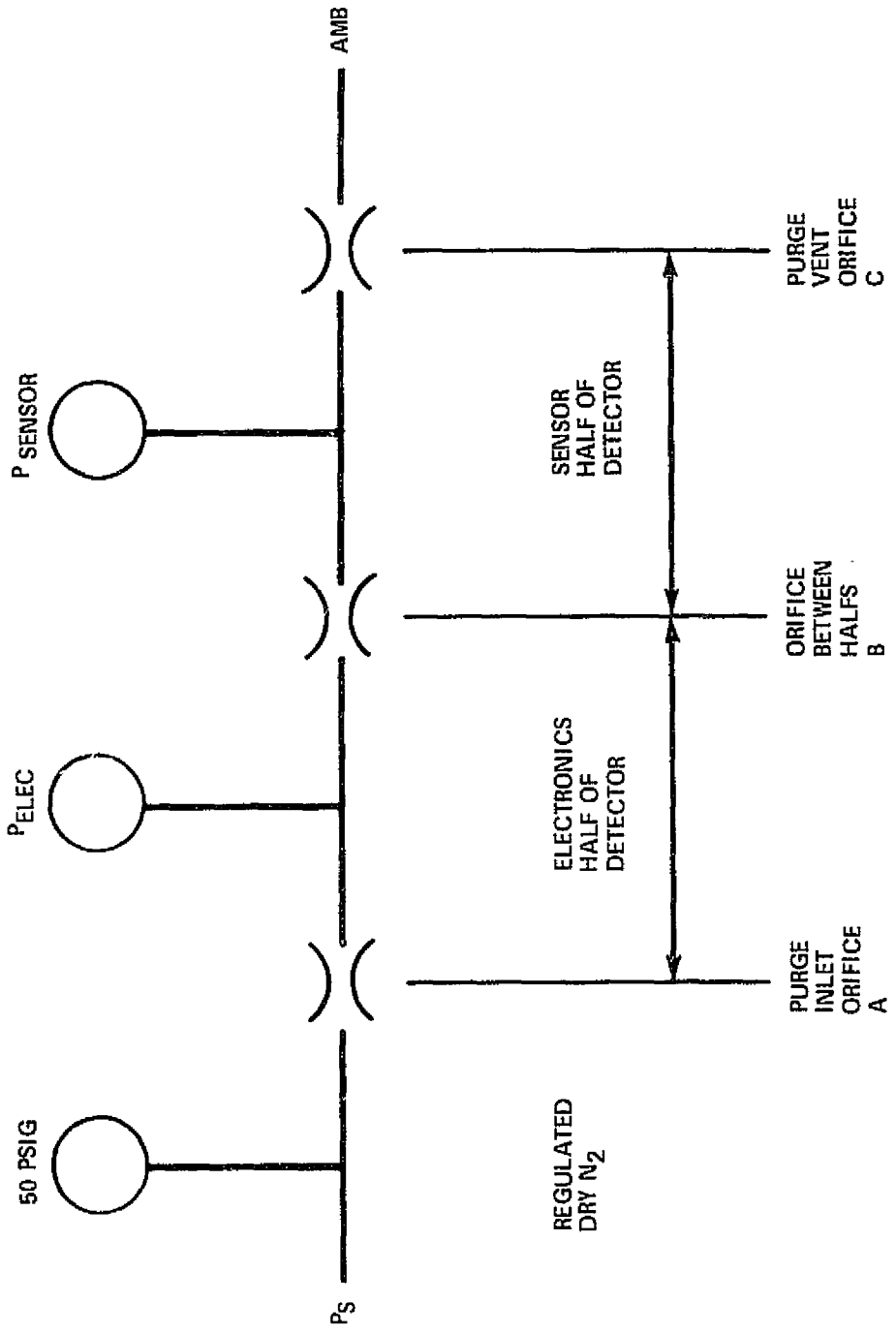

FIGURE G-2 PURGE SCHEMATIC

Flow Conditions for Orifice "B"

P_1 = 2.0"H_2O gage P_2 = 1.0"H_2O gage

Q = 0.635 SCFM

Orifice Size Selected 4 - 0.11" dia. holes #35 drill

Flow Conditions for Orifice "C"

P_1 = 1.0"H_2O gage P_2 = Ambient

Q = 0.635 SCFM

Orifice Size Selected D = 0.22 in.

Use 5/16" elbow ftg.